Investigating Local Surface Displacements Associated with Anthropogenic Activities by Satellite Radar Interferometry: Application to Staufen im Breisgau and Ketzin

Christin Lubitz

A cumulative dissertation

in partial fulfillment of the requirements for the academic degree of
“doctor rerum naturalium” (Dr. rer. nat.)
in the academic discipline "Geoinformatics"

submitted to the Faculty of Science
Institute of Geography
of Potsdam University
and
the German Research Centre for Geosciences (GFZ)

Place and date of the disputation: Potsdam, 11.07.2018
Primary supervisor: Prof. Dr. Hartmut Asche
Further reviewers: Prof. Dr. Hermann Kaufmann, Prof. Dr.-Ing. Wolfgang Niemeier

Published online at the
Institutional Repository of the University of Potsdam:
URN urn:nbn:de:kobv:517-opus4-416002
http://nbn-resolving.de/urn:nbn:de:kobv:517-opus4-416002

Content

Declaration of Authorship

I hereby declare that the submitted thesis is my own original work. All direct or indirect sources that were used are acknowledged as references.
This thesis was not previously presented to another examination board and has not been published.

_____ _____

(Place, Date) (Signature)

Acknowledgements

I am deeply grateful to Prof. Dr. Hermann Kaufmann, who gave me the chance to do my PhD here at the German Research Centre for Geosciences. I appreciate every advice that he gave on my research, scientific life, and career planning. I enjoyed all of our breakfasts, filled with laughter and good talks.

I am very thankful to Prof. Dr. Hartmut Asche of the University of Potsdam for all the deep discussions on different perspectives regarding the overall research of this thesis.

In gratitude, I want to name Dr. Mahdi Motagh, who was my first contact for every professional question and who supported me in all the years of my PhD study.

Regarding my studies on Staufen im Breisgau, I want to thank Prof. Dr. Ingo Sass for sharing his profound knowledge on the situation on site, Rudi Asal from Landratsamt Breisgau Hochschwarzwald for support with questions related to the applied leveling campaigns, the municipal planning and building control office of Staufen, namely Wilma Tönnies, and mayor Michael Benitz for allowing data sharing.

With respect to my studies at the Ketzin pilot site, I deeply appreciate all the support from the whole Ketzin team, especially, Sonja Martens, Thomas Kempka and Fabian Möller.

Sylvia Magnussen deserves deep appreciation here. Who are you and what is your research worth if you do not have such a professional, patient, emergency-solving, and wonderful person as asystem administrator and computer expert?

As science progress is stimulated by the exchange of knowledge, I want to mention all the scientists, whether PhD students, Post-Docs, senior scientist, or professors, who I was glad to meet through the years in the office and on conferences, field trips, or summer schools. Thank you for every discussion or even small hints that you have shared.

My deep thanks goes to Dr. Nina Bösche, who has become a close friend during the last few years and who supported me during the writing of this thesis with her honest and motivating way of discussing my research.

Last but not least, I am absolutely grateful for every support of my husband, Daniel, during the entire period. Doing a PhD is not only limited to office and field work, it is an attitude to life that shapes a couple of years. Personally, during this time family and friends are the most important support. Thanks to my mother, my parents-in-law, my lovely grandmother-in-law and my friends, Anna, Janine and Tobias.

I dedicate this thesis to my two wonderful children.

Preface

The present cumulative thesis joins three papers. For each, multiple authors are listed; they contributed differently to the manuscripts, but I was the primary researcher and first author.
Publication one, Remarkable Urban Uplift in Staufen im Breisgau, Germany: Observations from TerraSAR-X InSAR and Leveling from 2008-2011, was published in 2013 in the peer-reviewed open-access journal *Remote Sensing* that is operated by the Multidisciplinary Digital Publishing Institute (MDPI) in Basel, Switzerland. The second paper, Ground Surface Response to Geothermal Drilling and the Following Counteractions in Staufen im Breisgau (Germany) Investigated by TerraSAR-X Time Series Analysis and Geophysical Modeling, was published in 2014 in *Remote Sensing* as well.
The last manuscript, Integrated Assessment of Ground Surface Displacements at the Ketzin Pilot Site for CO_2 Storage by Satellite-based Measurements and Hydromechanical Simulations, was submitted to IEEE Journal of Selected Topics in Applied Earth Observations and Remote Sensing in December 2017 for possible publication. The presented Subchapters 4.3.3 and 4.4.3 were mainly written by Dr. Thomas Kempka.
All papers are presented as reprints except the numbering of figures, tables, and references to subchapters, which were adjusted according to the order of this thesis.

Christin Lubitz

Abstract

Direct anthropogenic influences on the Earth's subsurface during drilling, extraction or injection activities, can affect land stability by causing subsidence, uplifts or lateral displacements. They can occur in much localized as well as in uninhabited and inhabited regions. Thus the associated risks for humans, infrastructure, and environment must be minimized. To achieve this, appropriate surveillance methods must be found that can be used for simultaneous monitoring during such activities. Besides classical geodetic methods such as leveling or GPS, multi-temporal synthetic aperture radar interferometry (MT-InSAR) methods like the Persistent Scatterer Interferometry (PSI) and the Small BAseline Subsets (SBAS) have been developed as standard approaches for satellite-based surface displacement monitoring. With increasing spatial resolution and availability of SAR sensors in recent years, MT-InSAR can be a valuable alternative for the detection and mapping of even the smallest man-made displacements.

This doctoral thesis aims at investigating the capacities of the mentioned standard methods for this purpose, and comprises three main objectives against the backdrop of a user-friendly surveillance service:

(1) the spatial and temporal significance assessment against leveling, (2) the suitability evaluation of PSI and SBAS under different conditions, and (3) the analysis of the link between surface motion and subsurface processes.

Two prominent case studies on anthropogenic induced subsurface processes in Germany serve as the basis for this goal. The first is the distinct urban uplift with severe damages at Staufen im Breisgau that has been associated since 2007 with a failure to implement a shallow geothermal energy supply for an individual building. The second case study considers the pilot project of geological carbon dioxide (CO_2) storage at Ketzin, and comprises borehole drilling and fluid injection of more than 67 kt CO_2 between 2008 and 2013. Leveling surveys at Staufen and comprehensive background knowledge of the underground processes gained from different kinds of *in-situ* measurements at both locations deliver a suitable basis for this comparative study and the above stated objectives. The differences in location setting, i.e. urban versus rural site character, were intended to investigate the limitations in the applicability of PSI and SBAS.

For the MT-InSAR analysis, X-band images from the German TerraSAR-X and TanDEM-X satellites were acquired in the standard Stripmap mode with about 3 m spatial resolution in azimuth and range direction. Data acquisition lasted over a period of five years for Staufen (2008-2013), and four years for Ketzin (2009-2013). For the first approximation of the subsurface source, an inversion of the InSAR outcome in Staufen was applied. The modeled uplift based on complex hydromechanical simulations and a correlation analysis with bottomhole pressure data were used for comparison with MT-InSAR measurements at Ketzin.

In response to the defined objectives of this thesis, a higher level of detail can be achieved in mapping surface displacements without *in-situ* effort by using MT-InSAR in comparison to leveling (1). A clear delineation of the elliptical shaped uplift border and its magnitudes at different parts was possible at Staufen, with the exception of a vegetated area in the northwest. Vegetation coverage and the associated temporal signal decorrelation are the main limitations of MT-InSAR as clearly demonstrated at the Ketzin test site. They result in insufficient measurement point density and unwrapping issues. Therefore, spatial resolutions of one meter or better are recommended to achieve an adequate point density for local displacement analysis and to apply signal noise reduction. Leveling measurements can provide a complementary data source here, but require much effort pertaining to personnel even at the local scale. Horizontal motions could be identified at Staufen by only comparing the temporal evolution of the 1D line of sight (LOS) InSAR measurements with the available leveling data. An exception was the independent LOS decomposition using ascending and descending data sets for the period 2012-2013. The full 3D displacement field representation failed due to insufficient orbit-related, north-south sensitivity of the satellite-based measurements. By using the dense temporal mapping capabilities of the TerraSAR-X/TanDEM-X satellites after every 11 days, the temporal displacement evolution could be captured as good as that with leveling.

With respect to the tested methods and in the view of generality, SBAS should be preferred over PSI (2). SBAS delivered a higher point density, and was therefore less affected by phase unwrapping issues in both case studies. Linking surface motions with subsurface processes is possible when considering simplified geophysical models (3), but it still requires intensive research to gain a deep understanding.
Finally, it remains to be said that the investigations at Staufen for this thesis have led to the decision for further MT-InSAR based monitoring of the uplift area by the city administration and the survey authority concerned. This is an important step forward in the broader acceptance of this technology.

Zusammenfassung

Die Stabilität der oberen Gesteinsschichten kann durch anthropogene Aktivitäten, wie Bohrungen, Gas- oder Fluidextraktionen, beziehungsweise –injektionen, so beeinflusst werden, dass Oberflächenhebungen, Senkungen und seitliche Lageverschiebungen auftreten können. Diese Bewegungen können lokal begrenzt sein, in bewohnten als auch unbewohnten Gebieten in Erscheinung treten und ein Risiko für Mensch, Umwelt und Infrastruktur darstellen. Die Einschätzung und Überwachung dieser Risiken kann lokal durch geophysikalische und geodätische Verfahren erfolgen, und mittels fernerkundlichen Analysen in einen räumlich zeitlichen Zusammenhang gebracht werden. Neben klassischen geodätischen Methoden wie dem Nivellement oder GPS, haben sich multitemporale Methoden der Synthetischen Apertur Radar Interferometrie (MT-InSAR) wie die Persistent Scatterer Interferometry (PSI) oder das Small BAseline Subsets (SBAS) Verfahren als Standardanwendung für die satellitengestützte Messung von Oberflächenverschiebungen etabliert. Mit der Entwicklung hin zu immer hochauflösenderen Systemen sowie einer Zunahme an zur Verfügung stehenden Sensoren in den letzten Jahren, bietet MT-InSAR eine Alternative zum Aufspüren und Kartieren von kleinsten menschengemachten Bewegungen der oberen Gesteinsschichten.

Ziel dieser Doktorarbeit ist die Untersuchung der oben genannten Standardmethoden hinsichtlich ihrer Eignung zur räumlich zeitlichen Analyse von lokalen Bewegungen. Vor dem Hintergrund einer nutzerfreundlichen Anwendung werden dabei drei Punkte eingehend betrachtet: (1) die Bewertung der raum-zeitlichen Signifikanz gegenüber dem Nivellement, (2) die Eignungsbeurteilung beider Methoden unter verschiedenen Bedingungen und (3) die Analyse der Verknüpfbarkeit von Oberflächenbewegungen und Untergrundprozessen.

Als Grundlage für diese Untersuchung dienen zwei bekannte Bohrprojekte in Deutschland. Das erste ist ein fehlgeschlagenes Projekt zur geothermalen Energieversorgung eines einzelnen Gebäudes in Staufen im Breisgau im Jahr 2007. Damit in Verbindung steht eine ausgeprägte innerstädtische Hebung mit ernsten Schäden an der Wohnbebauung. Das zweite ist ein Pilotprojekt zur geologischen Speicherung von Kohlenstoffdioxid (CO_2) in Ketzin, welches Bohrungen und Fluidinjektionen von mehr als 67 kt CO_2 zwischen 2008 und 2013 umfasst. Die Nivellement-Messungen in Staufen sowie das umfangreiche Hintergrundwissen durch verschiedene *in-situ* Messungen zu den Untergrundprozessen an beiden Standorten bieten eine solide Grundlage für diese vergleichende Studie und ihre Ziele. Da beide Standorte sich stark unterscheiden, insbesondere hinsichtlich ihres städtischen beziehungsweise ländlichen Charakters, erlauben diese Fallstudien eine Untersuchungen der Grenzen in der Anwendbarkeit von den Methoden PSI und SBAS.

Für die Untersuchung wurden Bilddaten im X-Band von den deutschen Satelliten TerraSAR-X und TanDEM-X im Standardmodus Stripmap mit etwa 3m Azimut- und Entfernungsauflösung aufgenommen. Die Datenakquise für Staufen umfasste fünf Jahre (2008-2013) und für Ketzin vier Jahre (2009-2013). In Staufen wurde durch eine Inversion der InSAR-Resultate eine erste Näherung zur Lokalisierung einer Volumenexpansion im Untergrund erzielt, welche ursächlich für die an der Oberfläche beobachteten Hebungen ist. Für das Ketzin-Projekt wurden komplexe hydromechanische Simulationen durchgeführt und darauf basierende modellierte Hebungen zum Vergleich mit den MT-InSAR-Messungen herangezogen. Zusätzlich erfolgte eine vergleichende Korrelationsanalyse mit den Druckdaten aus der Injektionsbohrung.

In dieser Arbeit konnte gezeigt werden, dass Im Vergleich zu den gängigen Nivellement-Messungen ein deutlich höherer Detailgrad in der Kartierung der Oberflächenbewegungen durch das fernerkundliche MT-InSAR Verfahren erlangt werden konnte (1). Die klare Abgrenzung des elliptischen Hebungsfeldes in Staufen sowie seiner variierenden Magnituden an verschiedenen Positionen konnte deutlich gezeigt werden, mit Ausnahme einer Vegetationsfläche im nordwestlichen Abschnitt. Die Fallstudie zu Ketzin demonstriert ebenfalls die methodischen Einschränkungen bei MT-InSAR durch Vegetation und den damit einhergehenden Signalverlusten. Als Folge traten eine unzureichende Messpunktdichte und Probleme in der Phasenabwicklung auf. Eine räumliche Auflösungen von einem Meter oder besser würde die Wahrscheinlichkeit einer geeigneten

Punktdichte erhöhen. Außerdem ermöglicht sie die Anwendung passender Methoden zur Rauschreduzierung des Signals unter geringen Verlusten in der räumlichen Auflösung. Dennoch zeigte sich, dass Nivellement-Kampagnen als ergänzende Datenquelle wertvolle Informationen liefern, auch wenn diese einen hohen Arbeitsaufwand selbst für lokale Ereignisse erfordern.
Die Identifizierung von Horizontalbewegungen in Staufen war nur durch den Vergleich des zeitlichen Hebungsverlaufes von Nivellement- und den 1D InSAR-Resultaten festellbar. Eine Ausnahme bildete die davon unabhängige Verschneidung zweier Datensätze von je einem aufsteigenden und absteigenden Orbit für den Zeitraum 2012-2013. Die Darstellung eines kompletten, satellitengestützten 3D-Bewegungsfeldes scheitert an der ungenügenden, umlaufbahnbedingten Sensitivität in Nord-Süd-Richtung.
Die zeitlich dichte Kartierung durch TerraSAR-X und TanDEM-X alle 11 Tage ermöglicht eine ebenso detaillierte zeitliche Erfassung der Entwicklung wie mittels Nivellement.
Die Untersuchungen an beiden Standorten haben gezeigt, dass das SBAS-Verfahren im Allgemeinen nützlichere Ergebnisse liefert, als das PSI-Verfahren (2). Das SBAS-Verfahren lieferte die höhere Punktdichte und zeigte aufgrund dessen weniger Probleme bei der Phasenabwicklung.
Die Verknüpfung von Bewegungen in den oberen Gesteinsschichten mit deren ursächlichen Untergrundprozessen ist unter Einbeziehung vereinfachter geophysikalischer Modelle möglich (3), verlangt aber noch weiterführende Analysen für ein tieferes Verständnis.
Abschließend bleibt zu erwähnen, dass die in der dieser Arbeit präsentierten Untersuchungen zu Staufen zu einer Fortführung der MT-InSAR-basierten Überwachung der Hebungen führten. Diese von der Stadtverwaltung und dem verantwortlichen Vermessungsamt getroffene Entscheidung stellt einen wichtigen Schritt zur breiteren Akzeptanz dieser Technologie dar.

1. Chapter: Introduction

1.1 Motivation and Objectives of the Thesis

The worldwide demand for 'green' energy sources is increasing. Apart from sun, water and wind as classical alternatives, geothermal energy supply has become popular, and its usage has expanded. While geothermal energy supply is considered very effective and sustainable for operations, it comes with some risks during exploration for resources and drilling. Drilling can affect land stability, and may lead to unpredicted surface movements [1]. Another application that requires drilling is the underground storage of carbon dioxide (CO_2) in appropriate reservoirs to prevent its emission into the atmosphere. Such projects are mostly associated with the Carbon Capture and Storage (CCS) technology. Both geothermal energy supply and subsurface CO_2 storage directly affect the environment, especially through anthropogenic induced processes on the Earth's subsurface (amongst others, borehole drilling and fluid injection). Such interventions into the existing hydro-geological systems require responsible and careful handling, as well as continual monitoring and improvement of methods aimed at long-term, risk-minimized usage for humans and environment.
Satellite-based remote sensing, in particular Synthetic Aperture Radar Interferometry (InSAR) techniques, can be the appropriate solution for regular geodetic surveillance of surface displacements associated with the above stated activities. For example, it was successfully applied to investigations into large-scale deformation phenomena (earthquakes [2]–[5], volcanoes[6]–[9] , etc.). My doctoral research aims to evaluate the use of InSAR for the earlier mentioned cases of anthropogenic induced processes on the Earth's subsurface. The focus lies on the limitations and challenges for small-scale activities, which is especially important for locally restricted shallow geothermal energy resources. With increasing availability of high-resolution SAR sensors (1 m–5 m spatial resolution), such local analyses become feasible. In this context, and additionally from the user's point of view, the following key questions and objectives are investigated:

(1) Significance assessment of the spatial and temporal InSAR measurements as compared to classical point-wise terrestrial leveling measurements

(2) Comparison and evaluation of the standard time series methods of Persistent Scatterer Interferometry (PSI) and Small BAseline Subsets (SBAS)

(3) Which indirect conclusions can be made on subsurface processes based on displacement measurements at the top surface, and what factors are important, when considering the constructed relation between underground processes and surface motions?

As the future usage of these techniques is rather commercially driven (service provider) than scientifically driven, the following points are expressed as further objectives and questions of this thesis.

(4) Which factors define user-friendly and sufficient surface displacement surveillance?

(5) Definition of the conceptual aspects for future InSAR monitoring services for anthropogenic activities

To investigate the above mentioned objectives, two case studies representing anthropogenic induced processes on the Earth's subsurface were chosen. Both test sites are located in Germany with very small spatial extent (several 100 meters of affected area). The first pertains to shallow geothermal energy supply in Staufen im Breisgau (hereafter referred to as Staufen). The second deals with the underground CO_2 storage at the Ketzin pilot site. The two test sites are openly discussed because they affect the reputation of renewable energy and reduction of CO_2 emissions, respectively. The activities at these locations have raised doubts, and even a negative perception of the application of these new technologies among the German population. Therefore, the

investigation presented herein shall support increased knowledge and enhanced transparency for a better understanding of these technologies.

1.2 Composition of Thesis

The introduction provides the fundamentals on InSAR (Chapter 1.3). Since temporal investigations are requested for monitoring surface stability, Chapter 1.4 provides insights into the main issue with InSAR, which is the signal decorrelation that is affected primarily by spatial and temporal influences. Within the subchapters, the two main categories of processing algorithms to overcome this issue to a certain extent are introduced: PSI (Chapter 1.4.1) and SBAS (Chapter 1.4.2). Both have been developed as the accepted standard approaches, which are the most widely used in research and commercial projects currently. Their general procedures and differences are presented here. As this doctoral study is application oriented, it includes the evaluation of these standard techniques with regard to their suitability in the precise mapping of potentially instable and localized areas in time and space. Chapter 1.5 provides an overview of the simple geo-physical modeling strategies for deformation sources as usually applied in conjunction with InSAR, as well as presents the aspects that are relevant for model-refinement. These models allow the indirect linking of observed instability on the Earth's surface with subsurface processes.
An overview of both case studies (Chapter 1.6) concludes the introductory part of this thesis. It comprises the site locations, a summary of the events and activities in view of their international importance, their current state, and how the use of InSAR can help in these specific cases.
Chapter 2 deals with the capacity of the Multi-Temporal InSAR (MT-InSAR) method SBAS to clearly delineate the borders of instable ground surfaces, and to specify their magnitudes and temporal evolution in comparison to conventional terrestrial leveling measurements. The representative case study focuses on surface displacement analysis in conjunction with a failed shallow geothermal energy supply project at the old city center of Staufen, a small city in southwest Germany. Since the related anthropogenic activities are very small in their spatial extent (tens to hundreds of meters), this investigation must be considered as focusing on the question of details.
Chapter 3 extends the investigation at Staufen (Chapter 2) towards a 2D displacement field analysis, and the related added value for geophysical modeling and process understanding. It includes the differentiation of horizontal and vertical motion contributions from the 1D Line of Sight (LOS) InSAR measurement by using additional SAR images from an opposing orbit path. In order to link the InSAR surface displacement observation with the subsurface processes occurring at Staufen, the study is complemented by the computation of a rectangular opening-mode dislocation source in an elastic half-space. By using an inversion of the InSAR observations, the deformation source parameters can be constrained.
Chapter 4 considers the case in which anthropogenic induced subsurface processes do not lead to significant surface instability. The representative case study deals with the underground storage of CO_2 at the Ketzin pilot site, which is located west of Berlin, Germany. This investigation demonstrates the limitations and challenges for MT-InSAR methods (PSI and SBAS) as surveillance techniques. Complex hydromechanical simulations of the surface displacements related to CO_2 injection are used for comparison with the InSAR observations. They complement the discussion on the measurement boundaries for surface displacements.
A summation of the overall discussion in and the conclusion of this thesis are presented in Chapter 5. The capacity of the standard MT-InSAR techniques for surveillance of localized surface displacements associated with anthropogenic activities is assessed and outlined in detail. The results of all the contributing publications presented in the previous chapters with respect to the key questions and objectives listed in Chapter 1.1 are discussed in Chapter 5.1.
The significance assessment of LOS InSAR measurements against classical leveling is provided as the first point (Chapter 5.1.1), and it includes the evaluation to map the different spatial dimensions and the temporal evolution. Chapter 5.1.2 deals with linking the surface observations with the anthropogenic induced subsurface processes. The specific findings of the case studies, which

comprise simple geo-physical modeling at Staufen (Chapter 3) and complex hydromechanical simulations at the Ketzin pilot site (Chapter 4), are reviewed, leading to general conclusions on what InSAR measurement analyses can reveal regarding the constructed surface-subsurface-relation. The third main point of discussion (Chapter 5.1.3) reflects on technical and performance factors following the demand for a user-friendly and effective usage of MT-InSAR for future projects in this field of application.
Additionally, as both case studies are based on SAR images of the German TerraSAR-X (TSX) and Tandem-X (TDX) satellites, prognostic statements on the usage of the newly available Sentinel-1 data for the test sites analyzed herein will be presented in Subchapter 5.1.3.1. This is considered as relevant for future applications, because the open-data policy of the satellite's operator, the European Space Agency (ESA), guarantees free data access.
Based on the discussion of the results, a conceptual summary for a successful InSAR monitoring (Chapter 5.2) as well as an overall conclusion (Chapter 5.3) will end this thesis.

1.3 Introducing Synthetic Aperture Radar Interferometry as Remote Sensing Technique

Remote sensing by using Synthetic Aperture Radars (SAR) sensors exploits the microwave region of the electromagnetic spectrum (0.1 cm–100 cm). It is an imaging method that is based on the travel time measurements of actively transmitted, high-energetic signals in a side-looking geometry (Fig. 1.1). The echo received by the antenna comprises information on the distance from the sensor to the scattering object (range), the amplitude (strength of signal return), and the phase (angular difference between the transmitted and received waves).
The potential of phase information for detecting surface displacement was discovered in the early 1990s [10]. Prior to that, phase-based interferometric measurements were applied for topographical derivations. By comparing the travel time and phase of the SAR signals from at least two temporally separated images allows the mapping of surface displacements at intervals that are provided by the orbit revisit time of the satellite used or the flight repetition of the airplane, respectively. It is known as repeat-pass SAR Interferometry (InSAR). Methodological advancements in time series investigations have triggered the popularity of this geodetic technology. The use of Unmanned Aircraft Systems, also referred to as drones, is increasing in photogrammetry and remote sensing applications [11]. Since localized investigations do not require large areal coverage as provided by satellite-based imaging, drones are an interesting option for future demands for specific small area displacement surveillances.
Compared to optical systems, several advantages of the SAR systems lead to the decision for a microwave-based displacement monitoring. These are solar illumination-independence due to the active sensor and its own energy source, and a significantly reduced impact of atmospheric conditions (clouds, precipitation) on the image. The latter is due to the long wavelength of microwave signals, which reduces the impact of aerosol and precipitation driven scattering within the atmosphere, thereby allowing information retrieval from the ground.
Since microwaves are beyond the visible spectrum, only signal processing reveals an image that can be finally interpreted by the human eye. This leads to an aspect that is not negligible in radar remote sensing, which is complex signal processing and image interpretation. In this context, the side-looking geometry of SAR systems, which is a prerequisite for the signal separation of surface objects, can cause spatial distortions like layover and foreshortening. Even information loss due to radar shadow is possible, and it depends on the surface topography.
Another important aspect in SAR image analysis is the understanding of the different scattering mechanisms that exist, and which lead to different intensities of the signal's echo. The signal can either be reflected away from the antenna (specular reflection at smooth surfaces), backscattered with varying intensity depending on the surface roughness (diffuse scattering or volume scattering), or almost totally reflected back to the antenna in case of appropriate object geometry (corner reflection). The kind of scattering mechanism that occurs depends on the wavelength, the local

incident angle and the characteristics of the object that is hit by the SAR impulse (e.g. size, shape, orientation, surface roughness, and dielectric constant)[12].

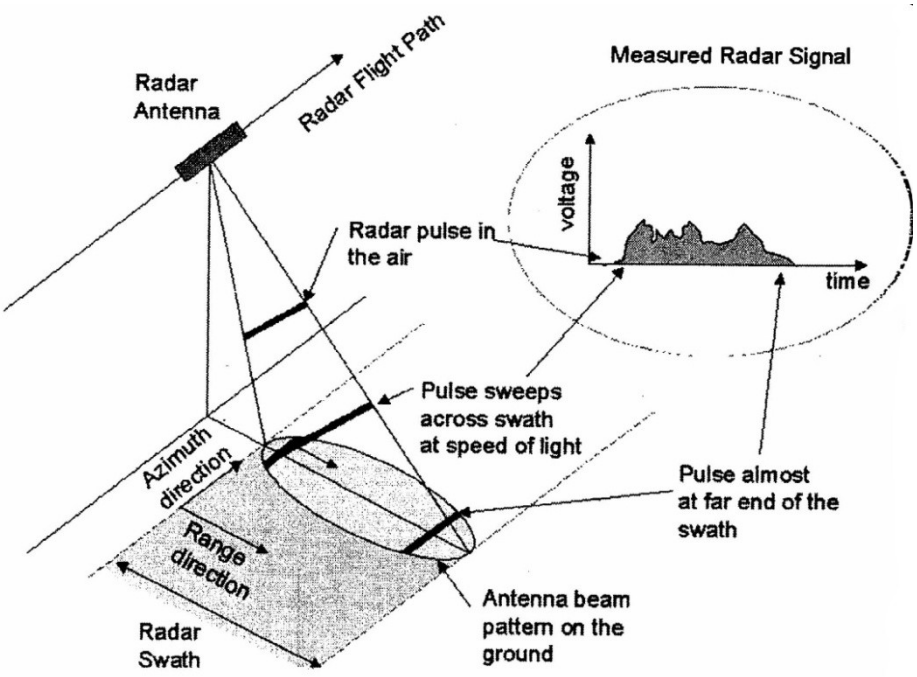

Fig. 1.1: Measurement principle for imaging SAR sensors [13].

1.4 Multi-Temporal InSAR Methodologies for Surface Displacement Analysis in Conjunction with Subsurface Processes

When surface displacements pertaining to subsurface processes are investigated, it is essential to have knowledge on their spatio-temporal evolution. It allows drawing conclusions on process triggers, analyses of the association with natural barriers and/or anthropogenic counteractions, and increases process knowledge itself. Geodetic surveillance techniques are useful for this purpose, but when considering InSAR here, there are certain restrictions that are related to the main limitation in the InSAR time series analysis: the signal decorrelation in the resolution cell of the SAR image.
This decorrelation can be either sensor geometry-driven (spatial and rotational decorrelation [14], [15]) or triggered by changes in the signal backscatter characteristics with time (temporal decorrelation) [14]. Temporal decorrelation occurs at short and long timescales in repeat-pass interferometry, e.g. immediate changes in signal response in vegetated areas under windy conditions or seasonal variations due to precipitation periods [16]. Also, sudden or slow surface displacements can cause signal loss. Therefore, the time difference between two SAR images (temporal baselines) of the acquired dataset must be considered for convenience in InSAR processing and result interpretation.
Spatial decorrelation is directly related to the spatial distance between the acquisition antennas, which is called the spatial baseline. A non-zero baseline causes changes in the look angle of the SAR acquisitions, and consequently causes slightly varying relative positions and scattering phases within each resolution cell [14], [17]. In interferometry, the spatial baseline results in a trade-off as follows. The shorter the distance, the lower is the sensitivity for phase change detection, but the longer the baseline, the stronger is the signal decorrelation. This can end in totally uncorrelated backscatter between the acquisitions at the so-called critical baseline [8], [18]. Noise caused by decorrelation corrupts the desired signal, and can lead to a false estimate of the desired information (in this case, surface displacement). It becomes apparent by an increase of the standard deviation of the interferometric phase estimates [14], and needs to be minimized.

Two categories of MT-InSAR methodologies have been developed as the standard approaches to overcome the decorrelation issue and to provide a time series analysis of the spatial surface displacement patterns: namely, the PSI and the SBAS techniques. There are several variations in procedures to process them, but the principle behind each category is common to all the individual algorithms, and this principle will be introduced in the following subchapters.

1.4.1 Persistent Scatterer Interferometry

PSI methods focus on the phase change of individual, dominant signal scatterers in time in a set of SAR images [19], [20]. The first algorithm published in 2001 by Ferretti et al. [19] is patented and known as Permanent Scatterer Interferometry™. Several alternative procedures were developed later, e.g. [20]–[22], followed by naming these class of algorithms as Persistent Scatterer Interferometry techniques with the acronym PSI. A permanent/persistent scatterer (PS) is a pixel showing a stable reflector that remains correlated to a certain extent through long periods, and which can be of spatially smaller dimension than the resolution cell [19]. As the signal response of a resolution cell is the sum of several scatterers, a pixel identified as PS must contain a dominant scatterer, whose brightness is stronger than its surrounding scatterers [17]. Therefore, a PS is not a physical characteristic [20], but rather requires a statistical signal distinguishability from its surrounding and from noise in order to retrieve the information of interest (displacement) at this point [17].

The general workflow of the PSI procedure is as follows. First an appropriate master image (reference) needs to be selected, to which all the remaining SAR images (slave scenes) of the acquired data stack are co-registered. The master image selection is essential in that it requires the optimal image from a set of SAR acquisitions that minimizes all the decorrelation related factors: perpendicular baseline, Doppler centroid frequency change, thermal noise, and time [17]. As large temporal baselines, and accordingly temporal decorrelation, can reduce the number of detectable PS [19], the master image is usually selected somehow temporally centered in the period under investigation. Moreover, the number and distribution of the available SAR images in time (preferably uniform without larger gaps) influence the applicability of PSI, in that it increases accuracy with increasing number of scenes.

Second, the interferograms of all master-slave combinations are created by pixel-wise multiplication of the complex signal of one image with the complex conjugate of the other. Later, the interferograms are corrected for topography-related phase contribution. This is achieved first by flattening of the interferogram and second, by subtracting the synthetically calculated topography phase term received from a Digital Elevation or Surface Model (DEM/DSM) [17], which represent the difference of the surface from the reference ellipsoid. If such a model is not available, this phase term can also be computed from an additional SAR image pair from the data stack that is assumed to not to show any displacement during acquisitions.

Then, the resulting differential interferograms are transformed to a geocoded reference frame with a positioning accuracy of several meters [17]. The PS candidates (PSC) are identified and analyzed with respect to their amplitude and phase stability in time to select the final set of PS. The unwanted phase terms contributing to the interferometric phase as the remaining geometric error, atmospheric delays and orbit inaccuracies as well as several minor error sources summarized as noise need to be estimated and removed. Within these steps (amplitude and phase stability analysis, and estimation and removal of unwanted terms), the different available algorithms provide deviating approaches. For example, Ferretti et al. (Ferretti et al., 2001) and Kampes et al. [15] use a predefined temporal model to estimate the displacement phase history for separation from the other contribution, whereas Hooper et al. [17] consider the spatial correlation of the individual phase terms.

A final and crucial step before the computation of displacement time series of the PS is phase unwrapping. This is needed to resolve the ambiguity in the wrapped differential interferometric phase, which is measured as modulo 2π radians. Unwrapping requires phase gradients smaller than π between the neighboring PS, and hence, a sufficient spatial density of PS. There are several

unwrapping algorithms, and they can be classified into 2D (spatial unwrapping)[23] and 3D (spatial and temporal unwrapping), e.g. [24], procedures. Since successful phase unwrapping requires an appropriate spatial sampling of PS, the method works best in urban or rocky regions due to the higher probability of dominant and temporally stable scatterers in these environments. For this reason, PSI seems to be a preferable technique when considering anthropogenic activities related to subsurface processes, especially when they are localized. The prerequisite is that the event is located within a settlement or that artificial objects in conjunction with the anthropogenic activities exist on the surface. If this is not the case, then SBAS is an alternative MT-InSAR surveillance technique that can be used.

1.4.2 Small Baseline Subset

The SBAS procedure was published shortly after the Permanent Scatterer Interferometry™ method as an alternative and complementary technique that does not focus on dominant scatterers, and is therefore also applicable in non-urban areas. In principle, it is the multi-temporal refinement of the classical two image Differential InSAR [25], and is named after the specifications for interferogram generation. Whereas, PSI intends to use all the available SAR images to form interferograms with respect to a single master with the consequence of potentially long spatial and temporal baselines (Fig. 1.2(a)), SBAS is a multiple master approach that aims at minimizing spatial and temporal baselines to reduce signal decorrelation effects. With this approach, an appropriate interferogram network (connected interferogram cluster) is established, which is also able to use all the available SAR data without including image pairs of long baselines (Fig. 1.2(b)). Therefore, this technique is not forced to use the most coherent radar targets with high phase stability over time. Also, moderate coherent pixels are included in the search for an underlying displacement signal. SBAS further deviates from PSI as it applies additional decorrelation reduction by using spectral filtering in range (sensor's look direction) and removal of non-overlapping Doppler frequencies in azimuth (sensor's flight direction) [26].

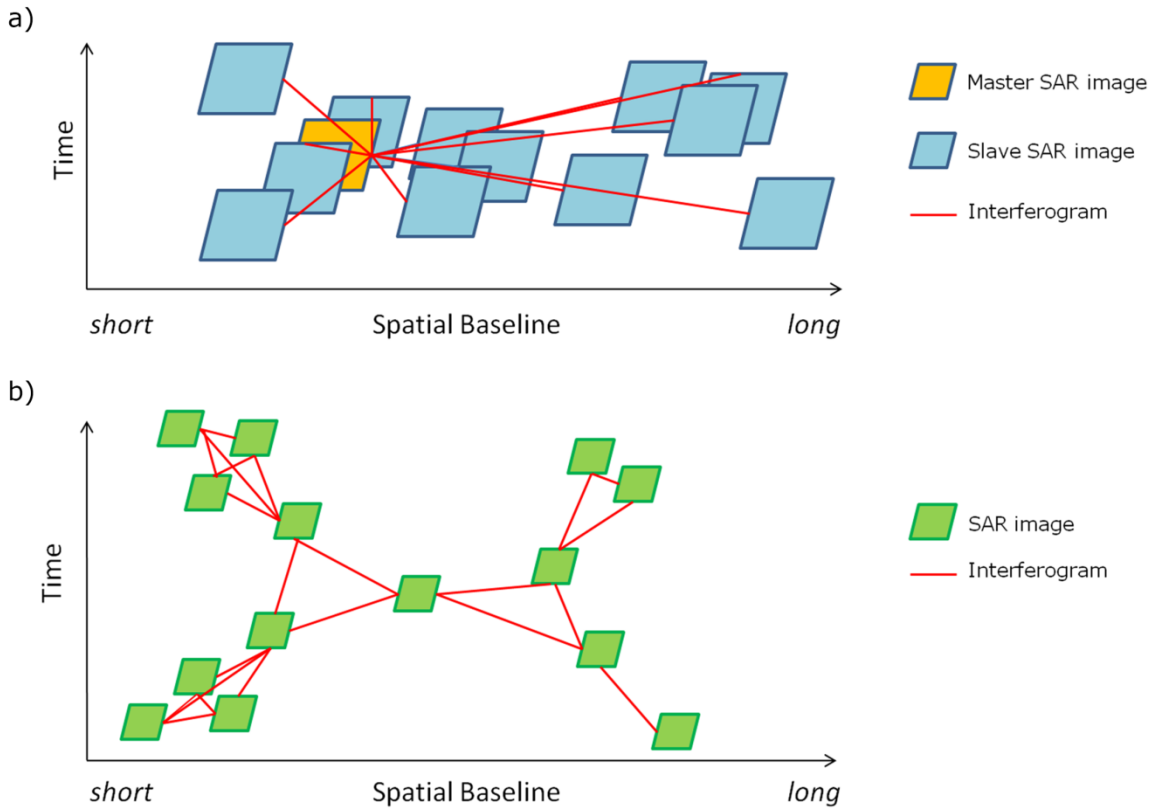

Fig. 1.2: Interferogram formation scheme of a) PSI and b) SBAS [figure by Christin Lubitz].

The initial SBAS algorithms by Berardino et al. [25] use spatially filtered, and hence low-resolution, but less noisy (multi-looked) SAR imagery for identifying atmospheric phase artifacts and analyzing large scale deformation phenomena. Mora et al. [27] refined this by additionally subtracting the detected atmospheric artifacts and deformation (modulo 2π) from single-look (high resolution) interferograms to identify additional localized deformations within the overall deformation pattern. Hooper et al. [28] developed a SBAS procedure that directly works on single-look images with the advantage of detecting isolated pixels within a decorrelating neighborhood as well.
The removal of unwanted contributions to the interferometric phase (topography, atmosphere, orbit inaccuracies, and noise) and phase unwrapping are also necessary for displacement retrieval in SBAS as in PSI.

1.5 InSAR for Usage in Geophysical and Hydromechanical Modeling

As InSAR surface measurements can detect displacements, the question of their source always accompanies the investigation for both natural and anthropogenic-induced phenomena. In detail, this means what can the observed surface displacements indirectly tell about the triggering phenomenon, the kind of process, its extent (dimension), its depth, its duration, bounding and triggering influences, and finally the potential threats. Here, the link between the observation and the arising questions can be an appropriate modeling that can offer geophysical and/or hydromechanical answers.
Theoretical formulations on dislocation theory have been introduced since 1958 [29], with increasing complexity, completeness and generality of source type and geometry as examined and summarized by Okada [30]. The focus lies on the point and the finite fault sources that usually find application in volcano (e.g. Mount Etna [31]) and earthquake source mechanism simulations (e.g. Eureka Valley, California Earthquake of 17 May 1993 [32]). Typically, an isotropic homogeneous half-space and a simple source configuration are assumed for simplicity as the first approximation [30]. The spherical point source by Mogi [33], the arbitrary oriented triaxial ellipsoidal point source by Davis [34], and the arbitrary oriented rectangular opening-mode dislocation by Okada [30] are commonly applied. The aspects that include a more realistic representation of the Earth model, such as the effects due to the Earth's curvature, surface topography, crustal layering, lateral inhomogeneity, and due to oblique layering have been investigated in numerous studies, which are summarized by Okada [30]. They have varying impacts on surface displacement depending on the depth of the source. Actually, there is a trade-off between the depth and the strength of source, additionally influenced by overburden rock mass and its material properties [35]–[38].
If only InSAR data is available, such simple physical models can provide the first statements on the source, and also for anthropogenic deformations, especially when they are related to pressure change. Here, the physical models can be applied in a forward model manner to fit the InSAR results by simulating an interferogram and subtracting it from the measured one for 'trial and error' comparison, or the model parameters can be estimated from the observed data by inversion [31].
Complexity and consequently more accurate and comprehensive knowledge can be gained by including additional data in the models. These can be local geological, stratigraphic, and hydrological maps that provide information on faults, layering, and groundwater levels, respectively, and which can be used to generate a geological model and hydromechanical simulations. Additional active investigations such as seismic measurements, well drilling, and associated campaigns with temperature and pressure logging support the development of precise source models. These aspects are relevant in cases where the occurring displacement is not sudden and unexpected, but rather surveyed as an accompanying phenomenon of a human activity. The simulations based on these other data sources can be computed beforehand or during the activities, and the collected InSAR data can be used for correlation and validation purposes. In particular, fluid related activities, e.g. groundwater extraction, usage of geothermal reservoirs, and injection for CO_2 storage, require a more complex consideration than a single pressure source.

1.6 Introducing the Case Studies

Two case studies, representing geothermal energy supply (Staufen) and geological CO_2 storage (Ketzin), respectively, are considered in this thesis. Their locations within Germany are shown in Fig. 1.3. The following subchapters introduce the two cases.

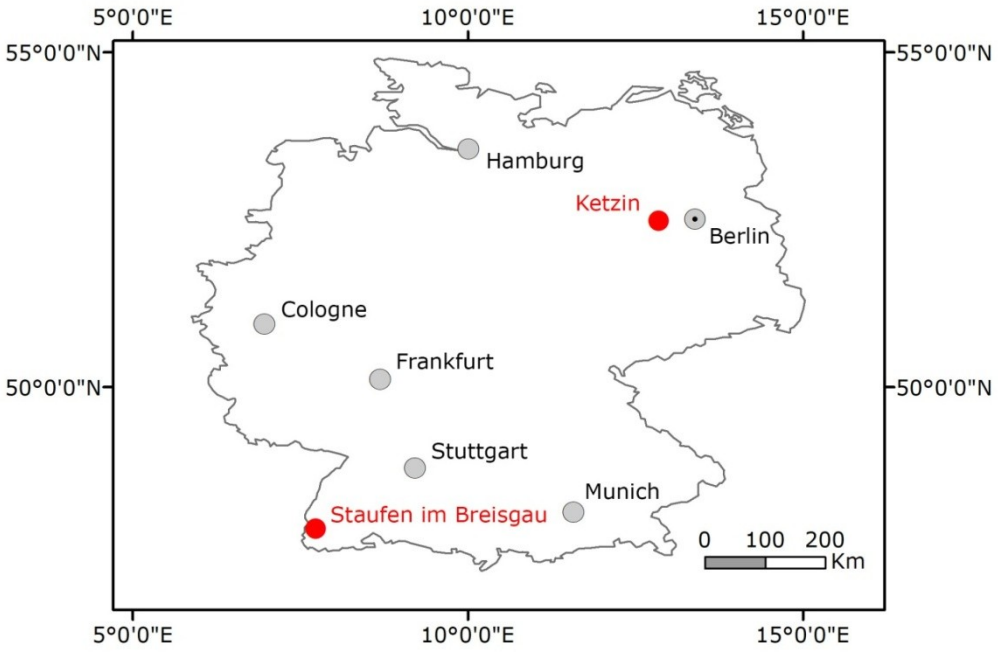

Fig. 1.3: Locations of Staufen and Ketzin in Germany [figure by Christin Lubitz].

1.6.1 Surface Uplift in Conjunction with Shallow Geothermal Energy Project in Staufen im Breisgau

The historical city hall of Staufen was renovated in 2006-2007, and is located at the old city center. There was a desire for shallow geothermal energy for the new heating and cooling management of this building due to environmental considerations and sustainability. The Upper Rhine Graben has the appropriate potential for such an application as the highest temperature gradients in Germany occur there (average gradients of 30 K/km up to anomalies of 110 K/km [39]).
In fact, the geothermal energy project at Staufen has turned into the most prominent case of damage associated with previous geothermal drillings that has also reached international awareness [40]–[42]. Small cracks appeared in 2007, and have since developed into threats of severe damages to nearly 270 buildings. The danger of collapsing finally led to the first building demolition in 2013. Comprehensive investigations on the causes were forced by the financial loss that ran to the range of double-digit millions, lawsuits, the establishment of an arbitration board, and the risk to the reputation of geothermal resource usage. The National Agency for Geology, Resources and Mining (LGRB) has attributed leaking geothermal probes as the initiating event. They triggered water contact with unknown anhydrite deposits (calcium sulfate), followed by their chemical transformation to gypsum, and an associated strong increase in volume. This deformation is visible at the surface as uplift.
Leveling campaigns have been used since January 2008 to discover the spatial extent and the magnitude of the displacement area. As the spatial dimension and the motion rate have turned out to be larger than initially expected, the survey campaigns were intensified with respect to increasing the number of survey points and smaller measurement intervals (up to two weeks). These classical

terrestrial measurements are both labor-intensive and expensive. The satellite-based MT-InSAR techniques are an alternative here, because data acquisition is simplified by the instantaneous mapping of the complete area under consideration at a fixed interval and viewing geometry.
Furthermore, a beneficial microwave scattering behavior can be expected due to the urban setting of Staufen (corner reflection). Depending on the available image resolution, the number of measurement points, and thus, the level of detail can be drastically higher as compared to leveling. Consequently, such MT-InSAR observations can provide a sound basis for source modeling and process interpretation. Moreover, the fixed acquisition interval can be used for monitoring the evolution of the displacement in order to enable the assessment of counter measurements.

1.6.2 Geodetic Surveillance at the Ketzin Pilot Site for Geological CO_2 Storage

The Ketzin pilot site comprises a comprehensive research program with all the phases of geological CO_2 storage: site construction and drilling of the injection and observation wells, the actual operation and monitoring period, as well as the final site closure, including post-injection monitoring and dismantling of the above-ground facilities. The details of the test site are given in Chapter 4.2. This is the first onshore project of its kind in Europe, following the increasing international demand for profound knowledge of safe operations and the associated subsurface processes.
At present, the Global CCS Institute lists 22 large industrial sites in operation or under construction worldwide, onshore and offshore, often coupled with enhanced oil recovery ([43]; overview table can be found in appendix A). The National Energy Technology Laboratory of the USA also names small-scale projects such as the Ketzin pilot site, which also deal with carbon capture or carbon storage only. Thus, it lists 274 CCS projects worldwide (November 2014), of which 128 are actively running [44]. Although current German legislation blocks the use of the CCS technology in Germany, the knowledge gained from it increasingly serves the international community.
The research project at the Ketzin pilot site started in 2004 with CO_2SINK (CO_2 storage by injection into a natural saline aquifer at Ketzin), followed by CO_2Man (CO_2 reservoir management), and CO_2CARE (CO_2 site closure assessment research) from 2010 through 2013, and is currently in the final stage with COMPLETE (CO_2 post-injection monitoring and post-closure at the Ketzin pilot site), ending in 2017. During the period from 30 June 2008 to 29 August 2013, about 67 kt CO_2 were injected underground. The complex monitoring of system integrity aimed at safe storage for man and environment comprises deep- (e.g. surface seismic, gravimetry, well logging, temperature/pressure measurement) and shallow-focused (e.g. atmospheric measurements and surface flux, geochemical sampling, geodetic surface deformation observation)[45] monitoring technologies.
Most of the methods mentioned as examples for both categories were applied at the Ketzin pilot site, but the surface displacement observation was not planned as it was not expected. The reason for this is that a small overall injection volume of maximum 100 kt CO_2 was approved, and it was not suspected to cause any displacement on the ground surface. Neither Differential Global Positioning Systems nor tiltmeters were installed at the Ketzin pilot site for the surveillance of potential surface displacement. As InSAR has developed into a widely used geodetic technique, its capacity for an adequate spatial and temporal mapping of the assumed surface stability at Ketzin shall be investigated. Here, the focus lies on the limitations and challenges of MT-InSAR, because Ketzin is located on agricultural land and experiences strong seasonal variations in vegetation growth and weather. Nevertheless, it is important to evaluate the operational capability of InSAR in non-ideal environments also because this field of application is not restricted to a certain above-ground situation, but rather to subsurface conditions. Due to the increasing global importance of CCS and carbon storage, the conclusions made from this case study shall support the prior assessment of MT-InSAR as a regularly applied shallow-focused monitoring technique.

2. Chapter: Remarkable Urban Uplift in Staufen im Breisgau, Germany: Observations from TerraSAR-X InSAR and Leveling from 2008-2011 (published: Remote Sens., 2013, *5*, 3082-3100; doi:10.3390/rs5063082)

Christin Lubitz *, Mahdi Motagh, Hans-Ulrich Wetzel and Hermann Kaufmann

GFZ German Research Centre for Geosciences, Section 1.4, Telegrafenberg, D-14473 Potsdam, Germany; E-Mails: chlubitz@gfz-potsdam.de (C.L.); mahdi.motagh@gfz-potsdam.de (M.M.); wetz@gfz-potsdam.de (H.W.); charly@gfz-potsdam.de (H.K.)

***** Author to whom correspondence should be addressed; E-Mail: chlubitz@gfz-potsdam.de; Tel.: +49-331-288-28621; Fax: +49-331-288-1192.

Received: 24 April 2013; in revised form: 31 May 2013 / Accepted: 4 June 2013 / Published: 20 June 2013

Abstract

As geothermal energy is of increasing importance as a renewable energy source, there is a high demand for comprehensive studies to prevent failure during implementation, as is the case in Staufen im Breisgau, Germany. The drilling of seven wells for the geothermal heating of the city hall in 2007 is thought to have disturbed the existing hydro-geological system in the complex structured transition zone of the Upper Rhine Graben and the Schwarzwald massif. This event has led to uplift, related to the transformation of anhydrite to gypsum, which affects the infrastructure of the city centre via the generation of large cracks. This study focuses on the application of the InSAR Small Baseline Subset (SBAS) approach using 50 X-band radar images from the German TerraSAR-X satellite (TSX) to map the spatial and temporal patterns of the deformation field in detail. X-band InSAR time series analysis for the three-year time period from July 2008 through May 2011 indicates maximum velocities of ~12 cm/yr in the line of sight (LOS) direction, from the ground to the satellite, approximately 50 m northeast of the drilling field. In comparison with leveling data for the same time period, TSX data analysis better delineates the border of the deformation area, and it is able to map the amount of deformation associated with different parts of the city. Moreover, this comparison indicates contributions of horizontal motion, as is expected for uplift patterns.

Keywords: InSAR; SBAS; geothermal drilling; uplift, Staufen im Breisgau

2.1 Introduction

Staufen im Breisgau (hereafter referred to as Staufen) is a small city in southwestern Germany, approximately 50 km north of Basel and 120 km south of Karlsruhe (Fig. 2.1). It is located at the eastern transition zone of the Upper Rhine Graben to the Schwarzwald massif, and their interaction controls the regional hydrology and geology [1]. A system of numerous faults has created a complex mosaic of blocks with varying strata sequences. Figure 2.1 shows the regional lineaments [2,3].

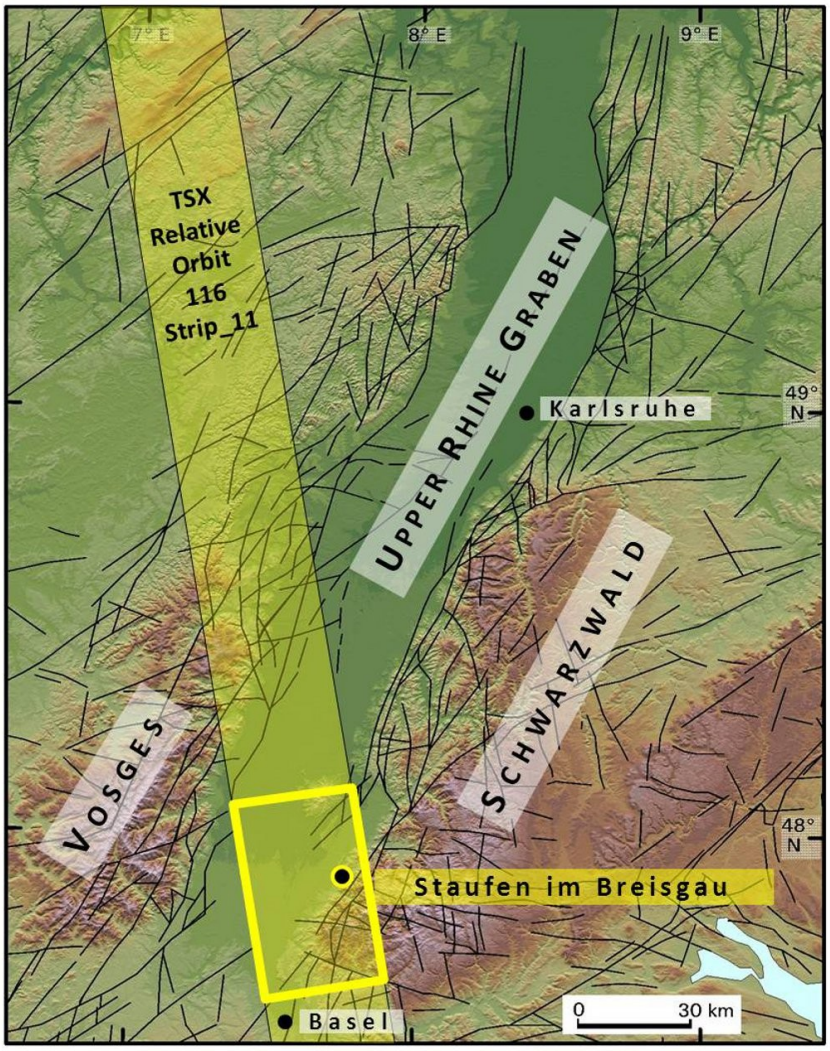

Fig. 2.1: Location of the city of Staufen and the regional lineaments. The Background Digital Elevation Model (DEM) is based on data from the Shuttle Radar Topography Mission (SRTM). The orbit path of the TerraSAR-X satellite (TSX) is shown, and the yellow frame indicates the boundaries of the Spaceborne Synthetic Aperture Radar (SAR) images acquired for this study.

As part of the renovation of the historical city hall of Staufen and its neighboring building in 2006–2007, renewable shallow geothermal energy was selected as the new heating source. The region of the Upper Rhine Graben has a high potential for this technology due to its high subsurface temperature gradients [4]. Borehole drilling to a depth of 140 m was permitted in Staufen after an assessment of the geological and hydrological conditions. In September 2007, seven boreholes for geothermal double-U-tube probes were drilled, adjacent to the city hall, up to the permitted depth of 140 m [5]. Their locations are presented in Fig. 2.2(a). At the end of the year, hairline cracks appeared in the city hall and in other neighboring buildings. The cracks (Fig. 2.2(b)) increased rapidly in size and number. As of November 2011, 262 private buildings and seven public buildings have shown severe damage [6].

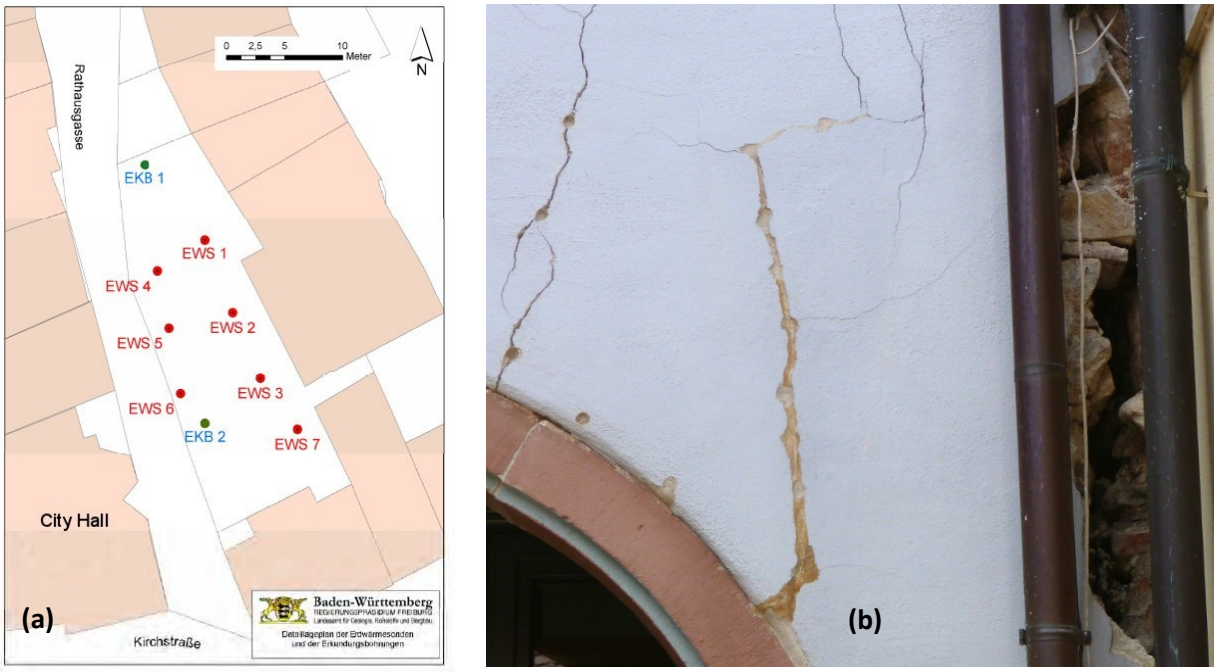

Fig. 2.2: (a) Location of the seven heat exchanger boreholes (red) and the two exploration wells (blue) next to the city hall sketched on an orthophoto (acquired by the State Survey Office of Baden-Württemberg). (b) One of the affected buildings in Staufen with large cracks (picture by C. Lubitz, 23 August 2012).

The deformation has been attributed to uplift that is caused by the disturbance of the existing subsurface hydro-geological system below the historical city centre. This disturbance is thought to have been triggered by the drilling, which most likely created connections between different groundwater horizons, above and below the strata of Keuper, and deposited anhydrite lenses. The mineral anhydrite (calcium sulphate) transforms into gypsum through contact with water and leads to a subsurface volume increase. As the drilling project has led to severe damage of buildings and some urban infrastructures, the project has since been stopped.

Deformation rates of up to 1 cm/month [5,7] were measured by conventional leveling surveys from February 2008 through February 2009. They have been carried out at regular intervals since January 2008, shortly after the first hairline cracks appeared, to map the spatial extent and magnitude of the surface deformation. Gradually, the number of survey points was increased to better capture the displacement field. The locations of the points are presented in Fig. 2.3, color-coded by the date of their first measurement to show the expansion of the survey network. Between March 2009 and May 2010, the survey interval was decreased to two weeks for a subset of points located in the uplift centre and marked with black dots in Fig. 2.3.

Although highly accurate, conventional leveling surveys are a time-consuming, labor-intensive, and expensive technique of providing adequately dense mapping of the spatio-temporal pattern of surface deformation. Spaceborne Synthetic Aperture Radar (SAR) sensors allow high-resolution monitoring of the earth's surface at regular intervals and over large areas. The revisit time of the German TerraSAR-X (TSX) satellite for a single location, and with the same viewing geometry, is 11 days, and the spatial coverage of images recorded in Stripmap mode (resolution of approximately 3 m), which are used in this study, is approximately 30 km in range and 50 km in azimuth.

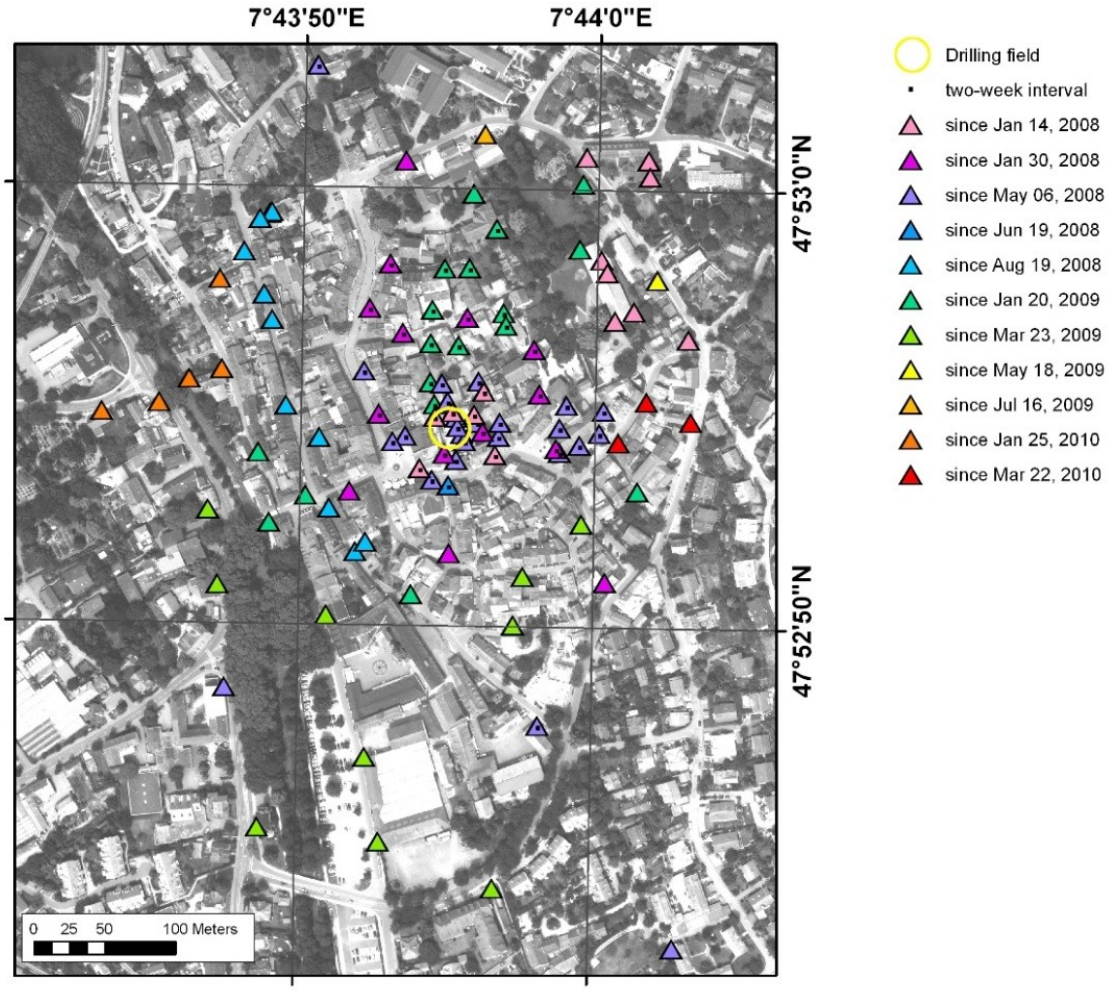

Fig. 2.3: Location of the leveling survey points (provided by Landratsamt Breisgau Hochschwarzwald, office Müllheim) plotted on an orthophoto of Staufen (acquired by the State Survey Office of Baden-Württemberg). The expansion of the network is color-coded. The points at which measurements are repeated every two weeks are marked with a black dot in their centre. The drilling field is indicated by a yellow circle.

By applying time series methods of SAR Interferometry (InSAR), in particular, the Persistent Scatterer Interferometry (PSI) or the Small Baseline Subset (SBAS) approach, surface displacements at centimeter- to millimeter-level accuracies can be measured over time [8–11]. Both methods have shown their applicability in different fields of natural hazards and anthropogenically induced events [12–15]. The first InSAR-based observations of ground uplift in Staufen [16] are based on the analysis of nine TSX Stripmap images from July 2008 through January 2009 using differential repeat-pass interferometry. Further monitoring of the deformation field is essential for a better understanding of the on-going subsurface processes, in particular to determine if the rates of motion vary, and is helpful for the evaluation of counter measures. Hence, in this study, we present the result of the SBAS time series analysis of 50 TSX images acquired over Staufen from July 2008 to May 2011. Comparison with data from leveling surveys for the same period allows the evaluation of this multi-temporal InSAR method. We are also interested in what additional information the remotely sensed deformation data contain with respect to the leveling surveys.

This paper is organized as follows. Section two provides information about the available SAR data. The details of the SBAS methodology as implemented in the StaMPS software [17] are introduced in section three. Section four presents the results of the time series processing. In section five, we compare the SBAS product with the leveling data, consider the aspects of horizontal motion and discuss the result with respect to the geological system and against the background of the subsurface processes. The conclusion and summary are given in section 2.6.

2.2 Data

For our study, data from the German TSX satellite over a time period of almost three years—from 22 July 2008 through 22 May 2011—are available. The SAR images were acquired in Stripmap mode in an ascending orbit path direction (relative orbit 116, beam strip_011) with HH polarisation. The orbit path and image frame are schematically shown in Fig. 2.1. The incidence angle ranges from 37.9° in the near range to 40.6° in the far range within the SAR image. The ground resolution is approximately 2.8 m in the range direction and approximately 3.3 m in the azimuth direction. In total, 53 TSX-images were acquired. Three images of the data stack, namely those from 12 January 2010, 14 February 2010 and 27 November 2010, display snow coverage leading to strong decorrelation for interferometric processing with respect to the other images. Hence, only the remaining 50 images were used for data processing.
A timeline of the SAR image acquisitions and leveling surveys is presented in Fig. 2.4. It shows a high temporal sampling, in particular between March 2009 and June 2010, for both datasets with approximately similar periodicity: 11 days for the spaceborne data *versus* 14 days for the terrestrial recordings. This sampling allows the development of deformation over time to be resolved in detail and our remote sensing result to be compared with the terrestrial measurements.

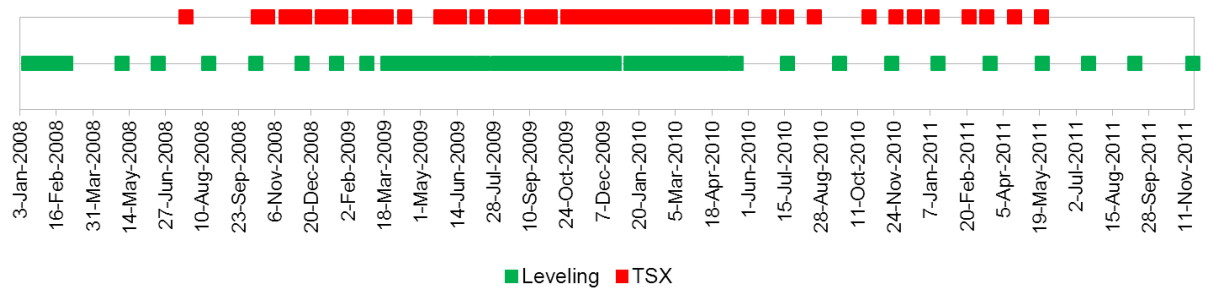

Fig. 2.4: Timeline of the leveling surveys and the available TerraSAR-X satellite (TSX) acquisitions.

2.3 Methodology

Classical repeat-pass SAR interferometry is a suitable tool for detecting surface displacement and monitoring coherent areas [18–21]. Interferometric coherence is a pixel-based measure of the signal similarity between two SAR images and ranges from 0 (total decorrelation) to 1 (total correlation). Temporal signal decorrelation is the limiting factor for InSAR, particularly in rural and vegetated areas due to the progressive change of the scattering properties [22] caused by vegetation growth, erosion, or harvesting. The InSAR time series methods of PSI and SBAS overcome this limitation. PSI focuses on identifying only coherent pixels dominated by a single scatterer mechanism that are imaged in every recorded SAR scene, while SBAS identifies those pixels showing only slow decorrelation over short time intervals [17]. Both techniques work better in urban areas because man-made objects, which often cause high-energy signal echoes, are highly coherent in time.
Due to strong uplift at a rate of several cm/yr in Staufen (inferred preliminary from leveling measurements), we applied the SBAS method as implemented in the StaMPS/MTI (Stanford Method for Persistent Scatterer/Multi-Temporal InSAR) software for the time series analysis. The SBAS approach refers to a network of individual differential interferograms (multi-master) that take into account minimized temporal, perpendicular and Doppler baselines to minimize decorrelation effects. In terms of high displacement rates, using multi-master interferograms with short temporal baselines reduces the number of phase difference ambiguities to be resolved, potentially allowing a more reliable phase unwrapping than the single-master PSI technique without a priori temporal model phase unwrapping.

Figure 2.5 shows the network of the small baseline interferograms used for the SBAS analysis of surface deformation in Staufen. The interferograms were computed from TSX single-look complex (SLC) images by using DORIS (Delft object oriented radar interferometric software [23]). Prior focusing was not necessary, as the TSX data are delivered in SLC format. Initially, 289 interferograms were processed, but only 249 interferograms were used in the SBAS-processing due to the removal of the three SAR images with strong snow cover.

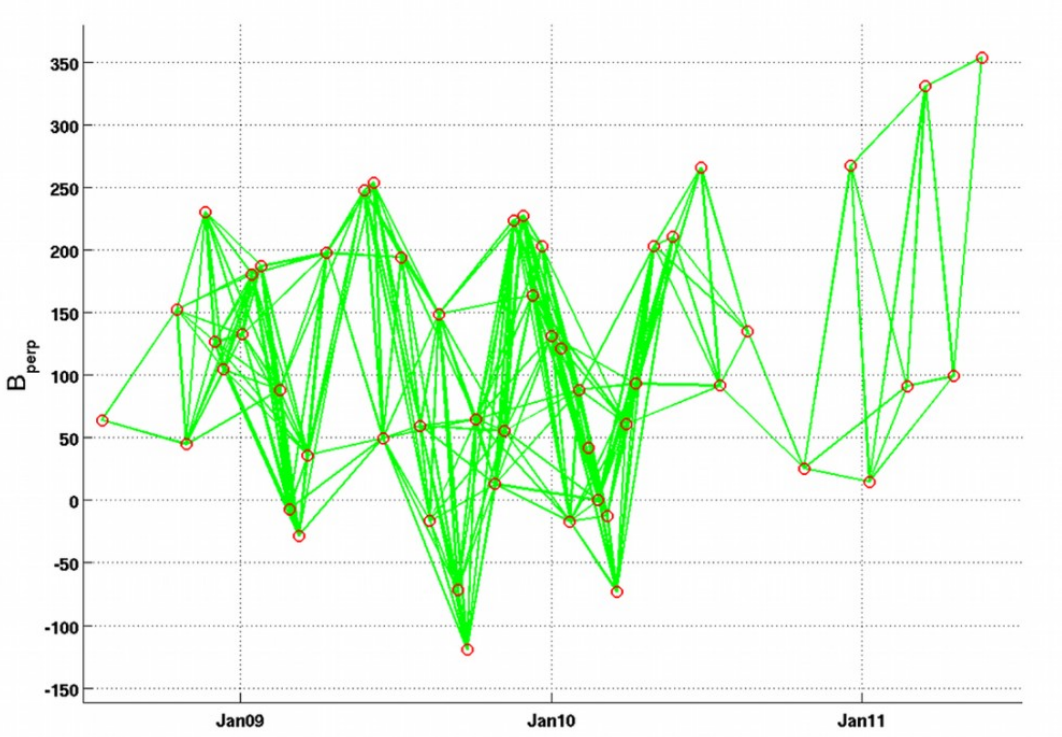

Fig. 2.5: The network of the individual Small Baseline Subset (SBAS) interferograms for the TSX dataset for Staufen. The red circles represent the images and the green lines the pairs from which interferograms were generated. The vertical axis is the perpendicular baseline in meters.

As differential interferograms are required for displacement analysis, we removed the topographic information from the interferometric phase by transforming a Digital Elevation Model (DEM) into phase values and subtracting it from the interferograms. We used a high-resolution LiDAR DEM with 1 m resolution (provided by the State Survey Office of Baden-Württemberg) for the topographic phase correction and geocoding of interferograms.
In the SBAS implementation of StaMPS/MTI, time series analysis is only conducted for those pixels for which the phase, after filtering of the azimuth and range spectra, shows slow decorrelation over short time intervals, the so-called slowly decorrelating filtered phase (SDFP) pixels [17]. The previous filtering aims to reduce decorrelation effects due to geometry and non-overlapping Doppler frequencies. A computational cost-effective initial selection of the SDFP candidates was performed at the highest resolution (single-look image) by setting a threshold (0.6) for the amplitude difference dispersion, which is the standard deviation of the amplitude difference between the master and slave divided by the mean amplitude. Afterwards, an iteratively conducted phase analysis yielded the phase stability estimation of each candidate. In the StaMPS algorithm, after the removal of topography and earth flatting, spatial correlation was assumed for the differential interferometric phase residuals of SDFP pixels related to deformation of the earth's surface, the spatially correlated height error, the atmospheric delay, and orbit inaccuracies. These contributions were estimated by the bandpass filtering of surrounding pixels. The statistical analysis of the spatially correlated terms, the spatially uncorrelated (look-angle error) terms, and the amplitude difference dispersion were used for the final SDFP pixel selection. This method estimates displacement time series without prior

consideration of a temporal model for the deformation and thus allows the derivation of temporally varying deformation processes.
Three-dimensional phase unwrapping was applied on the final sets of SDFP pixels by using a statistical cost flow algorithm that works for both single-master (PSI) and multi-master (SBAS) methods [24]. The time series of displacement for each SDFP pixel was derived by least-squares inversion. The reader is referred to [17] and [24–26] for further details on the SBAS algorithm, the unwrapping method, and StaMPS in general.

2.4 Results

The multi-temporal SBAS processing of the available TSX dataset reveals a clear NE-SW elliptical-shaped deformation pattern, as presented in Fig. 2.6. As the motion is towards the satellite, it is specified as uplift. Figure 2.6 shows the cumulative uplift on 22 May 2011, after three years of SAR observation. The displacement field extends approximately 290 m NE-SW and approximately 190 m NW-SE. A large part of the deformation field has risen more than 25 cm (dark blue to violet) in the line of sight (LOS), and the maximum three-year cumulative uplift of 33.5 cm is located approximately 50 m northeast of the drilling field.
The temporal evolution of the uplift at three-month intervals is illustrated in Fig. 2.7, which apparently shows a smooth increase in uplift over time. However, a closer look at the differences in deformation at the selected dates (Figure 2.8) reveals that with time, the uplift rate decreased since autumn/winter 2009. For example, comparing the uplift rates of a SDFP pixel located within the main deformation area (47.882313°N, 7.732191°E) for the same season in different years, we observe a decrease by 43 %; 4.12 cm between 29 October 2008 and 25 January 25 2009, compared to 2.35 cm between 27 October 2009 and 23 January 2010.

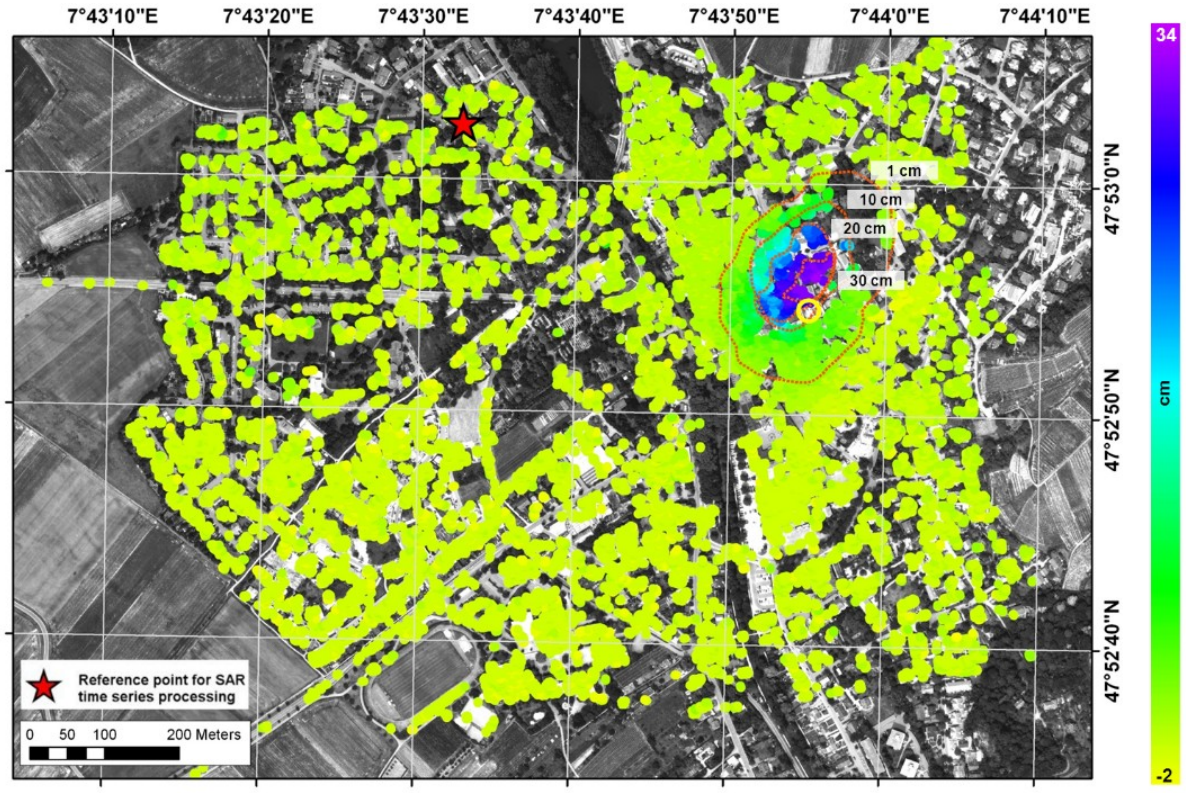

Fig. 2.6: SBAS-derived cumulative line of sight (LOS) displacement in cm from 22 July 2008 through 22 May 2011. The yellow circle indicates the drilling area and the red star represents the reference point for the LOS motion. The displacement boundaries of 1 cm, 10 cm, 20 cm, and 30 cm are highlighted.

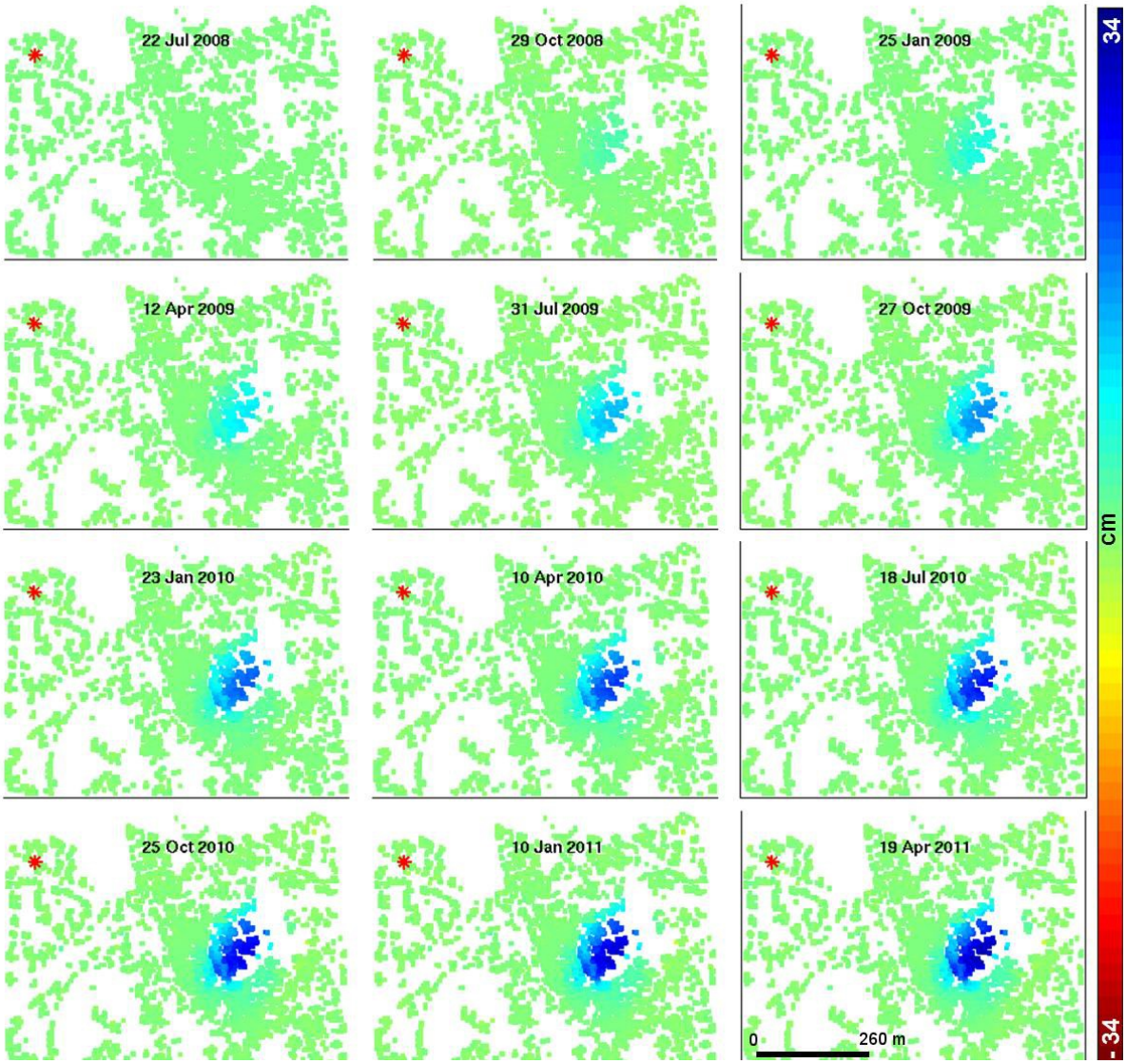

Fig. 2.7: Time series of the LOS displacement in Staufen. For simplicity, the uplift patterns of only 12 of 50 acquisition dates are shown.

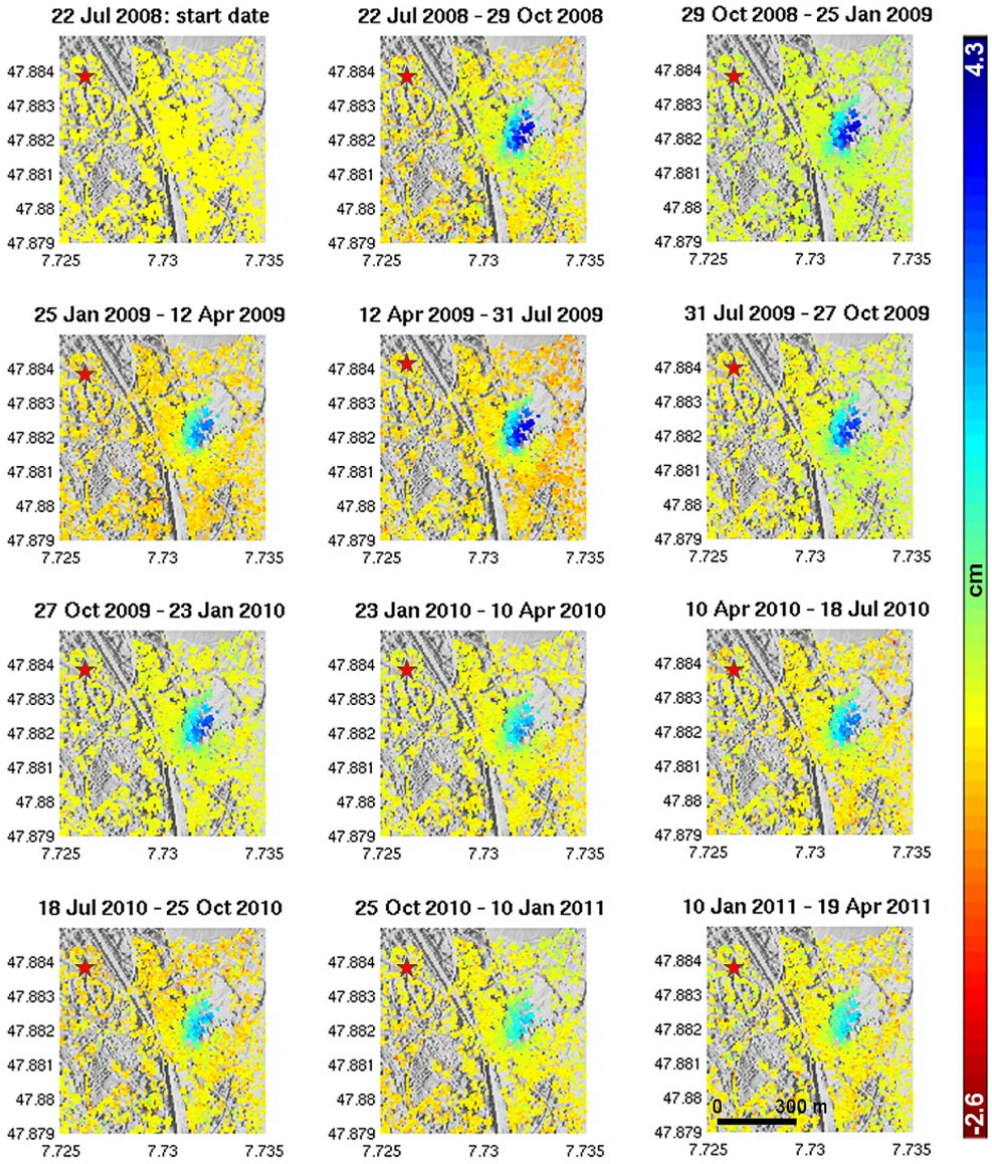

Fig. 2.8: Deformation differences (in cm) of the uplift field between the acquisition dates selected in Fig. 2.7.

2.5 Discussion

2.5.1 Leveling and InSAR Comparison

To evaluate the result of the TSX SBAS processing of Staufen, we compare it with leveling measurements that cover approximately the same period as the SAR imagery (Fig. 2.4). The cumulative vertical motion, measured from 19 August 2008 through 23 May 2011, of each survey point (triangles) is overlaid on the SBAS result (circles) in Fig. 2.9 and shown in the same color scale as the LOS displacement of the SDFP pixels. In comparison, the SBAS method represents the surface displacement at a higher level of detail due to the higher density of pixels in the InSAR analysis. Dense point clouds are an advantage of InSAR time series methods, especially if applied to urban areas. Man-made objects usually guarantee a high coherence over time. For vegetated areas, as in the upper right corner of Fig. 2.9, no SDFP pixels were found, demonstrating the decorrelation-

related limitation of the method. Although not yet performed, leveling surveys could fill such gaps and provide a complementary analysis to the InSAR and existing leveling data.
The boundary of the SBAS-derived uplift ellipse agrees well with the leveling measurements, as well as the amount of displacement of points at the border. Differences on the order of several centimeters occur in the inner part of the displacement area. To determine the cause of deformation differences, the displacement time series of several survey points (red square in Fig. 2.9) was compared with that of nearby SDFP pixels, which were intentionally selected from different parts of the deformation field. The selected points are labeled with letters (A-I) from west to east for simplicity, but for reconstruction purposes, the reader is referred to the official survey point IDs provided on the left side of Fig. 2.9.

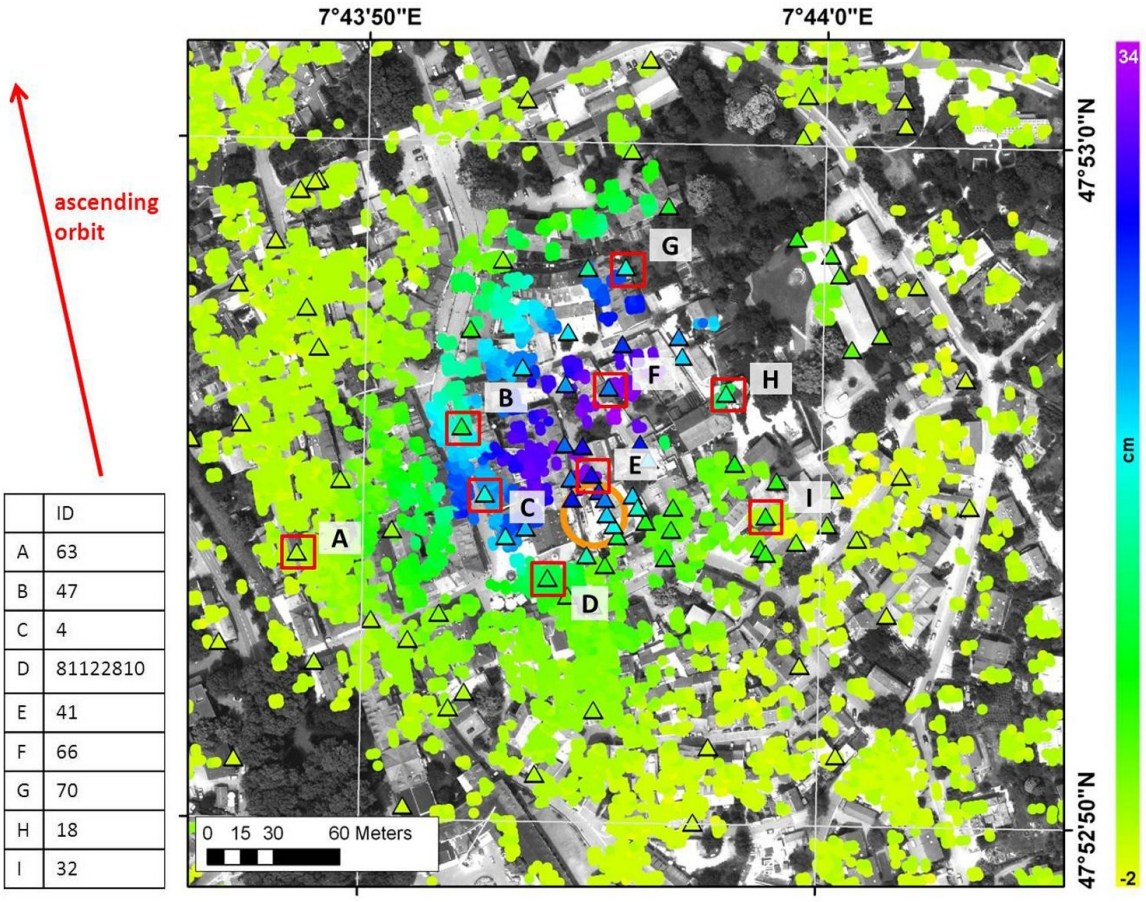

	ID
A	63
B	47
C	4
D	81122810
E	41
F	66
G	70
H	18
I	32

Fig. 2.9: The cumulative LOS uplift pattern based on the SBAS processing (22 July 2008–22 May 2011) and the vertical cumulative motion of the leveling survey points (19 August 2008–23 May 2011). The SDFP pixels are indicated by circles and the leveling survey points are indicated by triangles. The points selected for the time series investigation (Fig. 2.10) are highlighted with a red outline and labeled with a capital letter for easier connection with Fig. 2.10. The official survey point IDs are given on the left side of the figure for reconstruction purposes. An orange circle marks the drilling area.

The time series plotted in Fig. 2.10 show approximately uniform (linear) motion for both leveling and InSAR measurements, but the displacement rate decreases slightly over time, which generally coincides with the areal results presented in Fig. 2.8. The leveling points and SDFP pixels in Fig. 2.10 are marked with triangles and circles, respectively. Corresponding points are presented in the same color. As leveling and InSAR data acquisitions began on different dates, the time series have been adjusted to the same start date via linear interpolation. The time series start on 22 July 2008 (first TSX image), but the data for some points are shown only from 20 January 2009 due to the gradually increasing number of leveling marks.

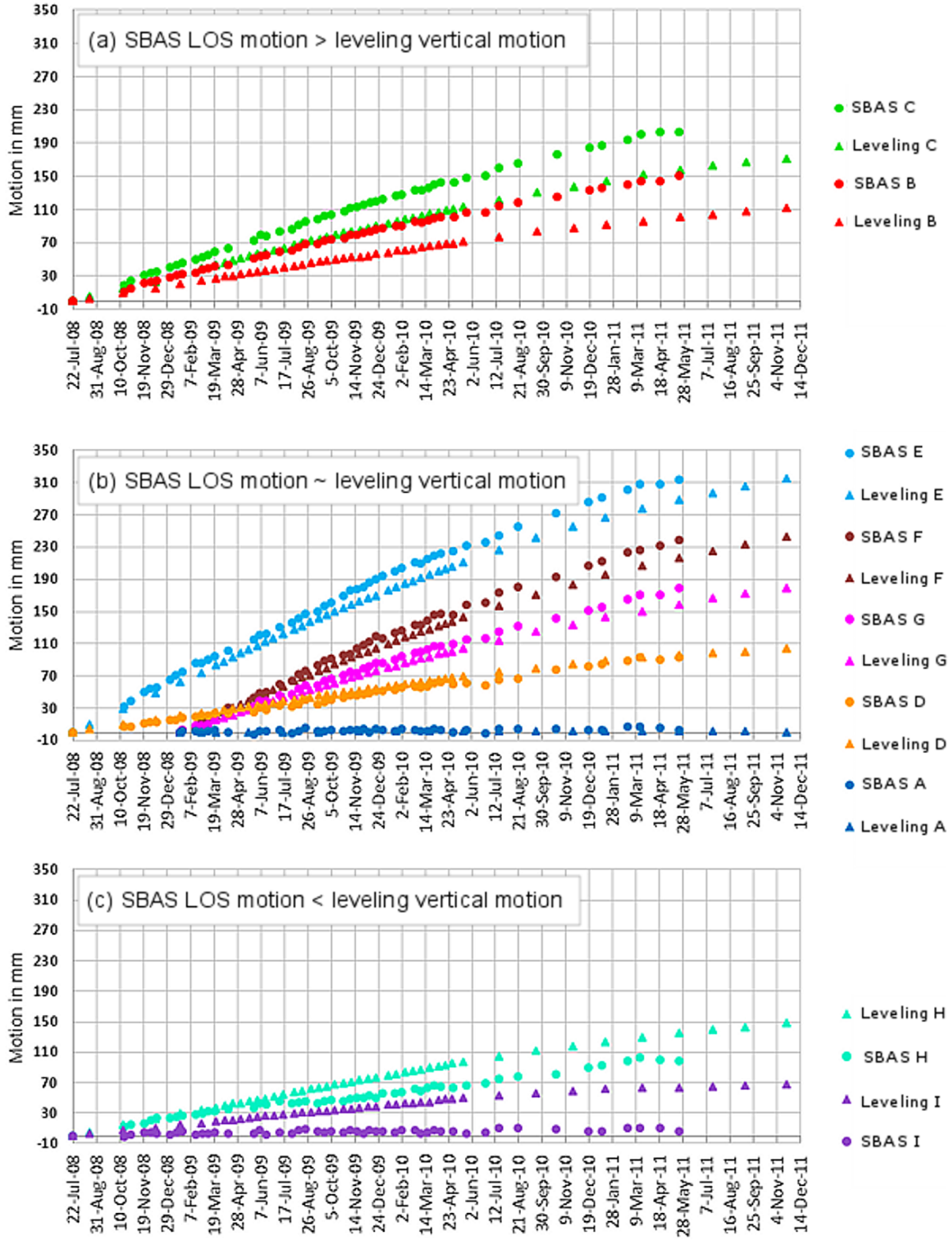

Fig. 2.10: Time series of the vertical motion of selected leveling points (Fig. 2.9) and the LOS displacement of SBAS SDFP pixels, which are located in their immediate vicinity. Corresponding points are in the same color. The separation into the three subfigures is due to the classification of three specific groups as indicated in the upper left corner of each diagram and described in the text (see Section 2.5.1).

As shown in Fig. 2.10, the selected points show different amounts of uplift depending on their location. Leveling point A and the corresponding selected SDFP pixel (SBAS A) are located at the border of the deformation field (Fig. 2.9), at which both types of measurements coincide

(Fig. 2.10(b)). Among the selected point pairs, pair E presents the largest cumulative uplift of 28.8 cm (leveling) and 31.2 cm (SBAS). This point pair is located north of, but close to, the drilling field. For all other points, the general trend is similar for both leveling and SBAS-derived time series, but the time series show discrepancies in magnitude between leveling and InSAR. According to those differences, Figure 2.10 is divided into three sub-charts: (a) shows the time series of points with larger SBAS values than leveling values, (b) gives those with small discrepancies between InSAR values and leveling values and (c) presents those with larger leveling values than SBAS values.

2.5.2 Implications of Horizontal Motion

The discrepancy between InSAR and leveling points, as depicted in Fig. 2.10, can be attributed to the contribution of horizontal displacement. Figure 2.11 provides a simplified scheme to visualize the "positive" or "negative" contribution of horizontal motion to the overall LOS displacement.

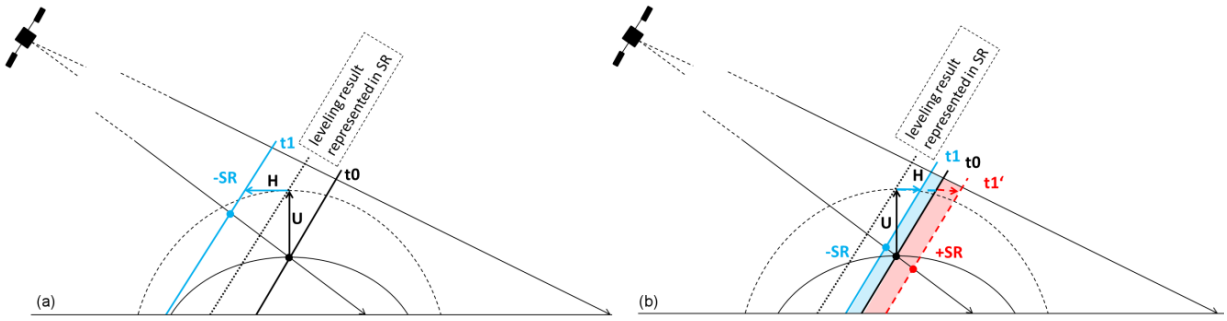

Fig. 2.11: Schematic sketch of the horizontal contribution to the overall LOS displacement. (a) When points move toward the satellite during the time interval from t0 to t1, uplift (U), and horizontal (H) components contribute in the same manner to the LOS motion (slant range decreases (-SR)). (b) When points move away from the satellite, the horizontal and uplift components have opposing impacts on the LOS motion. Depending on the magnitude of the horizontal motion, this effect can result in an increase of slant range (+SR) with respect to the state at t0.

In the case of horizontal motion toward the satellite, its contribution is added to the vertical motion (uplift), resulting in a LOS displacement of higher magnitude than measured by leveling (Fig. 2.11(a) and time series in Fig. 2.10(a)). All point pairs showing this type of difference in their time series are suggested to also experience horizontal motion towards the west. Point pairs showing no discrepancy in magnitude likely represent only vertical motion. The opposite case of Fig. 2.10(a) is shown in Fig. 2.10(c), where leveling measurements of selected points show larger magnitudes of motion than those based on SBAS. In the case of horizontal motion away from the ascending satellite (here, toward the northeast), the uplift and horizontal components have opposing impacts on the LOS motion (Fig. 2.11(b)). This results in a reduced LOS displacement compared to the leveling value. Depending on the incidence angle, the magnitude of uplift, and the magnitude and direction of horizontal motion, this effect can theoretically lead to an increase in slant range (see Fig. 2.11(b), t1 versus t1') and can be misleadingly interpreted as subsidence. Hence, a displacement field interpretation of a one-dimensional LOS result is limited, and ascending and descending data for the same period are required. Work is currently underway to precisely assess the amount of horizontal deformation in Staufen using ground- and satellite-based geodetic measurements [28,29].

2.5.3 Geological Considerations

The region surrounding the Upper Rhine Graben is a complex structured system of blocks and faults dominated by the extensional tectonics of the Upper Rhine Graben and its interaction with the Schwarzwald massif. The main fracture zones attributed to the Upper Rhine Graben strike NE-SW,

whereas those of the Schwarzwald crystalline primarily strike E-W or NW-SE (Fig. 2.1). The subsurface beneath the city centre of Staufen reflects this typical fault formation of the transition zone. Several horst and graben blocks are oriented NE-SW and are cross-bordered by faults striking NW-SE [5].
Potential natural causes for the uplift in Staufen are unlikely, not only due to the strong temporal and spatial correlation of the deformation field with the drilling activities but also due to a lack of evidence pointing to other causes. No earthquakes have been recorded in this particular period [5].
Different exploration activities have been performed by the National Agency for Geology, Resources and Mining (LGRB) to obtain information about surface and subsurface geological structures and to achieve a detailed understanding of the processes that have led to the observed surface deformation. These activities include analysis of samples from boreholes EWS 1, EWS 2, and EWS 3 (Fig. 2.2(a)), geological exploration by the drilling of wells EKB 1 and EKB 2 (location shown in Fig. 2.2(a) in blue), two-dimensional seismic surveys along five profiles in 2009, and temperature profiling in all seven wells. Based on the geophysical measurements (seismic surveys) and drilling samples, the locations of faults were identified and several blocks were characterized [5].
According to the LGRB investigations, the drilling area is located on a graben block, and the core sample analysis revealed the typical stratigraphic sequence of the region: upper Muschelkalk, lower Keuper, middle Keuper (Schilfsandstein and Keuper-Gypsum), and quaternary sediments. Anhydrite (calcium sulphate) and swellable clay minerals (mainly corrensite) were found in the non-lixiviated Keuper-Gypsum layer of the middle Keuper. Four hydraulically disconnected groundwater levels were also discovered in the graben block in which the drilling was performed. All boreholes dip to the southeast, and several of them cross faults that separate the graben block into smaller pieces [5]. Borehole EWS 7 reaches the hydraulically separated groundwater aquifer of the lower Keuper. During the drilling in September 2007, artesian groundwater was reported. It is suggested that water found a path through the insufficiently sealed annular space of one or more boreholes to anhydrite lenses. Temperature anomalies were detected in all boreholes except EWS 1 (maximum of 0.7 °C in EWS 7 between 12 February 2009 and 17 October 2009), which may indicate anhydrite swelling due to the exothermic character of the transformation into gypsum. This chemical transformation is accompanied by a volume increase that could theoretically reach 60%, if there is sufficient water [30]. Due to the pressure change, new cracks may occur into all directions within the Keuper-Gypsum, potentially forming additional paths for water to travel to other anhydrite lenses. The swelling is located between 61 m and 99 m depth [5], where the overlying rock mass is too small to hamper the swelling [16]. As the quantities and distribution of anhydrite and groundwater influx are unknown, the complex spatio-temporal evolution of subsurface processes cannot be described in detail. Nevertheless, the observed uplift at the surface can be considered an effect of the described chemical reactions.
The existing geological and hydro-geological system may have an influence on the spatial pattern of the uplift in Staufen [31,32]. The localized elliptical shape of the deformation field is oriented NE-SW (Fig. 2.6), and thus a significant structural control by the Upper Rhine Graben related horst- and graben-blocks can be assumed. In Fig. 2.12(a), the SBAS-derived cumulative uplift pattern from 22 May 2011 is overlaid with the geological structures derived from the geophysical explorations of the LGRB and from the 1:25,000 geological map to investigate potential spatial correlations. To better assess the deformation field with respect to the geology, we extracted two profiles across the area of uplift: profile A (NW-SE) and profile B (NE-SW). As observed in Fig. 2.12(b) and 2.12(c), both profiles show convex-downward curvature as they reach their area of maximum uplift. For Profile B, no measurement points are available in the vegetated area in the northeast, which reduces the mapping of deformation there.
As shown in Fig. 2.12(a,b), the southeastern boundary of the deformation field seems to be controlled by one of the NE-SW striking faults, which are derived from geophysical measurements of the LGRB. Due to the limitation of temporal decorrelation in vegetated areas, the InSAR data do not provide enough information on the northeastern part of the deformation area (Fig. 2.12 (a,c)). Hence, the possible bounding of the uplift field on its eastern edge by the assumed “Roter-Berg” Fault, which strikes NW-SE, cannot be confirmed nor excluded by the existing data. Leveling measurements from a dense network of survey points in this area could fill such a data gap and would show the complementary benefit of the two measurement techniques. The current

geophysical knowledge is not sufficient to explain the spatial limit of the deformation field to the north and west as detected by applying InSAR. Evidence for bounding faults are not yet obtained, but cannot be excluded from the considerations.
Counter measures against the on-going subsurface swelling have been applied, namely the backfilling of the wells since November 2009 and the pumping of water since September 2009 to reduce the water inflow to the swellable strata [33]. Exploration well EKB 2 is used for this purpose, with a constant pumping rate of 1.9 L/s. Since March 2011, this has been supported by an additional well southeast of the drilling field that pumps at a rate of 2.6 L/s [28]. Figure 2.8 and both the SBAS and leveling time series provided in Fig. 2.10 show a deceleration of uplift that can likely be attributed to these remediation activities. Another possible scenario, as described by [34], may be the natural evolution of the geochemical process of transforming anhydrite to gypsum, which can stop under certain external conditions (depending on the temperature and salinity of groundwater and the stiffness of the surrounding rock mass). Although theoretically possible, this scenario cannot be evaluated because the amount of anhydrite, gypsum, and water that has entered the system is unknown. An estimation of the time until complete transformation, the total volume change, and hence the final amount of uplift is not possible. Alternatively, a reduced rate of anhydrite transformation due to the isolation of anhydrite from water by the recently created gypsum crust, which acts as low-permeability barrier [37], could explain the deceleration of observed uplift in Fig. 2.8 and the time series in Fig. 2.10. However, the effectiveness of counter measures does seem reasonable.

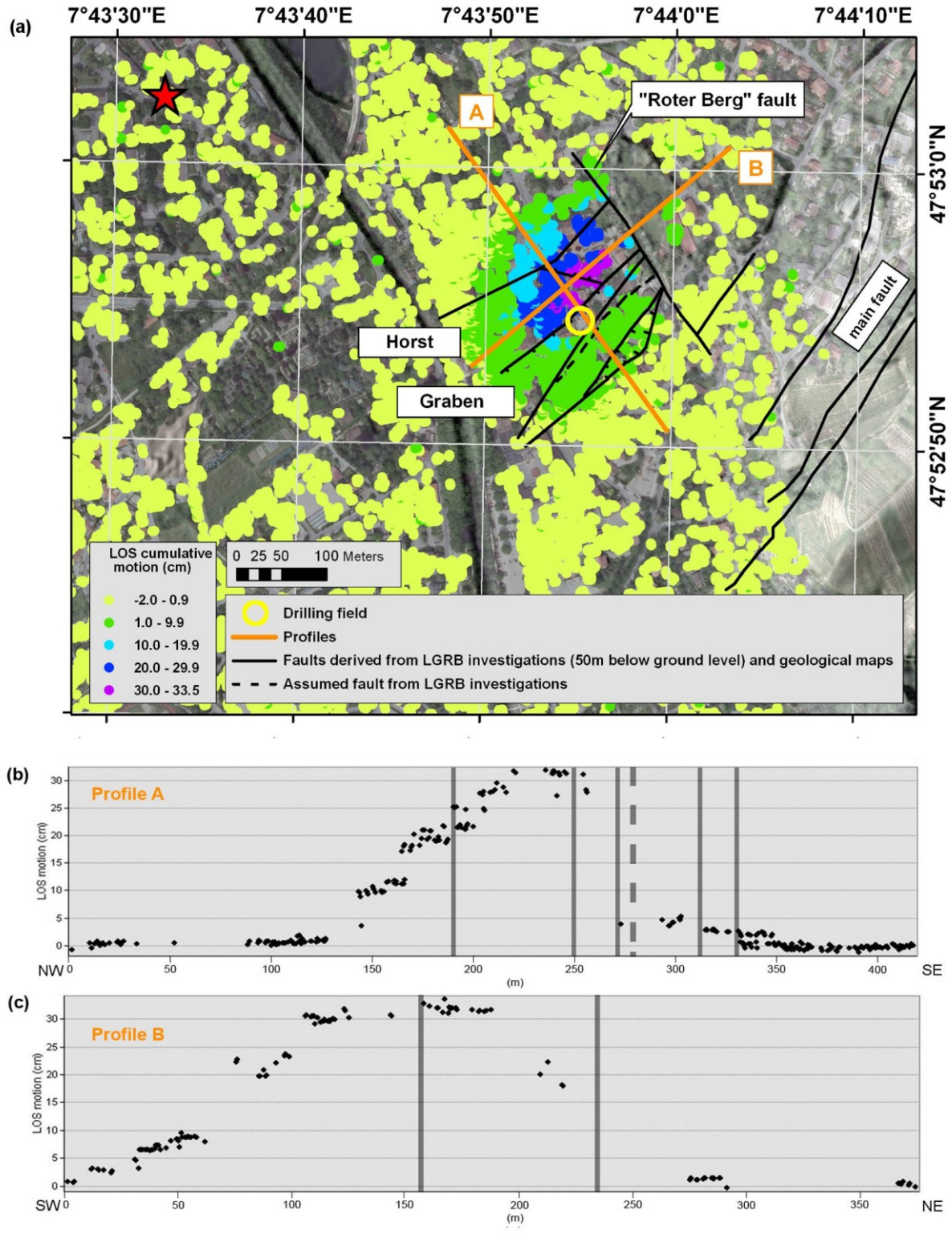

Fig. 2.12: (a) SBAS-derived LOS displacement presented in five classes overlaid on geological structures [5]. The red star represents the reference point for the displacement, and the yellow circle shows the location of the drilling field. The locations of the two profiles as presented in (b) and (c) are highlighted with orange lines. (b) Cumulative LOS deformation along profile A. (c) Cumulative LOS deformation along profile B. The intersection of faults derived by the geophysical measurements of the LGRB with both profiles is shown by vertical lines.

A potential future scenario may arise: the dissolution of the recently formed gypsum in water (karstification), leading to a volume loss. The risk involved is in this the structural collapse of possible subsurface cavities [35], which may lead to small-scale sinkholes [16], thus causing further damage.

SBAS time series analysis has the potential of capturing early signs of subsidence caused by gypsum dissolution due to more densely sampled points than leveling measurements and the small image acquisition interval of 11 days. Considering the current spatio-temporal results (Fig. 2.6 and Fig. 2.10), indications of such a process are not currently visible. Continued monitoring of the area is therefore strongly recommended.

2.6 Conclusion

In this study, we have demonstrated the capability of X-band InSAR time series analysis to record surface displacements occurring at rapid rates in Staufen, Germany. Because this method considers interferograms of small temporal baselines, it is suitable for detecting and correctly unwrapping the rapid surface uplift in Staufen, which occurs at rates greater than 10 cm/yr. The spatially limited deformation field is precisely reflected in the SBAS time series; its spatial extent and the trend coincide with the leveling measurements. Missing survey points and the incapability of the InSAR technique to overcome temporal decorrelations in vegetated areas result in a lack of information northeast of the uplift area. The availability and analysis of both remote sensing and terrestrial survey data indicate horizontal velocity contributions of several centimeters. As neither detailed terrestrial measurements of horizontal deformation, nor proper TSX data acquisitions from a descending orbit are available for the observation period, the full three-dimensional velocity field cannot be determined. Accordingly, the evaluation and validation of the InSAR-based deformation field at Staufen by using leveling data is only partially possible. Future data acquisitions in ascending and descending orbits, in combination with recent GNSS measurements, enable the discrimination between horizontal and vertical displacement. The combination of these various datasets together with either numerical or analytical geophysical modeling could provide additional details for geological interpretations and lead to a better understanding of the complex subsurface processes.

2.7 Acknowledgments

This work was supported by Initiative and Networking Fund of the Helmholtz Association in the frame of Helmholtz Alliance “Remote Sensing and Earth System Dynamics”. The leveling data have been provided by the Landratsamt Breisgau Hochschwarzwald, office Müllheim, under permission of the city council of Staufen im Breisgau. All TSX data are kindly provided by DLR under proposal number GEO0717. Special thanks to Jan Anderssohn for initiating the project and to Ingo Sass for comprehensive discussions. The authors would also like to thank the reviewers for their careful work in enhancing the quality of this paper.

Conflict of Interest

The authors declare no conflict of interest.

2.8 References

[1] Illes, J.H. The Rhine graben rift system plate tectonics and transform faulting. Surv. Geophys. 1972, 1, 27–60.

[2] Franzke, H.J.; Wetzel, H.U.; Werner, W. Welche Informationen können uns Fernerkundungsdaten zu Paläostressfeldern und zu Mineralisationsprozessen im Schwarzwald geben? Deutsche Gesellschaft Photogramm. Fernerkundung. 2001, 9, 340–353.

[3] Franzke, H.J.; Werner, W.; Wetzel, H.U. Die Anwendung von Satellitenbilddaten zur tektonischen Analyse des Schwarzwalds und des angrenzenden Oberrheingrabens. Jb. Landesamt Geologie Rohstoffe Bergbau Baden Württemberg. 2003, 41, 1–35.

[4] Münch, W.; Sistenich, H.P.; Bücker, C.; Blanke, T. Möglichkeiten der geothermischen Stromerzeugung im Oberrheingraben- Eine Analyse der geologischen Bedingungen, der Bohr- und Fördertechnik sowie der Kraftwerkstechnik und Wirtschaftlichkeit. VGB PowerTech. 2005, 10.

[5] LGRB Landesamt für Geologie, Bergbau und Rohstoffe Baden-Württemberg. Geologische Untersuchungen von Baugrundhebungen im Bereich des Erdwärmesondenfeldes beim Rathaus in der historischen Altstadt von Staufen i. Br; Sachstandsbericht Az. 94-4763//10-563; 2010. Available online: http://www.lgrb.uni-freiburg.de/lgrb/home/schadensfall_staufen_bericht (accessed on 9 January 2012).

[6] Presseerklärung zu den Hebungsrissen; Presseerklärung vom 22.12.2011. Available online: http://www.staufen.de/aktuelles-nachrichten/hebungsrisse/presseerklaerungen/presseerklaerung-zu-den-hebungsrissen~1556/ (accessed on 27 March 2013).

[7] Stadt Staufen. zu den Hebungsrissen an den Gebäuden der historischen Altstadt von Staufen. Presseerklärung vom 09.04.2009. Available online: http://www.staufen.de/default.asp?pn=1030&dn=&p1=1&ln=0&nk=20 (accessed on 9 January 2012).

[8] Berardino, P.; Fornaro, G.; Lanari, R.; Sansosti, E. A new algorithm for surface deformation monitoring based on small baseline differential SAR interferograms. IEEE Trans. Geosci. Remote Sens. 2002, 40, 2375–2383.

[9] Casu, F.; Manzo, M.; Lanari, R. A quantitative assessment of the SBAS algorithm performance for surface deformation retrieval from DInSAR data. Remote Sens. Environ. 2006, 102, 195–210.

[10] Ferretti, A.; Prati, C; Rocca, F. Permanent scatterers in SAR interferometry. IEEE Trans. Geosci. Remote Sens. 2001, 39, 8–20.

[11] Strozzi, T.; Teatini, P.; Tosi, L. TerraSAR-X reveals the impact of the mobile barrier works on Venice coastland stability. Remote Sens. Environ. 2009, 113, 2682–2688.

[12] Anderssohn, J.; Motagh, M.; Walter, T.R.; Rosenau, M.; Kaufmann, H.; Oncken, O. Surface deformation time series and source modeling for a volcanic complex system based on satellite wide swath and image mode interferometry: The Lazufre system, central Andes. Remote Sens. Environ. 2009, 113, 2062–2075.

[13] Lanari, R.; Lundgren, P.; Manzo, M.; Casu, F. Satellite radar interferometry time series analysis of surface deformation for Los Angeles, California. Geophys. Res. Lett. 2004, 31, L23613.

[14] Motagh, M.; Hoffmann, J.; Kampes, B.; Baes, M.; Zschau, J. Strain accumulation across the Gazikoy-Saros segment of the North Anatolian Fault inferred from Persistent Scatterer Interferometry and GPS measurements. Earth Planet. Sci. Lett. 2007, 255, 432–444.

[15] Vasco, D.W.; Rucci, A.; Ferretti, A.; Novali, F.; Bissell, R.C.; Ringrose, P.S.; Mathieson, A.S.; Wright, I.W. Satellite-based measurements of surface deformation reveal fluid flow associated with the geological storage of carbon dioxide. Geophys. Res. Lett. 2010, 37, L03303.

[16] Sass, I.; Burbaum, U. Damage to the historic town of Staufen (Germany) caused by geothermal drillings through Anhydrite-Bearing formations. Acta Carsol. 2010, 39, 233–245.

[17] Hooper, A. A multi-temporal InSAR method incorporating both persistent scatterer and small baseline approaches. Geophys. Res. Lett. 2008, 35, L16302.

[18] Bell, J.W.; Amelung, F.; Ramelli, A.R.; Blewitt, G. Land subsidence in Las Vegas, Nevada, 1935–2000: New geodetic data show evolution, revised spatial patterns, and reduced rates. Environ. Eng. Geosci. 2002, 8, 155–174.
[19] Fielding, E.J.; Blom, R.G.; Goldstein, R.M. Rapid subsidence over oil fields measured by SAR interferometry. Geophys. Res. Lett. 1998, 25, 3215–3218.
[20] Galloway, D.L.; Hudnut, K.W.; Ingebritsen, S.E.; Philips, S.P.; Peltzer, G.; Rogez, F.; Rosen, P.A. Detection of aquifer system compaction and land subsidence using interferometric synthetic aperture radar, Antelope Valley, Mojave Desert, California. Water Resour. Res. 1998, 34, 2573–2585.
[21] Motagh, M.; Walter, T.R.; Sharifi, M.A.; Fielding, E.; Schenk, A.; Anderssohn, J.; Zschau, J. Land subsidence in Iran caused by widespread water reservoir overexploitation. Geophys. Res. Lett. 2008, 35, L16403.
[22] Rocca, F. Modeling Interferogram Stacks. IEEE Trans. Geosci. Remote Sens. 2007, 45, 3289–3299.
[23] Kampes, B.M.; Hanssen, R.F.; Perski, Z. Radar Interferometry with Public Domain Tools. In Proceeding of Third International Workshop on ERS SAR Interferometry, Frascati, Italy, 1–5 December 2003.
[24] Hooper, A. A Statistical-Cost Approach to Unwrapping the Phase of InSAR Time Series. In Proceeding of International Workshop on ERS SAR Interferometry, Frascati, Italy, 30 November–4 December 2009.
[25] Hooper, A.; Zebker, H.; Segall, P.; Kampes, B. A new method for measuring deformation on volcanoes and other natural terrains using InSAR persistent scatterers. Geophys. Res. Lett. 2004, 31, L23611.
[26] Hooper, A.; Segall, P.; Zebker, H. Persistent scatterer interferometric synthetic aperture radar for crustal deformation analysis with application to Volcan Alcedo, Galapagos. J. Geophys. Res.-Solid Earth 2007, 112, B07407.
[27] Stadt Staufen. Hebungsrisse: Runder Tisch vom 14.01.2013. Available online: http://www.staufen.de/ aktuelles-nachrichten/hebungsrisse/protokolle-runder-tisch/hebungsrisse-runder-tisch~164881/ (accessed on 26 April 2013).
[28] LGRB Landesamt für Geologie, Bergbau und Rohstoffe Baden-Württemberg. Zweiter Sachstandsbericht zu den seit dem 01.03.2010 erfolgten Untersuchungen im Bereich des Erdwärmesondenfeldes beim Rathaus in der historischen Altstadt von Staufen i. Br. 2012. Zweiter Sachstandsbericht Az. 94-4763//12-2487. Available online: http://www.lgrb.uni-freiburg.de/lgrb/ home/schadensfall_staufen_bericht_2012 (accessed on 30 April 2013).
[29] Stadt Staufen. Presseerklärung vom 23.02.2012 zu den Hebungsrissen an den Gebäuden der historischen Altstadt von Staufen. Available Online: http://www.staufen.de/aktuelles-nachrichten/ hebungsrisse/presseerklaerungen/presseerklaerung-zu-den-hebungsrissen~627 (accessed on 30 April 2013).
[30] Müller-Salzburg, L.; Götz, H.P. Heaving of invert in tunneling. Bull. Int. Assn. Eng. Geol. 1975, 14, 51–53.
[31] Amelung, F.; Galloway, D.L.; Bell, J.W.; Zebker, H.A.; Laczniak R.J. Sensing the ups and downs of Las Vegas: InSAR reveals structural control of land subsidence and aquifer-system deformation. Geology 1999, 27, 483–486.
[32] Motagh, M.; Djamour, Y.; Walter, T.R.; Wetzel, H.U.; Zschau, J.; Arabi, S. Land subsidence in Mashhad Valley, northeast Iran: Results from InSAR, leveling and GPS. Geophys. J. Int. 2007, 168, 518–526.
[33] Stadt Staufen. Presseerklärung vom 12.11.2009 und 17.12.2009 zu den Hebungsrissen an den Gebäuden der historischen Altstadt von Staufen. Available Online: http://www.staufen.de/ default.asp?pn=1030&dn=&p1=1&ln=0&nk=20 (accessed on 9 January 2012).
[34] Zabank, C.; Arthur, R.C. Rock Mechanics Aspects of Volume Changes in Calcium Sulfate Bearing Rocks due to Geochemical Phase Transitions. In Proceeding of The 25th US Symposium on Rock Mechanics (USRMS), Evanston, IL, USA, 25 June 1984.

[35] Pando, L.; Pulgar, J.A.; Gutiérrez-Claverol, M. A case of man-induced ground subsidence and building settlement related to karstified gypsum (Oviedo, NW Spain). Environ. Earth Sci. 2013, 68, 507–519.

3. Chapter: Ground Surface Response to Geothermal Drilling and the Following Counteractions in Staufen im Breisgau (Germany) Investigated by TerraSAR-X Time Series Analysis and Geophysical Modeling (published: Remote Sens., 2014, *6*, 10571-10592; doi:10.3390/rs61110571)

Christin Lubitz *, Mahdi Motagh and Hermann Kaufmann

GFZ German Research Centre for Geosciences, Section 1.4, Telegrafenberg, D-14473 Potsdam, Germany; E-Mails: mahdi.motagh@gfz-potsdam.de (M.M.); charly@gfz-potsdam.de (H.K.)

***** Author to whom correspondence should be addressed; E-Mail: chlubitz@gfz-potsdam.de; Tel.: +49-331-288-28621; Fax: +49-331-288-1192.

External Editors: Richard Gloaguen and Prasad Thenkabail

Received: 24 April 2014; in revised form: 20 October 2014 / Accepted: 21 October 2014 / Published: 31 October 2014

Abstract

The city of Staufen im Breisgau in southwest Germany suffers from a localized land uplift, which has occurred in the past six years in relation to geothermal drilling activities in 2007. So far, severe damages at 269 buildings have been recorded. The chemical transformation of anhydrite and water to gypsum, resulting in a volume increase, has been attributed as the cause of the uplift. Previous studies provide knowledge on the spatio-temporal displacement evolution from 2008 through 2011 using leveling and spaceborne Synthetic Aperture Radar Interferometry (InSAR) measurements, but lack a detailed representation of vertical and horizontal displacement contributions as well as geophysical modeling. This study focuses not only on continued observation analysis from June 2011 through July 2013, but also on obtaining and evaluating horizontal displacements in Staufen based on combined analysis of TerraSAR-X satellite imagery from both ascending and descending orbits. Applying the Small BAseline Subset (SBAS) approach a deceleration of annual cumulative line of sight (LOS) uplift is observable from 13.8 cm ± 0.3 cm (July 2008–July 2009) to 3 cm ± 0.3 cm (July 2012–July 2013) within area of maximum deformation NNE of the drilling zone. Conducting displacement decomposition on ascending and descending data of a common period (October 2012 through July 2013) yields in an approximately symmetric east- and westward motion with maximum values approximately 1 cm and 1.4 cm, respectively. The joint inversion of ascending and descending InSAR data for the common period from October 2012 through July 2013 shows that a horizontal rectangular source with length, width and depth of 177 m ± 19 m, 69 m ± 15 m and 89 m ± 9 m, respectively, can satisfactorily model the observation. The amount of opening at depth shows a decrease in time by about 71% for the period 2011–2012 as compared to period 2008–2009.

Keywords: Staufen im Breisgau; uplift; SBAS; horizontal displacement; source modeling

3.1 Introduction

The uplift process occurring in Staufen im Breisgau (hereafter called Staufen), southwest Germany (Fig. 3.1(a)), is a remarkable localized event with first signs of damages being recognized at the end of 2007. Comprehensive investigations [1–5] have already been conducted to investigate the spatial and temporal pattern of deformation area in the city and to evaluate the causes to which the ongoing subsurface processes can be attributed to.

Seven boreholes for geothermal probes were drilled in September 2007 for the purpose of thermal management of the city hall. This is supposed to have facilitated water contact with anhydrite (calcium sulfate) lenses that are deposited within the Keuper-Gypsum strata. Anhydrite was found at depth between 61.5 m and 126.1 m and between 73.5 m and 105.75 m below ground level by analyzing core samples of the well drillings EKB2 and BB3, respectively [1,2], both located close to the city hall (Fig. 3.1(b)). The chemical transformation of anhydrite and water to gypsum results in a volume increase [1]. Investigations by Sass and Burbaum [4] show that the swelling pressure cannot be compensated by the overburden, leading to surface deformation and severe damages. Until now, 262 private and seven municipal buildings sustained substantial crack damage; one building was demolished completely in August 2013 as it was damaged beyond repair [6].Continuous monitoring is essential as it provides invaluable data for local authorities and stakeholders to reliably track ground deformation and assess its associated hazards.

Terrestrial leveling measurements have been performed since January 2008 [1] and regular data acquisition for applying Synthetic Aperture Radar Interferometry (InSAR) techniques started in July 2008, both aiming to assess the deformation area in space and time. The first InSAR study using Synthetic Aperture Radar (SAR) imagery of the TerraSAR-X (TSX) satellite from July 2008 through January 2009 revealed a localized displacement field oriented NE-SW. Displacement rates of up to 12 mm/month (14 cm/y in the case of linear motion) in the satellite's line of sight (LOS) were derived for this period [4]. A more intensive investigation by Lubitz et al. [3] using time series analysis of TSX data from July 2008 to May 2011 found maximum LOS velocities of up to ~12 cm/y and showed evidences for distinct horizontal motions of several centimeters by comparing leveling and InSAR results. Moreover, Lubitz et al. [3] found a slowdown of uplift in time, which they relate to the countermeasures, namely groundwater pumping and borehole sealing, that have been conducted since September 2009 in the region [1].

The displacement analysis presented by Lubitz et al. [3] lacks a detailed representation of horizontal and vertical contributions. Whereas leveling measurements provide only information on the vertical component of displacement field, InSAR analysis combines both the vertical and horizontal motion contributions into one dimension, which is the line of sight from the ground to the satellite. Annually performed terrestrial position measurements by using tachymeter (distance and angular measurements) show strong evidences for horizontal dislocations, e.g., a survey point approximately 70 m NNE of the drilling zone moved about 6.4 cm in a northwestern direction from October 2009 through September 2010 and further 7.8 cm until November 2012. However, those measurements yield in a relatively poor spatial resolution and do not capture the potentially high spatial variability of displacement field. Therefore, from October 2012 through July 2013 we started TSX data acquisition in Staufen from a descending track in addition to the regular data acquisitions from the ascending track with the aim of differentiation between horizontal and vertical motion for the common time interval. We analyzed the new dataset in this study and also used the observed signals to constrain parameters of a geophysical pressure source model at depth, which in turn can be used to reconstruct surface deformation field [7]. The added value of standard deformation source modeling here is to obtain a first-order model for physical understanding of the source of the observed deformation in Staufen. The estimation of source depth is of main interest and will be considered with respect to anhydrite occurrences as detected by core sample analysis of the EKB2 and BB3 boreholes.

This paper is organized as follows: Section 3.2 is devoted to the data which we use in this research. In Sections 3.3.1 and 3.3.2 we introduce briefly the InSAR methodology and the geophysical modeling, respectively. Results are presented in Section 3.4, separated into InSAR derived results

(Section 3.4.1) and outcome of the source modeling (Section 3.4.2). Sections 3.5 and 3.6 are devoted to the discussion and conclusion, respectively.

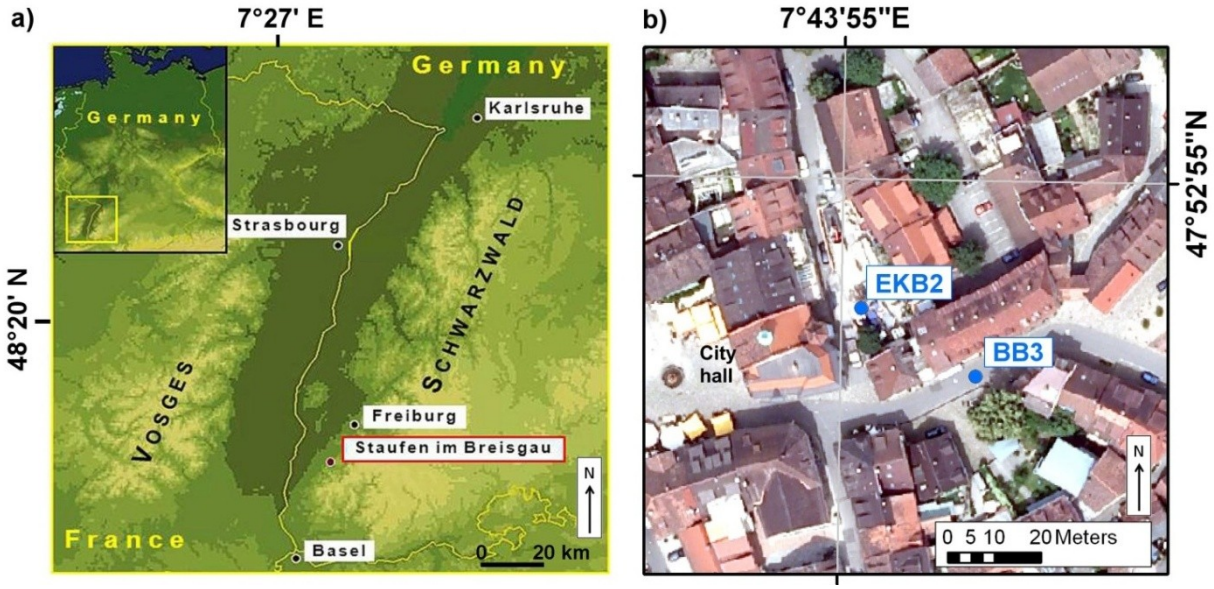

Fig. 3.1: (a) Location of the city Staufen im Breisgau; (b) Sketch of well locations EKB2 and BB3 that are currently used for ground water pumping. An orthophoto was used as background (acquired by State Survey Office of Baden-Württemberg).

3.2 Data

All SAR imagery used in this study were acquired by the German TerraSAR-X satellite. The ascending dataset from the relative orbit 116 (Stripmap mode, beam strip_011, HH polarized) covers the period from 2 June 2011 through 11 July 2013 and hence follows the time period investigated by the previous study [3]. Descending Stripmap data from the relative orbit 154 (beam strip_009R, HH polarized) were acquired from 1 October 2012 through 14 July 2013 and have an overlap period of 276 days (approximately nine months) with the ascending data. Larger data gaps in the winter periods 2011/2012 and 2012/2013 occurred due to mission conflicts with the TerraSAR-X add-on for Digital Elevation Measurement (TanDEM-X) data acquisition for the WorldDEM™.

As mentioned earlier, leveling measurements have been performed since 2008. However, for comparison with InSAR results in this study, we use only those leveling measurements that were conducted from 23 May 2011 through 15 July 2013. Until November 2012, the surveys were repeated at a two-month interval, followed by quarterly measurements in 2013. The reduction of repeated measurements was justified with the deceleration of the uplift and in consequence with the reduced capability of leveling instruments to capture displacements at small temporal intervals [8]. Additionally, the horizontal dislocation measurements were performed at several survey points once a year on 2 October 2009, 28 September 2010, 26 September 2011, 11 September 2012 and 7 October 2013.

3.3 Methodology

3.3.1 InSAR

Interferometric time series analysis of the SAR images was done using the Small BAseline Subset (SBAS) algorithm as implemented in the StaMPS/MTI (Stanford Method for Persistent Scatterer/Multi-Temporal InSAR [9]) software. Differential interferograms were generated with DORIS (delft object oriented radar interferometric software [10]) by using a Light Detection and Ranging (LiDAR) Digital Elevation Model (DEM) with 1 m spatial resolution (from the State Survey Office of Baden-Württemberg) for topographic correction. The SBAS method in StaMPS identifies single-look slowly-decorrelating filtered phase (SDFP) pixels directly from full resolution SAR images [9] and therein differs from SBAS methods of Berardino et al. [11] and Lanari et al. [12]. For interferogram generation of the ascending data, the perpendicular and temporal baselines were constrained to be below 450 m and 250 days, respectively. In the case of the descending dataset, we could decrease the temporal baseline below 100 days as the image acquisitions show a denser temporal distribution, which reduces the problem of network connectivity. The networks of the interferograms with small spatial and temporal baselines of the ascending and descending images of this study are shown in Fig. 3.2(a,b), respectively. The network of the ascending dataset consists of 113 interferograms based on 30 SAR images that cover about two years, and 21 descending SAR images of a nine-month period are the basis for 82 interferograms of the descending network.

3.3.2 Source Modeling

InSAR derived surface displacement inversion can be used for estimating geophysical source models at depth that cause surface deformation [13–15]. In this paper, we use a finite rectangular opening-mode dislocation source in homogeneous elastic half-space [7] to simulate the observed uplift in Staufen. This model yields a convenient first-order approximation to evaluate complex source characteristics of deformation. However, it should be noted that this model is not aiming at a detailed and realistic representation of the Earth's situation, since it does not include effects due to local structures, surface topography, crustal layering, lateral inhomogeneity or effects due to an obliquely layered medium.

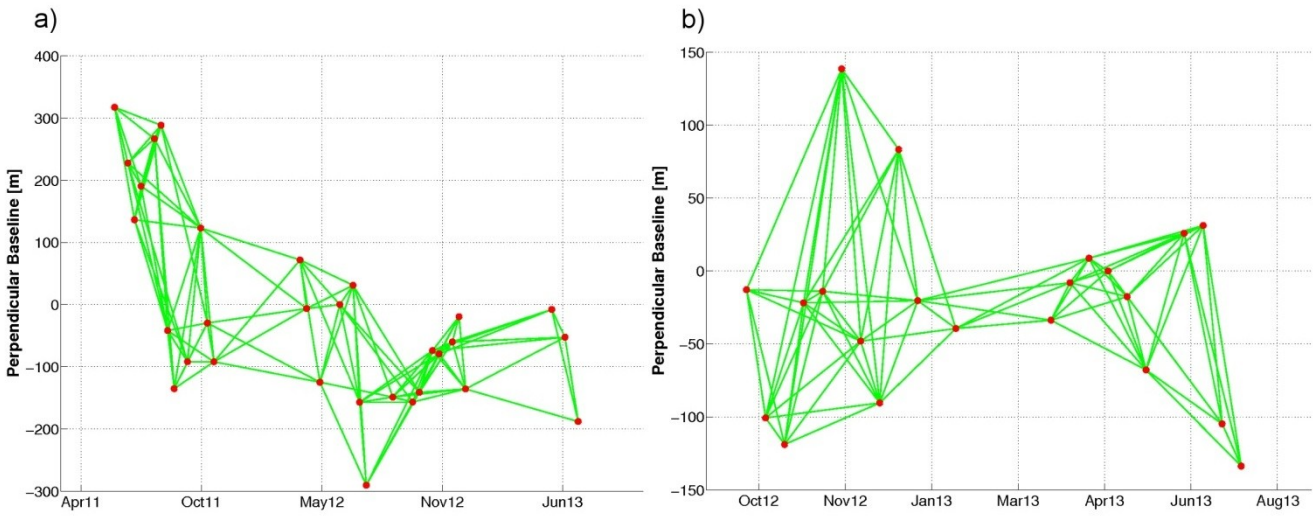

Fig. 3.2: The network of Small BAseline Subset (SBAS)interferograms used for the time series analysis of ascending (a) and descending (b) TerraSAR-X images. Red dots show the individual Synthetic Aperture Radar (SAR) images and green lines represent the image pairs for interferogram generation.

Several geometrical parameters define the source. These are: length, width, depth, strike (orientation in clockwise direction), dip, midpoint coordinates of the upper edge as well as the amount of uniform opening. Relating these unknown source parameters (x) and known InSAR displacement results in [16]:

$$d = G(x) + e\ , \tag{1}$$

where *d* is LOS displacement, *G* the Green's function and *e* the observation error, yields in a non-linear inverse problem, which we solved for the parameter vector (x) by using a Genetic Algorithm [17] with Bayesian probabilistic approach as described in [18].
To improve the efficiency of the inversion we selected a priori bounds for the parameters that are considered to be optimized. For example, exploration activities in Staufen, summarized in [1], locate the swelling area between 61.5 m and 99.5 m depth, which could be used to constrain the model's boundaries of the source depth. We have decided to select 0–1 km as boundary conditions for depths to avoid an overly restrictive setting. Further a priori bounds for source parameters (length, width and strike) were selected based on displacement maps (spatial dimension and orientation) from the previous study by Lubitz et al. [3]. The chosen boundaries are listed in Table 3.1, forming the parameter framework of the applied Genetic Algorithm that starts the first generation by using a population of 500 random source models. In order to find robust source parameters, 500 generations were then created.

Boundaries	Length (km)	Width (km)	Depth (km)	Dip (°)	Strike (°)
Lower Boundary	0	0	0	−20	0
Upper Boundary	0.5	0.5	1	0	90

Table 3.1: Lower and upper boundaries used in the inversion.

3.4 Results

The multi-temporal analysis of TSX SAR images from both ascending and descending orbits by applying the SBAS method is the main basis of the present study. The results provide not only information on the spatial and temporal evolution of the surface displacement, but also serve as important input for the source modeling.

3.4.1 InSAR Derived Motion

Figure 3.3(a,b) present the cumulative LOS displacement obtained from ascending data acquired between 2 June 2011 and 11 July 2013 and from the descending dataset for the period 1 October 2012 through 14 July 2013, respectively. It shows an elliptical-shaped uplift bowl oriented NE-SW. The LOS displacement values are with respect to a reference area marked by a red star. For consistency, the reference area was chosen at the same position as for the data analysis in [3] and is located within a non-deforming area. The drilling area has been highlighted with a black circle. For comparison with previous study, a red dashed contour has been added representing the 1 cm uplift contour of the cumulative LOS displacement of the 2008–2011 period from [3]. Symbols for reference point, drilling zone and 1 cm boundary of the 2008–2011 SBAS result apply for all figures in this paper when needed.
By looking at the red contour in Figure 3.3(a), we observe that compared to 2008–2011 the displacement pattern of 2011–2013 period has not changed significantly in its spatial extent. The local cumulative LOS uplift maximum for 2011–2013 is 8.5 cm, which is located approximately 50 m northward the drilling zone. Fig. 3.3(b) shows a similar motion pattern derived from the descending

dataset as compared to the ascending dataset. For this nine-month observation period the maximum cumulative uplift is 2.4 cm, which is located directly east of the drilling site. In comparison with the ascending data of both the 2008–2011 (red dashed contour) and the 2011–2013 (Fig. 3.3(a)) periods, the descending result shows further expansion of displacement field to the east.

3.4.2 Modeled Source Parameters

For the geophysical modeling we considered not only the SAR data processed in this study (period June 2011 through July 2013), but also the SBAS results of the period July 2008 through May 2011 as presented in [3]. Investigating different periods of surface ground motion helps us to better assess the spatial and temporal variability of the deformation source at depth. Figure 3.4 provides an overview about the best-fit modeling results (left column) in comparison to the observed LOS displacements (middle column) for different periods. The 2008–2011 period is presented at four different intervals: from 22 July 2008 through 12 December 2008 (five months, Fig. 3.4(a)), from 22 July 2008 through 11 August 2009 (eleven months, Fig. 3.4(b)), from 22 July 2008 through 24 May 2010 (22 months, Fig. 3.4(c)) and from 22 July 2008 through 22 May 2011 (34 months, Fig. 3.4(d)). The 2011–2013 period is shown at two intervals: from 2 June 2011 through 21 June 2012 (12 months, Fig. 3.4(e)) and from 2 June 2011 through 11 July 2013 (25 months, Fig. 3.4(f)). Finally, modeling of the descending result is shown in Fig. 3.4(g) covering the period from 1 October 2012 through 14 July 2013 (nine months).

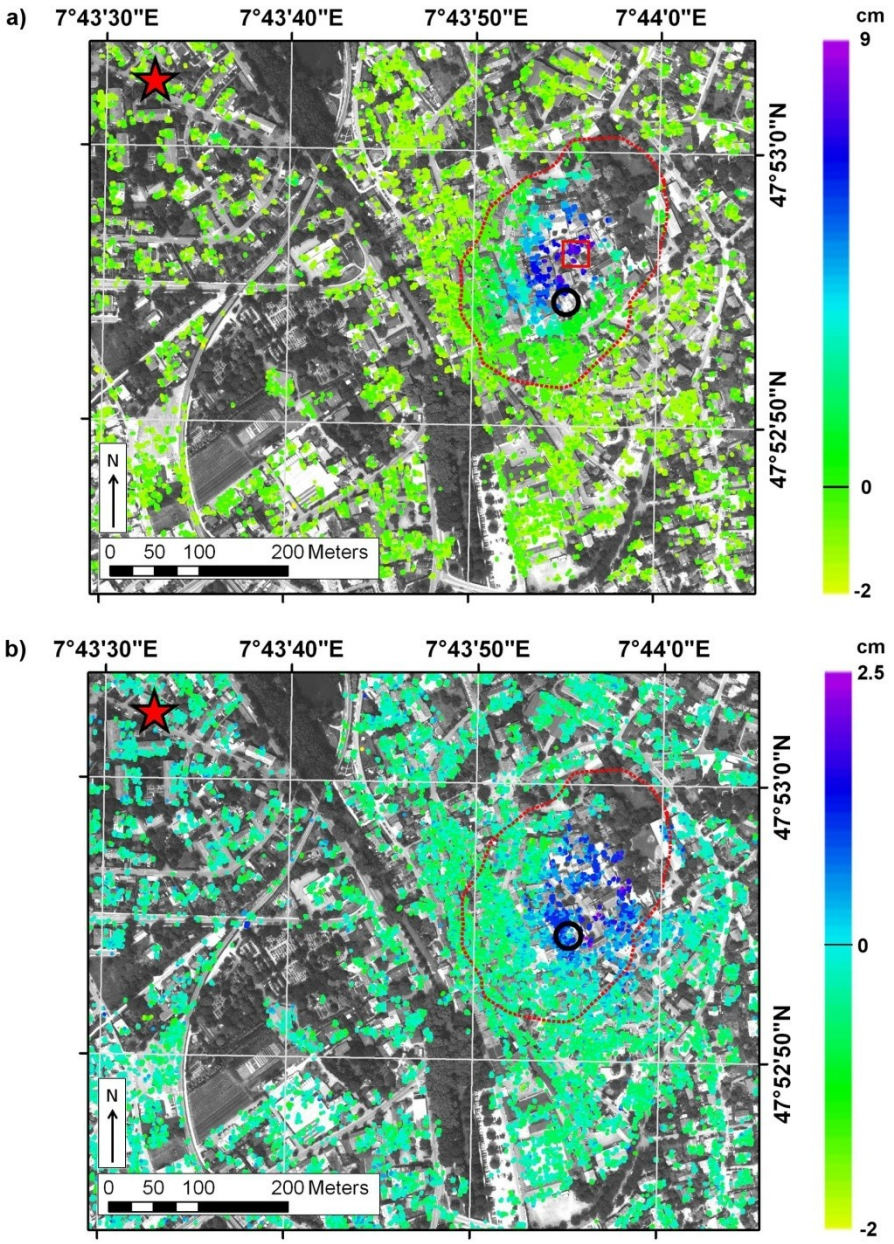

Fig. 3.3: (a) Cumulative line of sight (LOS) displacement in cm derived by using the Small BAseline Subsets (SBAS) approach based on the ascending data from 2 June 2011 through 11 July 2013. The red rectangle highlights the area of maximum deformation that is statistically analyzed in Section 3.5.1. (b) Cumulative LOS pattern based on the descending data from 1 October 2012 through 14 July 2013. The red star shows the reference area to which the displacement refers, the black circle indicates the drilling site and the red contour represents the 1 cm boundary of the ascending LOS displacement from 2008–2011 [3] for comparison.

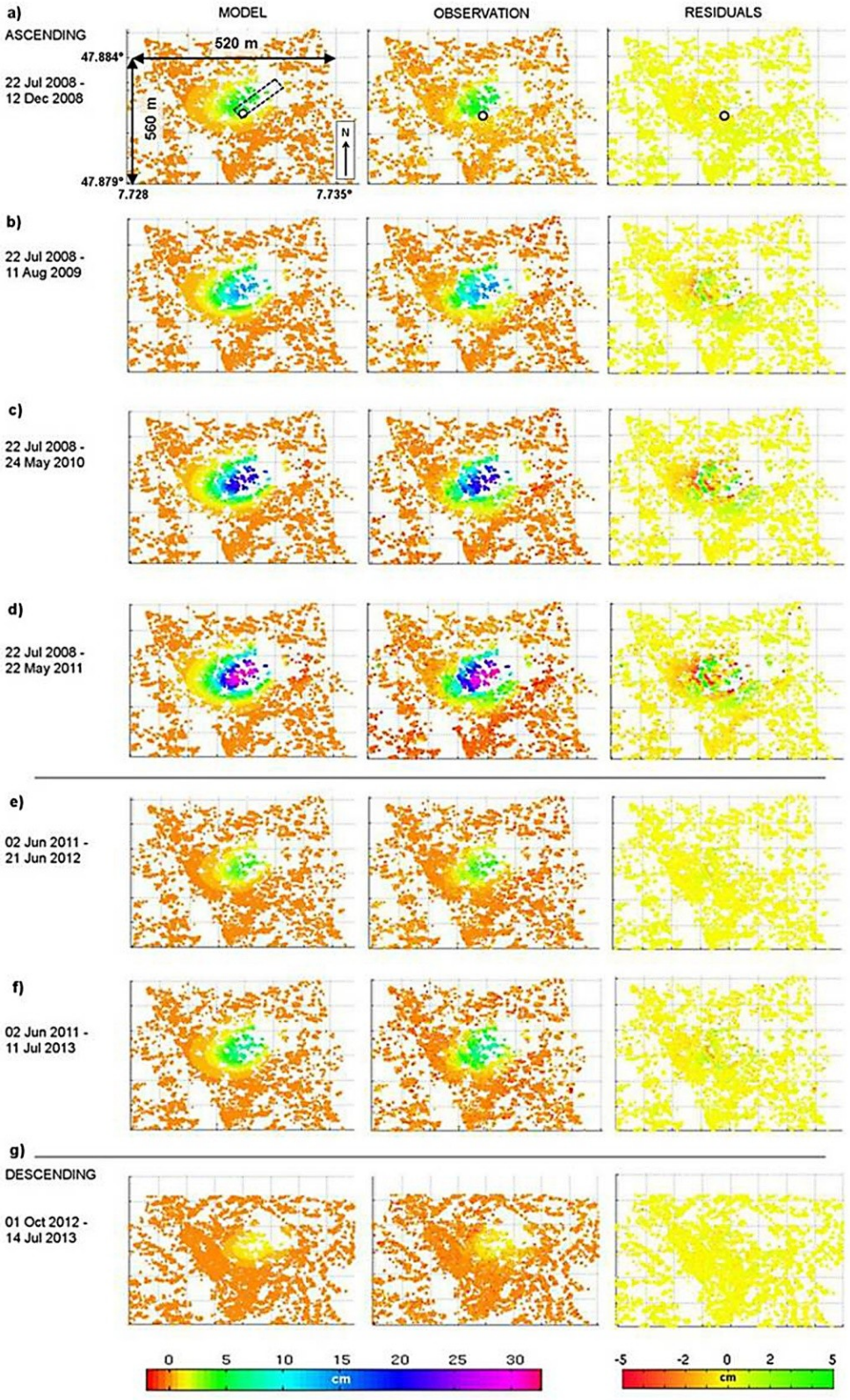

Fig. 3.4: Modeled surface displacement (first column) due to a rectangular finite dislocation source for different periods of the ascending data of [3] in (a)–(d) and of those processed in this study in (e)–(f). In 3.4(g) the descending outcome is shown. Corresponding source characteristics are listed in Table 3.2. Observed line of sight (LOS) cumulative displacements and residuals (difference between observation and model prediction) are shown in column two and three, respectively. Model-image in (a) shows exemplarily the outline (dashed) of the source as estimated for the corresponding period and the black circle indicates the drilling field location.

In general, the model solutions for all individual periods fit observations well, confirmed by residual images (observation minus model) in the right column of Fig. 3.4. However, noticeable residuals can be observed for datasets covering long periods (Fig. 3.4(c,d)). Interestingly, later observations of similar time intervals (Fig. 3.4(f)) show a significantly reduced magnitude of displacement, but a similar residual pattern as in Fig. 3.4(b,c,d), although of lower values. Several possibilities may be attributed to the residuals, which are discussed in Section 3.5.
The estimated source parameters corresponding to best-fit models in Fig. 3.4 are summarized in Table 3.2. Similarities in the results of different periods need to be considered with care, since they are based on different observation geometries and separated processing.

Source Parameters	Ascending						Descending
	Jul 2008–Dec 2008	Jul 2008–Aug 2009	Jul 2008–May 2010	Jul 2008–May 2011	Jun 2011–Jun 2012	Jun 2011–Jul 2013	Oct 2012–Jul 2013
Length (m)	175 ± 27	173 ± 15	171 ± 14	164 ± 12	171 ± 32	174±24	167±26
Width (m)	51 ± 8	65 ± 9	69 ± 2	71	64 ± 14	64±12	101±12
Depth (m)	63 ± 12	49	46	45	51 ± 4	52±2	48±23
Dip (°)	−1 ± 4	0 ± 3	0 ± 2	0 ± 2	0 ± 5	0±4	0±6
Strike (°)	39 ± 9	38 ± 5	39 ± 5	38 ± 4	34 ± 10	33±8	41±12
Opening (cm)	15	28	42	56	8	15	2
Opening rate (cm/month)	3	2.6	1.9	1.7	0.7	0.6	0.2

Table 3.2: Source parameters from inversion of different Synthetic Aperture Radar Interferometry (InSAR) datasets for different time periods as presented in Fig. 3.4. The standard deviation has been computed from conditional posterior probability density functions (PDF) as described in[18].Values shown without standard deviation resulted from unimodal posterior PDFs.

Based on the ascending data, the dislocation source is found to be located between 45–63 m depth with a length ranging between 164 m and 175 m and a width ranging between 51 m and 71 m. The estimated parameters from the descending data lie within the range of the ascending results, except for the width, which is 101 m. As Table 3.2 shows, the dip angle is found to be zero or close to zero, representing a horizontal plane, which is oriented about 38° from the north (strike). Modeled strike values vary by 4°–5° for different datasets and periods. Except for the amount of opening, other parameters are found to be approximately similar in all inversions.
A joint inversion of the ascending and descending data covering a nine month period from October 2012 through July 2013 yields in similar parameter values for length, width, dip and strike (Table 3.3) as the individual inversions of ascending data only. Interestingly, from this inversion the source is estimated deeper (89 m ± 9 m) as compared to the single-data inversions, showing that combined data analysis enhances the geophysical modeling. The opening value from the combined inversion is three times larger than of descending data inversion only, resulting in a rate similar to that from ascending data inversion for June 2011–June 2012 and June 2011–July 2013 periods. The modeled and observed surface displacements as well as the residuals are presented in Fig. 3.5.

As seen in Table 3.2 a relative opening of 56 cm was estimated within the first three years of SAR observation in Staufen, reaching to 15 cm for the following two years (2011–2013), and 2 cm for the nine month covered by descending data and 6 cm from joint inversion (Table 3.3), respectively. Considering the rate of opening (last row of Tables 3.2 and 3.3), a decrease in time is clearly observable.

Source Parameters	Oct 2012–Jul 2013
Length (m)	177±19
Width (m)	69±15
Depth (m)	89±9
Dip (°)	0±1
Strike (°)	37±5
Opening (cm)	6
Opening Rate (cm/month)	0.7

Table 3.3: Estimated source parameters from joint inversion of ascending and descending data for the period from October 2012 through July 2013.

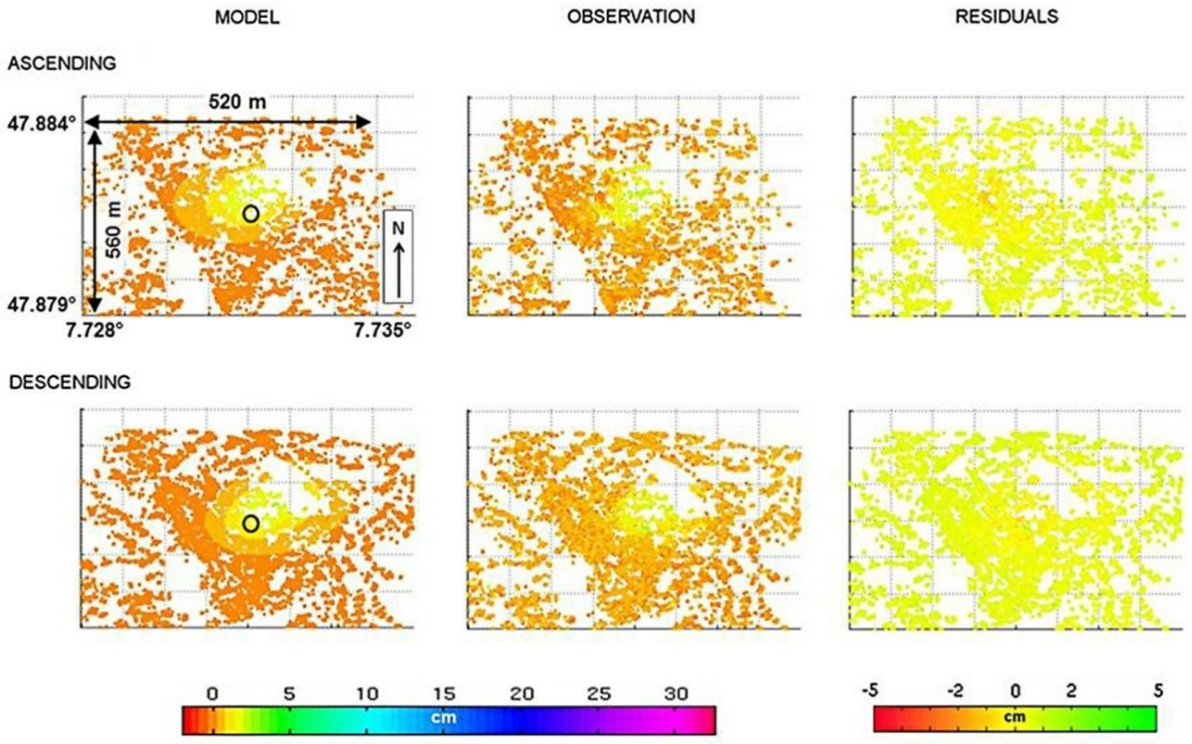

Fig. 3.5: Modeled surface displacements (first column), observed line of sight (LOS) cumulative displacements (second column) and residuals (third column) from joint inversion of ascending and descending data for the period from 9 October 2012 through 11 July 2013. The black circle in the model-images indicates the location of the drilling site.

Our inversion ran with a Poisson ratio of 0.25. The Okada dislocation model that we have applied here does not include the effects of layering. The influence of material properties can be relevant, in particular in shallow, inhomogeneous and geologically complex regions as they can have an effect on the spatial extent of the surface deformation [19–22]. A study by Pritchard and Simons [23] analyzing dislocation models in elastic half-space suggests that the material properties seem to be of secondary relevance for source depth estimation as compared to other geometry parameters [23].

We tested our inversion with varying Poisson ratios for the dislocation source (0.09, 0.1, 0.13, 0.15 and 0.3) and found deviations of up to 5% for the source parameters listed in Tables 3.2 and 3.3.

3.5 Discussion

In the following, we first discuss the temporal evolution of uplift, and then assess horizontal motions by evidences from comparing time series of SBAS and leveling, from combination of ascending and descending data as well as from source modeling. Finally, we discuss our modeling results.

3.5.1 Uplift Deceleration in Response to Counteractions

Monitoring of temporal variations in the displacement patterns allows us to evaluate the response of ground surface to countermeasures (borehole sealing and groundwater pumping) implemented in autumn 2009 and spring 2011 [2]. For this, we statistically analyze an area of 30 m by 30 m within the region of maximum LOS displacement about 50 m NNE of the drilling zone (red square in Fig. 3.3(a)). At this location, we observe a cumulative LOS uplift of 13.7 cm ± 0.3 cm (mean value within the defined area) from July 2008–July 2009, which then was reduced to cumulative LOS uplift of 3 cm ± 0.3 cm four years later from July 2012–July 2013 (Table 3.4). The deceleration in uplift is significantly observable when comparing the periods 2009/2010 with 2010/2011 as well as the periods 2010/2011 with 2011/2012. A correlation with the permanent groundwater pumping at the new well BB3 since spring 2011 in addition to well EKB2 seems reasonable. When considering the decrease in the amount of opening (Table 3.2), we find compatible indications of the effectiveness of countermeasures.

Statistics	22 July 2008–31 July 2009	31 July 2009–18 July 2010	18 July 2010–22 May 2011	5 July 2011–13 July 2012	13 July 2012–11 July 2013
Minimum (cm)	12.8	10.3	6.4	3.7	2.3
Maximum (cm)	14.2	11.7	7.8	4.8	3.5
Mean (cm)	13.7	11.1	6.9	4.01	3
Median (cm)	13.8	11	6.8	4.1	3
Standard deviation (cm)	0.3	0.3	0.3	0.2	0.3

Table 3.4: Line of sight (LOS) uplift statistics within area of maximum displacement (red square in Fig. 3.3(a)) for different periods. The first three columns refer to the Small BAseline Subsets (SBAS) analysis of Lubitz et al. [3] (24 slowly-decorrelating filtered phase (SDFP) pixels within the defined area) and the last two represent the period under investigation of this study (27 SDFP pixels within the defined area).

3.5.2 Horizontal Displacement Estimation

3.5.2.1 Evidence from Comparing Time Series of SBAS and Leveling Measurements

Comparisons between ascending SBAS results and time series of leveling measurements for the 2011–2013 period at 13 selected locations within or in close distance to the uplift area are plotted in Fig. 3.6. Nine locations (A, B, C, G, H, I, J, K, M) have been selected from previous study conducted for the 2008–2011 period [3] in order to better assess the temporal evolution of displacement. Three points have been selected to investigate the northeastern area (D, E, F) and one point has been selected south of the drilling zone (L). Similar to our earlier study, we compared directly vertical

leveling measurements with LOS SBAS displacements to assess the contribution of horizontal motion in the deformation field. For each presented location the vertical displacements as measured by leveling are shown as red triangles and the mean LOS displacements as derived from SBAS are presented as blue dots. Mean values and error bars of SBAS results were computed from a window size of 7.5 m by 7.5 m with leveling point as center location.

The SBAS results show good consistency with leveling measurements obtained for points outside the displacement field (location A) and some locations in its interior (e.g., location M with approximately linear uplift). However, some clear discrepancies are observable at some locations. For example, at locations I, K and L (southeastern part of uplift area) significant deviations of the SBAS result from the leveling motion evolution are observed from the beginning of the investigated period (e.g., up to 2.4 cm for point I). Generally, contributions of eastward, northward and southward motion in addition to uplift yield in smaller LOS values than leveling measurements for observations from an ascending orbit. Such cases can be seen for locations I, K and L, which are located on the southeastern part of the graben block (Fig. 3.7). The situation at point K is striking as the declining trend is not due to downward movement, but rather due to contribution of eastward and/or southward motion to overall LOS.

Comparison between InSAR and leveling measurement at point E indicates contributions of westward and/or northward motion in addition to the uplift, resulting in slightly larger LOS values than leveling measurements.

The other time series plots at locations B, C, D, F, G, H, and J show an interesting feature. First, their corresponding SBAS and leveling observations agree well until the winter period of 2011/2012, then a shift in spring 2012 is observed in which the SBAS derived motions show smaller magnitudes than leveling. No unwrapping problems have been recognized at those locations during processing, which may account for the observable shift. Among these points, B, C, G, H and J were analyzed before by [3], for which larger SBAS magnitudes than leveling for the period 2008–2011 were observed, an indication for the westward horizontal motion contributions. An explanation for the shift in the current uplift trend observable at these locations may be related to a transient deformation caused e.g., by reduction of westward motion or/and increase in northward motion since spring 2012. This observation cannot be verified against current ground reference measurements because of their poorer temporal resolution; the dislocation measurements were performed only annually in autumn season. Interestingly, all affected locations are at the horst block (Fig. 3.7), which may indicate an influence of the fault system on the change of the motion rates. Complex situations of surface deformation bulges in interaction with faults can lead to complex effects on magnitude and direction of displacements [24]. Whether the observed shift reflects such complexity or even a reactivation of the fault system requires further investigations.

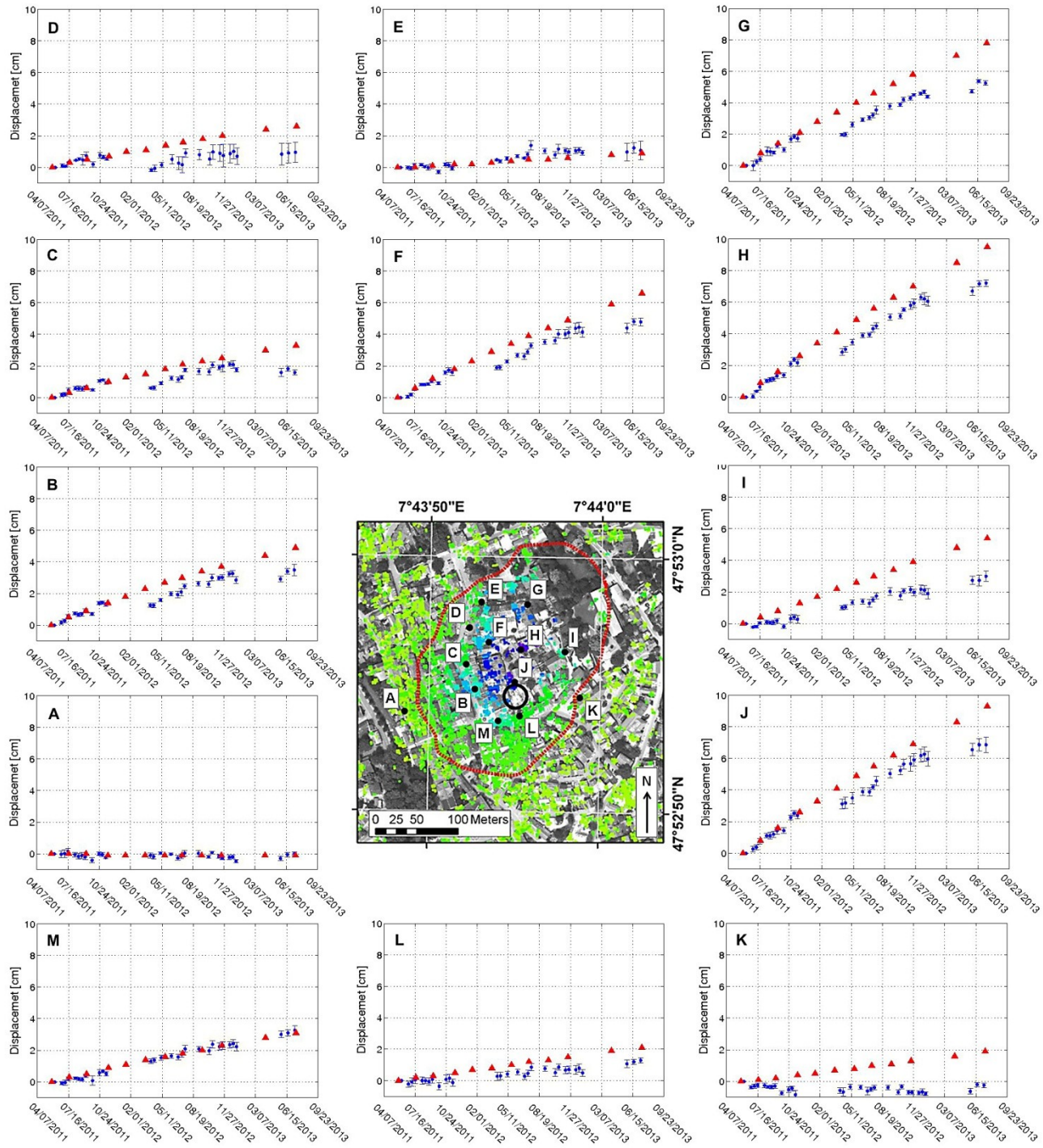

Fig. 3.6: Time series of displacements at selected locations. Red triangles correspond to leveling measurement and blue dots with error bars to Small BAseline Subsets (SBAS) results using the ascending data from 2011–2013 time period. The locations are highlighted as black dots in the centered image (enlarged subset of the displacement field of Fig. 3.3(a)).

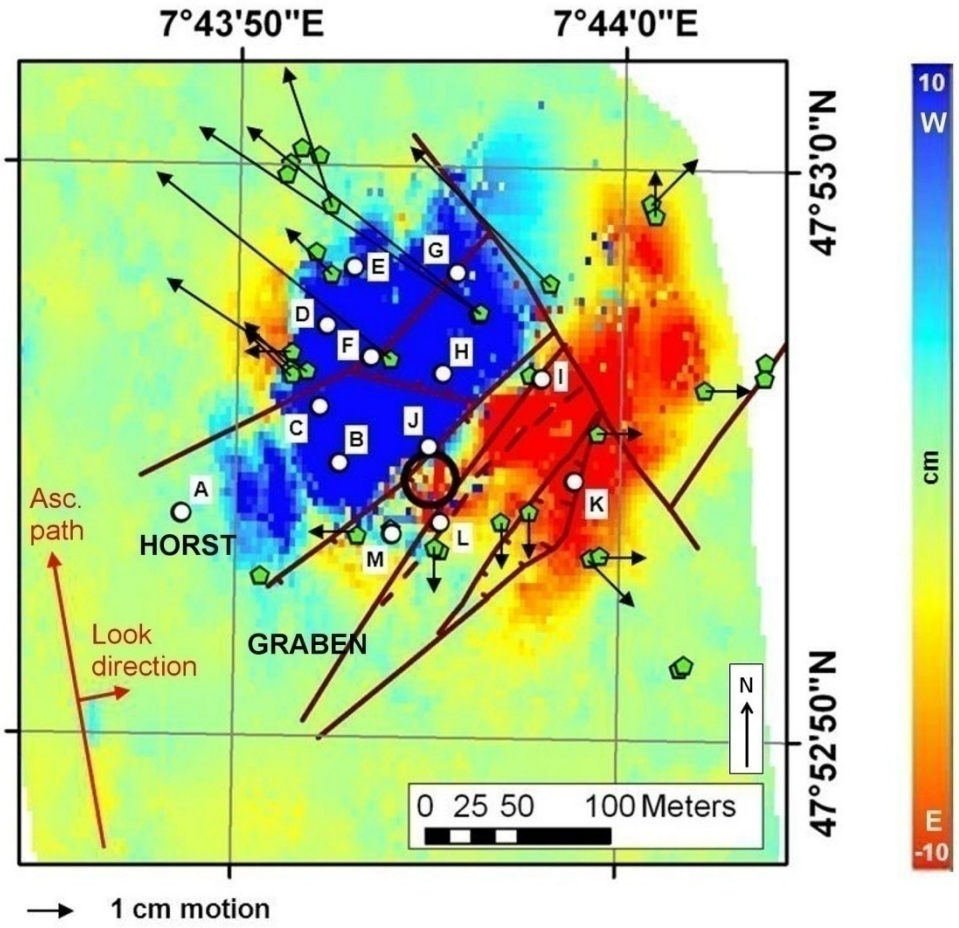

Fig. 3.7: Indication of horizontal motions in approximately east- (red) and westward (blue) direction that is revealed by subtracting interpolated cumulative Small BAselines Subset (SBAS) line of sight (LOS) displacement and interpolated leveling results of the 2008–2011 period from [3]. Ascending orbit path and eastward look-direction (range) are displayed. Green filled pentagons show locations of survey points, for which annual dislocation measurements are performed. Arrows display horizontal motions for the period from 26 September 2011 through 7 October 2013. Local faults at 50 m depth (brown line features) as detected by the National Agency for Geology, Resources and Mining (LGRB) were added. The locations, whose time series are presented in Fig. 3.6, are marked with white filled cycles.

3.5.2.2 Evidence from Ascending and Descending Data Processing

Comparing Fig. 3.3(a,b), we observe a further extension of the displacement area to the east in the descending result. This observation can be explained in part by the different acquisition geometries of the two orbit paths (eastward and westward look direction, look angles of 39.7° and 36.1° for ascending and descending data, respectively) and by the orientation of the surface objects that scatter the radar signal back to the antenna. The influence of the object orientation may be evidenced by an increased number of SDFP pixels in the descending result, although the shorter time span (9 months) and in consequence a smaller descending dataset is also a reasonable explanation for a higher amount of SDFP pixels. Approximately 1.66 times more SDFP pixels were found by the time series analysis in the descending data than in the ascending data (21,474 versus 12,943).
Although different acquisition geometries cause small variations in the pattern of displacement obtained from using ascending and descending data, the overall pattern in both results is similar to each other. This demonstrates that the vertical process is dominant in Staufen. However, the contribution from horizontal displacement as discussed in the previous section make slight differences between ascending and descending results.

Subtraction of interpolated SBAS LOS results from interpolated leveling data for the 2008–2011 period (Fig. 3.7) shows a pattern that is divided into an approximately westward (blue) and an eastward motion field (red) separated along a roughly NE-SW axis. This orientation agrees with the overall displacement field orientation and represents the consequent horizontal motion of a surface bulge. Interestingly, the westward motion occurs at the horst and the eastward motion at the graben block. Dislocation measurements at several survey points confirm this pattern for the later period from 26 September 2011 through 7 October 2013 as highlighted with arrows in Fig. 3.7, showing the difference map between leveling and InSAR data from the ascending orbit.

In order to assess the pattern observed in Fig. 3.7,we also compute horizontal motions by combining LOS displacements from ascending and descending SAR data. The common period covers approximately nine months, from 9 October 2012 through 11 July 2013. The magnitudes of SBAS derived displacements are similar for both datasets, with maximum of 2.4 cm for descending and 2.8 cm for ascending measurements. Data gaps in both ascending and descending results occur due to temporal decorrelation of the signal in vegetated areas (not shown here). To avoid noisiness or misinterpretation due to interpolation, we decided to consider only the measured point information. Hence, we have chosen the ascending SDFP locations to be the locations of interest and therefore computed a descending value at those positions by taking the mean of all descending SDFP values within a search window of 30 m by 30 m with the ascending SDFP location being the center point.

Horizontal motions were obtained by conducting the LOS decomposition [25,26] that takes into account the satellite heading (α) and look angles (ϑ) of the ascending (α_{asc}= 350.05°, ϑ_{asc} = 39.7°) and descending (α_{desc} = 190.45°, ϑ_{desc} = 36.1°) acquisitions. Applying [25]:

$$d_{LOS} = \cos(\theta) d_V - \sin(\theta)\cos(\alpha) d_E + \sin(\theta)\sin(\alpha) d_N \quad (2)$$

the sensitivity decomposition of LOS displacement for ascending data is *[0.77 − 0.63 − 0.11]* $[d_V, d_E, d_N]^T$ and for descending data *[0.81 0.58− 0.11]* $[d_V, d_E, d_N]^T$. It shows that the east-west (d_E) motion sensitivity for both orbit paths is considerably large compared to the north-south (d_N) sensitivity and of similar relevance as the vertical motion (d_V). Due to near-polar orbit and right-looking viewing geometry of the sensor, north-south sensitivity is lowest in InSAR measurements. Therefore, we only focus on decomposing east-west and vertical motion by solving the linear system of equations. The results d_V and d_E are presented in Fig. 3.8(a,b), respectively.

Having a closer look at the east-west component (Fig. 3.8(b)), the motion pattern is divided into two opposed parts following the expectations of the surface bulge's expansion. Oriented in NE-SW direction, the deformation area is expected to experience horizontal motion westwards for the northwestern part and an eastward horizontal motion for the southeastern part. The magnitudes reach up to 1 cm for the eastward motion (positive values) and 1.4 cm for the westward motion (negative values). Annually performed dislocation measurements at survey points revealed maximal values for eastward and westward motion of 1 cm and 3 cm, respectively, from 9 November 2012 through 7 October 2013. Comparing these measurements with decomposed maxima (slightly different periods), we find comparable values for eastward motion and underestimation of westward motion (Fig. 3.8(b)) by applying LOS decomposition. Although not comparable according to the magnitudes, the spatial distribution of horizontal motions of the nine-month-period is similar to the pattern derived by subtracting leveling information from 2008–2011 ascending SBAS result as shown in Fig. 3.7.

It is worth noting that applying a forward model by using the best-fit Okada solution for the period 2 June 2011 through 11 July 2013 (source parameters from Table 3.2) provides a modeled surface displacement field that also can be decomposed into all three directions and hence help for better understanding of horizontal motions. For comparison with the LOS decomposed results, the vertical and east-west components are shown in Fig. 3.8(c,d), respectively. Although the modeled motion patterns represent a longer period, a pronounced similarity can be observed between Fig. 3.8(a,c,b,d), respectively, which provides another evidence for the contribution of horizontal displacement to the overall deformation phenomenon operative in Staufen.

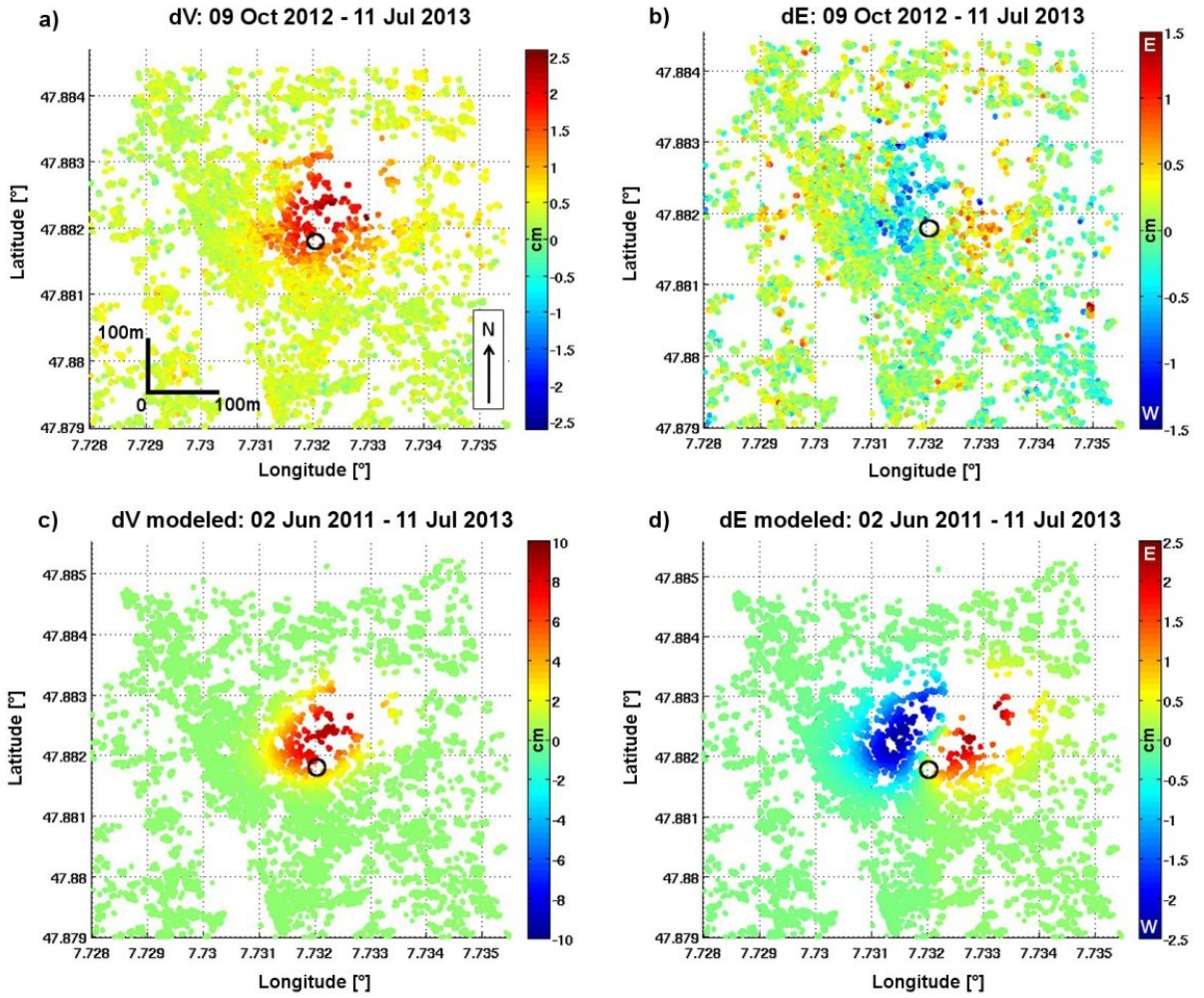

Fig. 3.8: (a) Vertical and (b) horizontal east-west motion contributions derived from line of sight (LOS) decomposition of ascending and descending SBAS results for the period 9 October 2012 through 11 July 2013. Estimated vertical (c) and east-west (d) motion from Okada modeling for the period 2 June 2011 through 11 July 2013 for comparison purposes. The black circle indicates the drilling site.

Although there is the potential issue of small-scale sinkholes due to water-driven dissolution of the recently formed gypsum (karstification) [3–4], we currently do not see any evidence in the new data that was analyzed in the present work. The InSAR results from both ascending and descending orbits do not show any subsidence, when considered individually and in combined analysis (vertical motion component dV based on LOS decomposition (Fig. 3.8(a)).

3.5.3 Model Evaluation

Although the source model used in this study is simple, the estimated source characteristics (Table 3.2) appear to infer well some parameters obtained independently with geophysical investigations. The estimated source depth of 51 m ± 6 m (mean of inversion results of ascending data) from single-data inversion represents a shallow source located several meters above the upper anhydrite layer at 61.5 m depth, as obtained from core sample analyses of the well drilling EKB2, which is directly located within the drilling field of the geothermal probes (Fig. 3.1(b)). The analysis of the excavation well BB3, which is located about 30 m east of the city hall revealed the upper anhydrite layer to be at 73.5 m depth [2]. By considering spatial variations of the depth of the upper anhydrite layer and the simplicity of the model, the estimated depth of the dislocation source

represents the opening process to be operative close to the upper anhydrite layer based on single-data inversion (Fig. 3.9(d)). The combined inversion of ascending and descending data leads to a source depth estimation of 89 m ± 9 m, which represents a depth within the interval of swellable region (61.5 m and 99.5 m below ground level) as assumed by LGRB [1]. Discussion about the estimated depth of a modeled source requires considering the trade-off between source strength and its depth. A deep and strong source can lead to the same surface deformation as a weak and shallow source [23]. Fixing the depth of the source to the upper anhydrite layer of the EKB2 well sample (61 m below ground level) for single-data inversion leads to an increase of source opening of 102% for the period 2008–2011 (56 cm vs. 113 cm). However, this will not affect the decrease in time for the amount of relative opening as shown in Table 3.2.

The situation, however, is quite complex. As anhydrite occurs as lenses, one could conclude multiple sources in combined action leading to the observed signal at the surface. This is hard to model as the deformation is localized and in consequence a single source model, despite being simple, was considered as an adequate first-order representation of the subsurface behavior.

The occurrence of residuals between modeled surface displacements due to a single pressure source and SBAS observations (Fig. 3.4, right column) may partly indicate the described source complexity. Moreover, as mentioned in Section 3.3.2, the applied model does not include factors such as local geological structures, surface topography or crustal layering, which all can account for residual occurrence. Surface topography in terms of steep slopes can significantly influence modeled source geometry and depth leading to misinterpretation of deformation as Cayol and Cornet [27] have described for volcano deformations. As our study area is generally flat, this impact has not been considered in our source estimation. Influencing topographic effects can be related to urban features, which we considered by using a high-resolution LiDAR-DEM to remove the topographic phase contribution from the signal.

Figure 3.9(a) shows an orthophoto of the historical city center of Staufen overprinted with local faults located 50 m below ground level that were derived from LGRB investigations. To better investigate the residual pattern derived from modeling, we plot the residuals of the period from 22 July 2008 through 22 May 2011 in Fig. 3.9(b) and show a profile in NW-SE direction across the residuals with cross sections of the faults (Fig. 3.9(c)). The residual plot and profile show spatial correlation with geological blocks that are separated by faults, in particular of the graben block S and SE of the drilling zone (see profile between 225 m and 250 m distance).

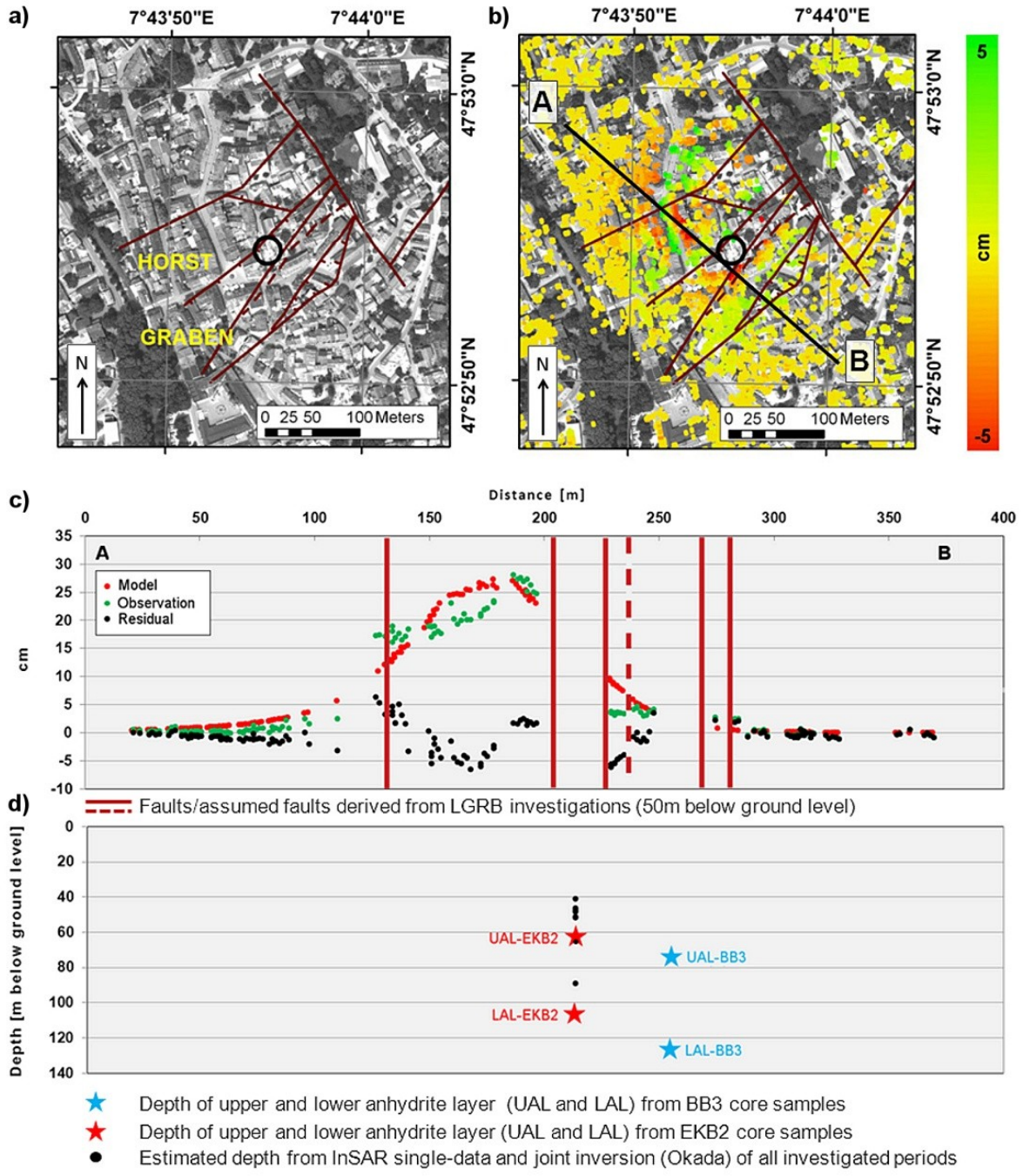

Fig. 3.9: (a) Orthophoto of the city center of Staufen (acquired by the State Survey Office Baden-Württemberg) overprinted with faults at 50 m below ground level derived from investigations of the National Agency for Geology, Resources and Mining (LGRB). (b) Residuals between observation and model for the period from 22 July 2008 through 22 May 2011 (Fig. 3.4(d)) were added to the orthophoto that is shown in 9(a). The black circle shows the location of the drilling area. (c) Model, observation and residual values (in cm) for the period from 22 July 2008 through 22 May 2011 along the profile AB that is presented in 9(b) with cross sections of the faults. (d) Sketch of estimated source depth from Synthetic Aperture Radar Interferometry (InSAR) inversion (single and joint inversion) compared to upper and lower anhydrite layer boundaries known from core sample analysis of the boreholes EKB2 and BB3. The location is not with respect to the profile, but related to the corresponding geological block.

Heterogeneous geological conditions as for example different anhydrite concentrations and varying rock masses can cause different swelling pressures at the surface [5], which cannot be predicted by our single source model. In addition, correlation with building locations and orientations, in particular NW of the drilling zone, are observable when comparing Fig. 3.9(a,b). Different building

foundations and loads react differently to subsurface opening process, and hence different building stresses can influence the detectable surface deformation. For further information the reader is referred to [5]. Both heterogeneous geology (complex source situation) and building stress may explain the residuals between model and observation. Moreover, the assumed elastic character of the model is restricted here, in that the damages at the buildings are permanent and consequently non-elastic.
As there exists a potential relation between residuals and geological features, we recommend a detailed seismic monitoring or a transect of permanent GPS stations across the faults (from NW to SE) to assess their potential kinematics. The development of a complex hydro-mechanical model including not only different strata (material properties), faults and ground water levels, but also the possibility of several interacting swelling sources (anhydrite lenses) is suggested as potential future work.

3.6 Conclusions

In this study, we have focused on extending the knowledge about the remarkable urban uplift in Staufen by a combined analysis of TerraSAR-X images from both ascending and descending orbits. Interferometric time series analysis of spaceborne Synthetic Aperture Radar (InSAR) imagery confirms deceleration of uplift as measured with terrestrial surveying techniques [1–2]. Within the area of maximum deformation NNE of the drilling zone, we found a reduction of the annual cumulative line of sight uplift of up to 78% when comparing the periods July 2008–July 2009 and July 2012–July 2013.
Although uplift is the dominant process, the decomposed horizontal motions for the common nine-month period of ascending and descending data (October 2012 through July 2013) demonstrate significant east- and westward motions (up to 1.4 cm in westward and up to 1 cm in eastward direction) in an approximately symmetric pattern along the horst-graben boundary. Inversion of ascending and descending InSAR data individually suggest a shallow horizontal rectangular source with length ranging between 164 m and 175 m, width ranging between 51 m and 101 m and depth between 45 m and 63 m. Performing a joint inversion of both datasets of the period October 2012 through July 2013 results in length, width and depth of 177 m ± 19 m, 69 m ± 15 m and 89 m ± 9 m, respectively. Although the single-data inversion provides a good fit to the observation, the source depth resulted by joint inversion agrees more closely with the depth of swellable region inferred from independent core sample analysis. The strength of the source (the amount of relative opening) varies in time and shows a decrease by a factor of 3.5 when comparing the periods before counteraction in autumn 2009 and after permanent implementation in spring 2011. The amount of opening at depth has reduced by 71% for period 2011/2012 as compared to period 2008/2009. Although the model adopted in this paper is a well-fitted first-order approximation, residuals between model and observation indicate potential influences of varying building stresses and fault kinematics. More geophysical investigations are required for their assessment and to also better resolve for additional deformation sources that may account for the complex subsurface situation.

3.7 Acknowledgments

This study was supported by the Initiative and Networking Fund of the Helmholtz Association in the frame of Helmholtz Alliance “Remote Sensing and Earth System Dynamics”. The data from leveling and dislocation measurements have been provided by the Landratsamt Breisgau Hochschwarzwald, office Müllheim, under permission of the city council of Staufen im Breisgau. All TerraSAR-X data are kindly provided by DLR under proposal GEO0717. Special thanks go to Pegah Faegh-Lashgary for providing Matlab scripts for the Bayesian analysis. The authors also express their gratitude to reviewers, whose comments and suggestions greatly improved the quality of the manuscript.

Author Contributions

All authors contributed equally to the work with ideas, interpretations and discussions. Christin Lubitz processed the SAR data and wrote the manuscript, Mahdi Motagh contributed to the modeling, data interpretation and manuscript revision, and Hermann Kaufmann supervised the work. All authors read and approved the final manuscript.

Conflicts of Interest

The authors declare no conflict of interest.

3.8 References

[1] Geologische Untersuchungen von Baugrundhebungen im Bereich des Erdwärmesondenfeldes beim Rathaus in der historischen Altstadt von Staufen i. Br.; LGRB Landesamt für Geologie, Bergbau und Rohstoffe Baden-Württemberg: Regierungspräsidium Freiburg, Germany, 2010.

[2] Zweiter Sachstandsbericht zu den seit dem 01.03.2010 erfolgten Untersuchungen im Bereich des Erdwärmesondenfeldes beim Rathaus in der historischen Altstadt von Staufen i. Br.; LGRB Landesamt für Geologie, Bergbau und Rohstoffe Baden-Württemberg: Regierungspräsidium Freiburg, Germany, 2012.

[3] Lubitz, C.; Motagh, M.; Wetzel, H.-U.; Kaufmann, H. Remarkable urban uplift in Staufen im Breisgau, Germany: Observations from TerraSAR-X InSAR and leveling from 2008 to 2011. Remote Sens. 2013, 5, 3082–3100.

[4] Sass, I.; Burbaum, U. Damage to the historic town of Staufen (Germany) caused by geothermal drillings through anhydrite-bearing formations. Acta Carsologica 2010, 39, 233–245.

[5] Sass, I.; Burbaum, U. Geothermische Bohrungen in Staufen im Breisgau: Schadensursachen und Perspektiven. Geotechnik 2012, 35, 198–205.

[6] Frühere Schlossberg-Wäscherei wurde abgerissen. Available online: www.staufen.de/ aktuelles-nachrichten/hebungsrisse/fruehere-schlossberg-waescherei-wurde-abgerissen-~164934/ (accessed on 4 December 2013).

[7] Okada, Y. Surface deformation due to shear and tensile faults in a half-space. Bull. Seismol. Soc. Am. 1985, 75, 1135–1154.

[8] Hebungsrisse: Runder Tisch vom 14.01.2013. Available online: www.staufen.de/ aktuelles-nachrichten/hebungsrisse/protokolle-runder-tisch/hebungsrisse-runder-tisch-~164899/ (accessed on 25 October 2013).

[9] Hooper, A. A multi-temporal InSAR method incorporating both persistent scatterer and small baseline approaches. Geophys. Res. Lett. 2008, 35, doi:10.1029/2008GL034654.

[10] Kampes, B.M.; Hanssen, R.F.; Perski, Z. Radar interferometry with public domain tools. In Proceedings of The Third International Workshop on ERS SAR Interferometry, Frascati, Italy, 1–5 December 2003.

[11] Berardino, P.; Fornaro, G.; Lanari, R.; Sansosti, E. A new algorithm for surface deformation monitoring based on small baseline differential SAR interferograms. IEEE Trans. Geosci. Remote Sens. 2002, 40, 2375–2383.

[12] Lanari, R.; Mora, O.; Manunta, M.; Mallorquí, J.J.; Berardino, P.; Sansosti, E. A small-baseline approach for investigating deformations on full-resolution differential SAR interferograms. IEEE Trans. Geosci. Remote Sens. 2004, 42, 1377–1386.

[13] Anderssohn, J.; Motagh, M.; Walter, T.R.; Rosenau, M.; Kaufmann, H.; Oncken, O. Surface deformation time series and source modeling for a volcanic complex system based on satellite wide swath and image mode interferometry: The Lazufre system, central Andes. Remote Sens. Environ. 2009, 113, 2062–2075.

[14] Motagh, M.; Wang, R.; Walter, T.R.; Bürgmann, R.; Fielding, E.; Anderssohn, J.; Zschau, J. Coseismic slip model of the 2007 August Pisco earthquake (Peru) as constrained by Wide Swath radar observations. Geophys. J. Int. 2008, 174, 842–848.

[15] Stramondo, S.; Moro, M.; Tolomei, C.; Cinti, F.R.; Doumaz, F. InSAR surface displacement field and fault modelling for the 2003 Bam earthquake (southeastern Iran). J. Geodyn. 2005, 40, 347–353.

[16] Pedersen, R.; Jónsson, S.; Árnadóttir, T.; Sigmundsson, F.; Feigl, K.L. Fault slip distribution of two June 2000 Mw 6.5 earthquakes in South Iceland estimated from joint inversion of InSAR and GPS measurements. Earth Planet. Sci. Lett. 2003, 213, 487–502.

[17] Sambridge, M.; Mosegaard, K. Monte carlo methods in geophysical inverse problems. Rev. Geophys. 2002, 40, doi: 10.1029/2000RG000089.

[18] Faegh-Lashgary, P.; Motagh, M.; Sharifi, M.-A.; Saradjian, M.-R. Source parameters of the September 10, 2008 Qeshem Earthquake in Iran inferred from the bayesian inversion of

Envisat and ALOS InSAR observations. In VII Hotine-Marussi Symposium on Mathematical Geodesy, International Association of Geodesy Symposia; Sneeuw, N., Novák, P., Crespi, M., Sansò, F., Eds.; Springer-Verlag: Berlin/Heidelberg, Germany, 2012; Volume 137, pp. 319–325.
[19] Lee, F.T.; Abel, J.F., Jr. Subsidence from underground mining: Environmental analysis and planning considerations. In Publications of the Geological Survey, 1983; U.S. Geological Survey: Reston, VA, USA, 1983; p. 28.
[20] Whittaker, B.N.; Reddish, D.J. Subsidence–Occurrence, Prediction and Control; Elsevier Science Publishers B.V.: Amsterdam, The Netherlands, 1989.
[21] Yao, X.L.; Whittaker, B.N.; Reddish, D.J. Influence of overburden mass behavioural properties on subsidence limit characteristics. Min. Sci. Technol. 1991, 13, 167–173.
[22] Singh, K.B.; Singh, T.N. Ground movements over longwall workings in the Kamptee coalfield, India. Eng. Geol. 1998, 50, 125–139.
[23] Pritchard, M.E.; Simons, M. An InSAR-based survey of volcano deformation in the central Andes. Geochem. Geophys. Geosystems 2007, 5, doi:10.1029/2003GC000610.
[24] Hernandez-Marin, M.; Burbey, T.J. The role of faulting on surface deformation patterns from pumping-induced groundwater flow (Las Vegas Valley, USA). Hydrogeol. J. 2009, 17, 1859–1875.
[25] Hanssen, R.F. Radar Interferometry—Data Interpretation and Error Analysis, 2nd ed.; van der Meer, F., Ed.; Kluwer Academic Publishers: Dordrecht, The Netherlands, 2001.
[26] Samieie-Esfahany, S.; Hanssen, R.F.; van Thienen-Visser, K.; Muntendam-Bos, A. On the effect of horizontal deformation on InSAR subsidence estimates. In Proceedings of The Fringe 2009 Workshop, Frascati, Italy, 30 November–4 December 2009.
[27] Cayol, V.; Cornet, F.H. Effects of topography on the interpretation of the deformation field of prominent volcanoes—Application to Etna. Geophys. Res. Lett. 1998, 25, 1979–1982.

4. Chapter: Integrated Assessment of Ground Surface Displacements at the Ketzin Pilot Site for CO_2 Storage by Satellite-based Measurements and Hydromechanical Simulations (submitted to IEEE Journal of Selected Topics in Applied Earth Observations and Remote Sensing, in December 2017)

Christin Lubitz*[1], Thomas Kempka[2] and Mahdi Motagh[1,3]

[1] GFZ German Research Centre for Geosciences, Telegrafenberg, D-14733 Potsdam, Germany, Section 1.4 Remote Sensing
[2] GFZ German Research Centre for Geosciences, Telegrafenberg, D-14733 Potsdam, Germany, Section 3.4 Fluid Systems Modelling
[3] Institute of Photogrammetry and GeoInformation, Leibniz University Hannover, 30167 Hannover, Germany

***** Author to whom correspondence should be addressed; E-Mail: chlubitz@gfz-potsdam.de; Tel.: +49-331-288-28621; Fax: +49-331-288-1192.

Received: 13 December 2017

Abstract

There has been growing interests in recent years for safe underground storage of carbon dioxide (CO_2) as a potential technology for preventing this greenhouse gas from entering into the atmosphere. As suitable locations for geological storage may be diverse in many kinds, the applicability of various geodetic and geophysical methods for surveillance and monitoring purposes must be investigated. In this research we evaluate ground surface displacement at the Ketzin pilot site for CO_2 storage in Germany, using satellite-based measurements and hydromechanical simulations.
InSAR observations, using more than 4 years of TerraSAR-X data from 2009 to 2013, reflect the stability of the Ketzin pilot site (long-term velocity <0.5 mm/y) in conjunction with accumulated CO_2 volume in the reservoir. This can be due to the low overall pressure change with a maximum of 16 bar that is not causing significant surface displacement. However, such overall stability can be interrupted temporally as detected within the InSAR time series for a distinct period of injection stop from May to December 2012 (subsidence of 2.8 mm). This is supported by our hydromechanical simulation results, exhibiting a maximum ground surface subsidence of about 1 mm during this period, and comparison with variations in bottomhole pressure, indicating a positive correlation of 80%.

Index Terms: Interferometry, Radar data processing, Synthetic aperture radar, Time series

4.1 Introduction

Synthetic Aperture Radar Interferometry (InSAR) techniques have become valuable to detect, monitor and analyze surface displacements directly or indirectly associated with fluid or gas injection or extraction. The Krechba gas field at In Salah, Algeria, is a well-known example for the Carbon Capture and Storage (CCS) technology and has been intensively explored [1]. Based on C-band Envisat ASAR images Onuma and Ohkawa [2] used classical Differential InSAR (D-InSAR) and interferogram stacking to monitor surface displacements from 2003-2008 that were spatially correlated with the locations of gas extraction (subsidence rate 4 mm/y) and re-injection (uplift rate 7 mm/y) of the Carbon Dioxide (CO_2). Vasco et al. [3] applied the Permanent Scatterer technique [4] on the same site and found uplift rates of 5 mm/y for the period from 2003-2007. It was the first test site for InSAR-based monitoring of CO_2 and represents the ideal case study, because the local rocky desert conditions (no vegetation, dry weather) prevent temporal SAR signal decorrelation, which is one of the main issues in Multi-Temporal InSAR (MT-InSAR). Kuehn et al. [5] summarized their experience by applying the Interferometric Point Target Analysis (IPTA, [6]) on C-band data of ERS-1, ERS-2 and Envisat ASAR to observe gas storage within Berlin city, Germany. This study clearly shows the potential of the method within urban areas to measure the gas storage related uplift with maximum circular area being about 1.5 km in diameter and uplift values >3 cm from 1992-2005. A recent study by Yang et al. [7] presents a significant uplift (about 10 cm in Line Of Sight (LOS) from 2007-2011) due to CO_2 injection at an enhanced oil recovery site in Texas, USA, measured by the Japanese L-band SAR satellite ALOS and derived by using the Small Baseline Subset approach [8].
The herewith presented field of application for MT-InSAR has risen with increasing relevance of greenhouse gas emission reduction and development of suitable technologies to store CO_2 in the underground. As of November 2014, the National Energy Technology Laboratory lists 274 projects worldwide that deal with carbon capture, carbon storage or CCS, 128 of them are actively running [9]. Due to injection of fluids in the subsurface and related pressure increase within the reservoir, deformation can occur that should be monitored carefully. Such observations can be used to constrain geomechanical models, e.g. as done for the In Salah CCS site [10]. Furthermore, precise delineation of surface displacements associated with unplanned subsurface pressure changes is highly important when they cause damages at above ground infrastructure and potentially risk human health in inhabited regions [11]. Such local environment occurrence can increase with increasing international demand on carbon storage.
C-band and L-band SAR data as well as several different InSAR methods were used in the examples mentioned above. In this study, the first European onshore pilot site for geological CO_2 storage that is located close to Ketzin, Germany, is investigated with respect to its suitability for InSAR-based surface displacement surveillance based on X-band data. Both Persistent Scatterer Interferometry (PSI) and the Small Baseline Subset (SBAS) approach as implemented in the non-commercial StaMPS software [12-14] were tested to evaluate their performance in this case. The pilot project on subsurface CO_2 storage at Ketzin comprises a comprehensive monitoring program, but lacks any ground-based surveys for potential displacement monitoring related to the injection. Hence, an InSAR analysis in this case may be a reasonable monitoring solution, although reference data for validation are missing. Due to this fact, the derived time series are compared with data from bottomhole pressure observations in the CO_2 injection well and with ground surface displacements calculated by using calibrated hydromechanical simulations.

4.2 Ketzin Pilot Site for CO_2 Storage

The Ketzin pilot site for geological CO_2 storage is situated in close distance to the city Ketzin, which is located approximately 25 km west of Berlin (Germany, Fig. 4.1(a)). Seasonally used as gas storage reservoir for town gas from the 1960s until 2004 [15], this site was already well explored before the CO_2 storage operation started. The town gas was stored in the Lower Jurassic strata at about 280 m depth, while CO_2 storage has been conducted in the fluviatile sandstone channels of the Upper

Triassic Stuttgart Formation, located at 630 m to 650 m depth. A multi-barrier-system of low-permeable mudstones, siltstones and anhydrites characterizes the caprocks, preventing CO_2 leakage into shallow strata (Fig. 4.1(b)) [16-17]. Figure 4.1(c) shows the strata sequence at the pilot site explored in 2007 from borehole logging at the Ktzi 200 well.

This geological setting was chosen to implement the first European onshore pilot project for subsurface CO_2 storage. The overall research at the pilot site aims at detailed monitoring and modeling of hydrological, geochemical, and geophysical processes associated with geological CO_2 storage to improve the understanding of the behavior of CO_2 injected into a saline aquifer during the entire site lifecycle. Furthermore, the investigation shall clarify whether a safe and sustainable storage of CO_2 is feasible without any risks for humans, health and environment [18]. This comprehensive research has been funded in the scope of different projects focusing on different aspects of the geological CO_2 storage [19-21]. In the period from June 2008 until August 2013 about 67 kt CO_2 were injected into the Stuttgart Formation.

In the course of the research activities, facilities required for the injection and monitoring of CO_2 as well as a visitor center were built. Figure 4.2 shows several aerial photographs of the pilot site through time with its surface infrastructure. Figure 4.2(a) is from 2011 showing the drilling of the observation well P300 in the upper right part, whereas Fig. 4.2(b) shows the drilling of the observation well Ktzi 203 in 2012 at the left side of the image. Further, Fig. 4.2(c) provides an impression of the pilot site at its last stage, the post-injection and post-closure phase in 2016, where most of the above ground facilities have already been removed. The two gas tanks that are clearly visible in Fig. 4.2(a,b) were used for the intermediate storage of CO_2. In their close vicinity, the injection facility is located, including ambient air heaters and pumps required for CO_2 injection. CO_2 is then transported via a short pipeline to the wellhead of the Ktzi 201 well (left side of the image 4.2(a)).

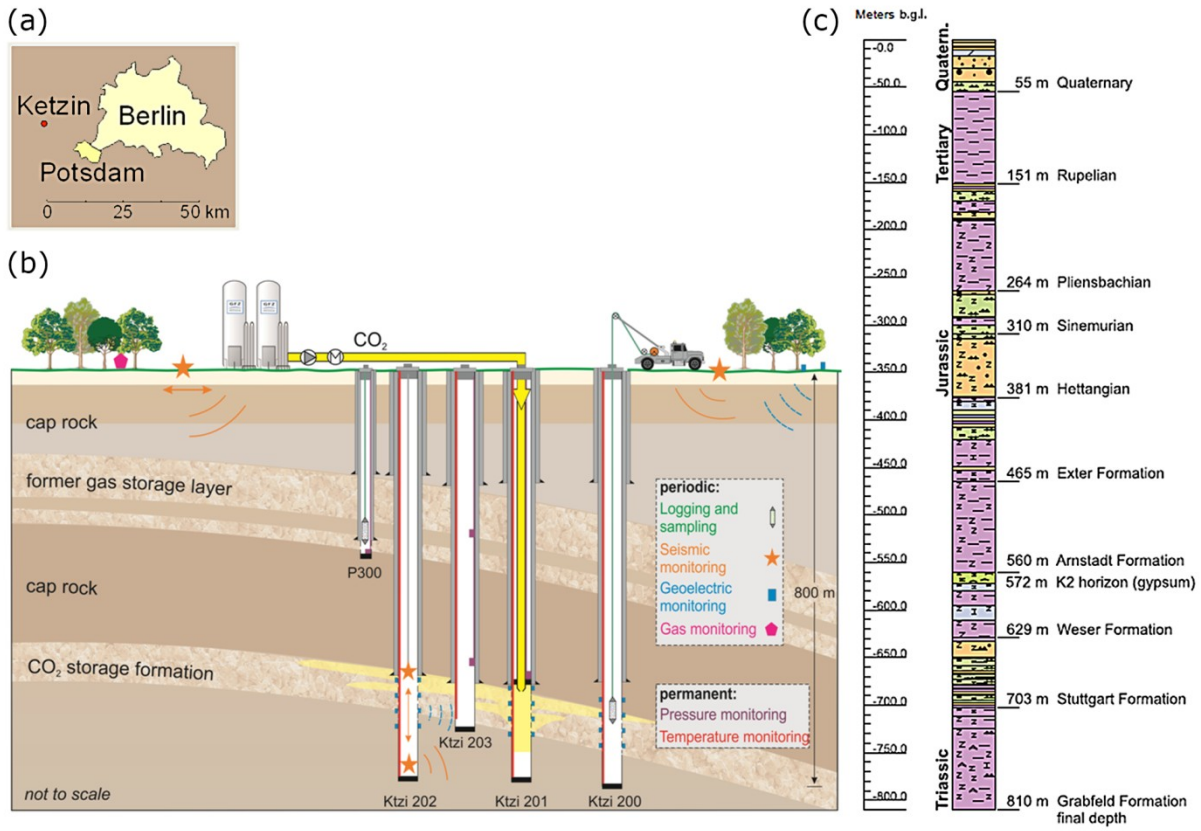

Fig. 4.1: (a) Overview map [18]. (b) Schematic illustration of the gas storage layers, injection and observation wells Ktzi 200, Ktzi 201, Ktzi 202, Ktzi 203 and P 300 as well as several measurement setups [adjusted after 18]. (c) Geological profile of Ktzi 200 well with the following lithology: mudstone (magenta), siltstone (green), sandstone (yellow) and anhydrite (light blue) [22].

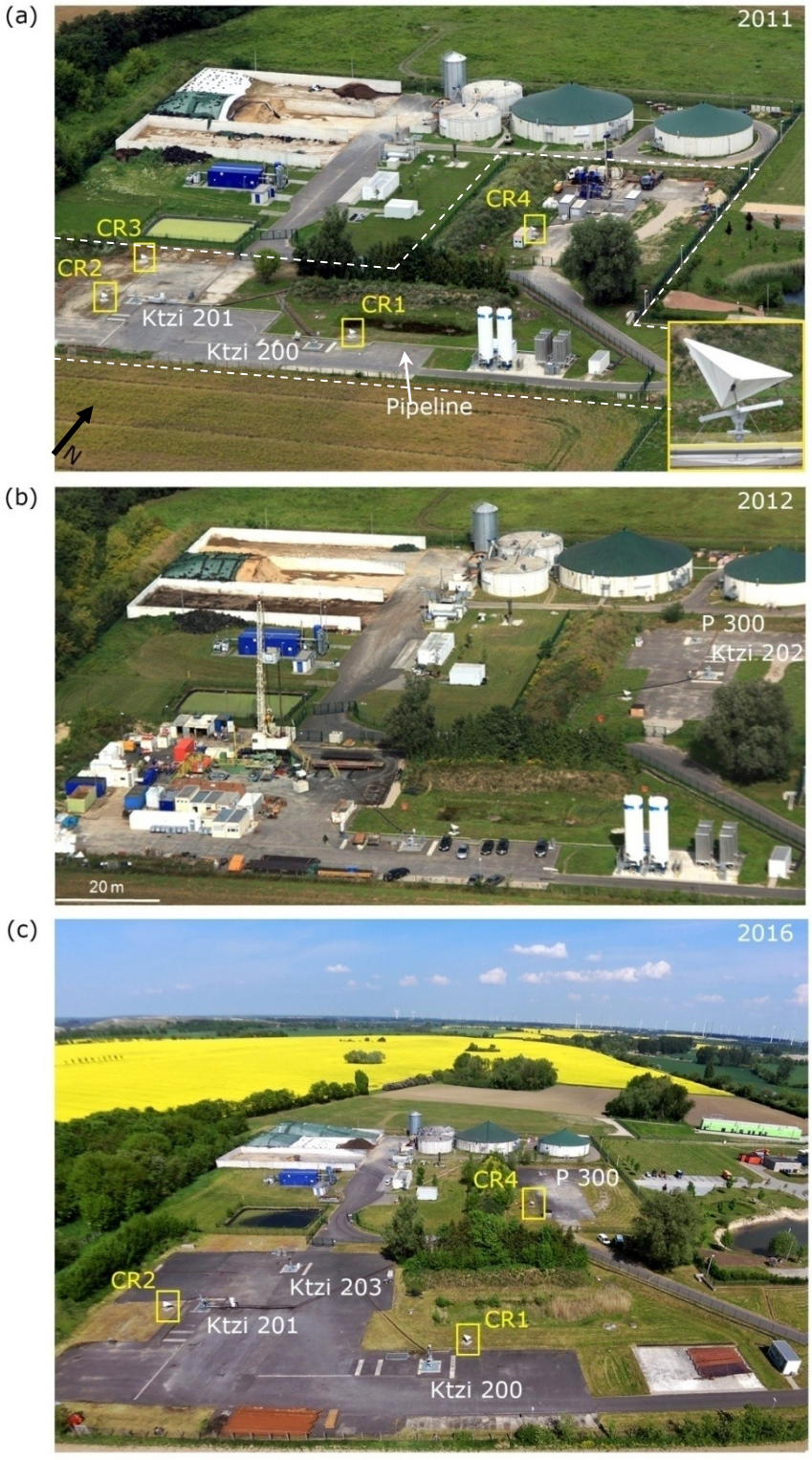

Fig. 4.2: Aerial photographs (a) and (b) were taken from airplane [M. Ludwig, GFZ] and (c) from a hexacopter [http://www.co2ketzin.de/en/media.html] over the Ketzin test site that is roughly marked in (a) with a white dashed contour. The location and identification numbers of the corner reflectors are highlighted by yellow frames. The labels for the injection well Ktzi 201 and all observation wells Ktzi 200, Ktzi 202, Ktzi 203 and P 300 are presented in all images when clearly visible. CR3 was removed and Ktzi 202 was back-filled and abandoned, therefore they are not shown in (c) anymore.

These surface facilities are essential for the application of InSAR time series techniques in vegetated regions as they serve as stable scatterers for the microwaves transmitted by the SAR sensor. Without such, there would be nearly no information content that could be analyzed over time in such a region. As the pilot site is located in an agricultural setting with varying states of field crops through the year and seasonal variations of vegetation, natural long-term stable scatterers are missing, and hence, artificial objects are required. The nearby bio-gas facility provides further objects that scatter the SAR signals (northward of the pilot site in Fig. 4.2(a-c)), and therefore enhances the information content about the desired area. Further support was expected by installation of four corner reflectors at strategic positions that scatter the transmitted signal back into its original direction. Oriented in satellite viewing direction, these corner reflectors are further fixed points for long-term monitoring of ground surface displacement at the pilot site. Their location is indicated in Fig. 4.2(a). All these scatterers allow indirect conclusions on surface motions by analyzing their behavior over time, but may also indicate their own structural instabilities. Overall interpretation of the local situation hence requires as many scatterers as possible and high resolution SAR images that map the area of interest.

4.3 Methodology

4.3.1 InSAR Analysis

MT-InSAR techniques have become an adequate alternative for geodetic surveys when large areal coverage is required instead of selected point-wise measurements by leveling or GPS that are labor-intensive, especially when long-term repetitive investigations are requested. InSAR limitations are mainly dependent on the data availability and on the region of interest, in detail its vegetation coverage, the land use changes and seasonal weather variations. The presented case study at the Ketzin pilot site combines all those limitations and is nonetheless intended to investigate the potential of the two main categories of MT-InSAR methods, PSI and SBAS, because suitable areas for CO_2 storage do not only occur at ideal regions for InSAR, but require surveillance.

4.3.1.1 TerraSAR-X Data

High-resolution image acquisition of the pilot site is conducted by the German twin satellites TerraSAR-X (TSX) and TanDEM-X (TDX) in Stripmap mode that record the region with about 3 m spatial resolution in azimuth (satellite's flight direction) and range (satellite's viewing direction). Data acquisition has started on 24 May 2009 for 4 ½ years until 29 November 2013. No TSX data exist from the period before and therefore the impact of storage on ground surface displacements cannot be assessed before May 2009. Potential signals from the acquired data need to be interpreted carefully, and only relatively and not absolutely.
Data acquisition occurred on regular basis every 11 days due to the satellite's orbit characteristics. Image recording was done until end of November 2013, that is several months after final injection. A larger data gap occurred from end of May until end of September 2011 that required the splitting of data processing into approximately two biennial periods. This data gap in the summer period prevented continuous monitoring using time series analysis. This is due to immediate change of vegetation in the growing season and strong agricultural activities that change the surface scattering leading to low coherence in X-band SAR interferograms. All together, 118 SAR images were acquired during the 4 ½ years of remote sensing observation, which were divided into two data sets: the first one (54 images) covers the period from 24 May 2009 through 31 May 2011 (two years) and the second one (64 images) covers the period from 29 September 2011 through 29 November 2013 (two years and two months).
The SAR images were acquired from a descending satellite orbit and one scene covers several tens of kilometers in range and azimuth. As the area of interest (pilot site) is comparably small with about

2.25 km² and in order to reduce computational costs, only a subset of the whole SAR image with 4000 by 4000 pixels with the pilot site in its centre was processed.

4.3.1.2 InSAR Time Series Analysis

By visual inspection, images showing a strongly deviating signal response through the year were initially removed from processing. They would prevent signal correlation that is required for time series analysis. Figure 4.3 shows a comparison of SAR amplitude images of the investigated area at different time steps. Here, mainly winter images are presented to exemplarily demonstrate the difference in their signal response compared to the summer image (4.3(c)). The most obvious variations occur along the Havel river and nearby lakes (black areas due to specular reflection of the transmitted signal at calm water areas) as radar signal response of water areas differs due to wind, freezing (Fig. 4.3(b,e)) and melting (Fig. 4.3(d)).

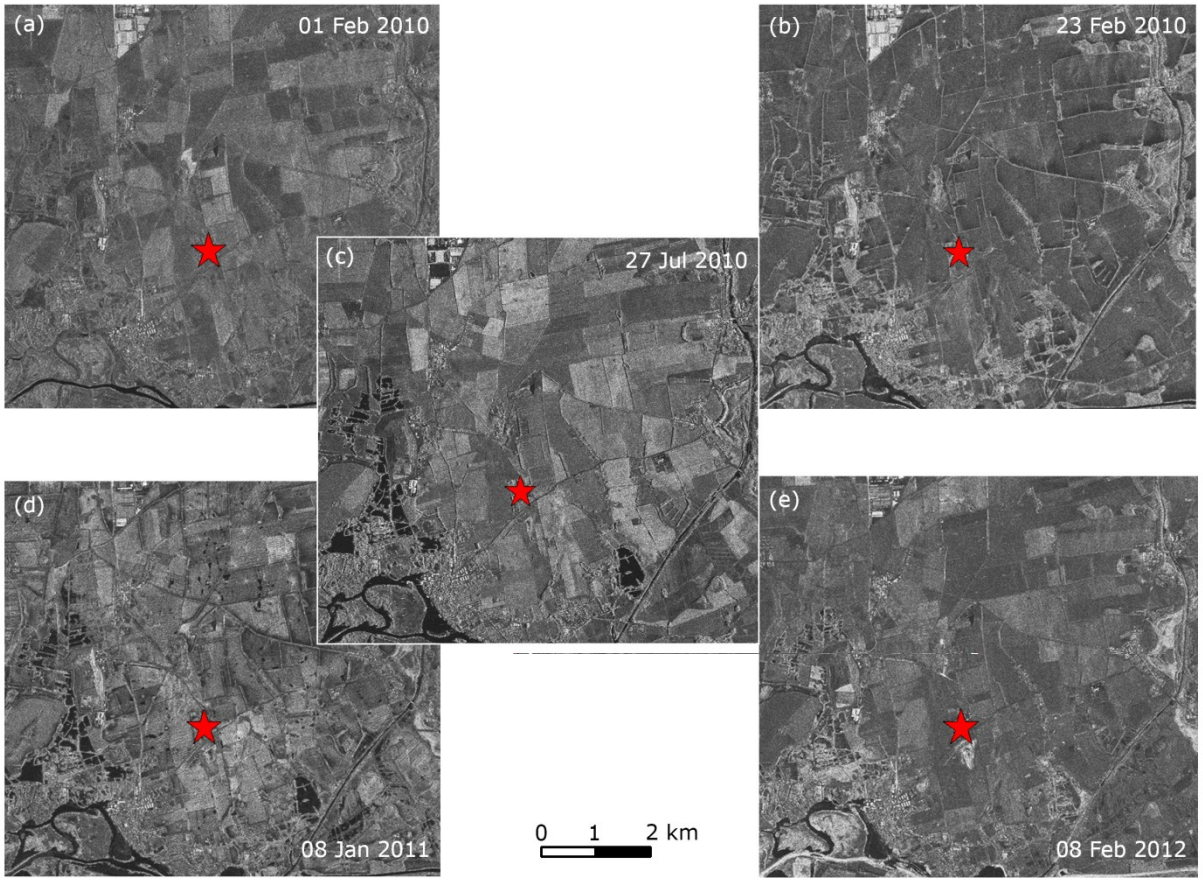

Fig. 4.3: Comparison of different SAR amplitude images of the investigated area. (a) Winter image with partly rough water areas visible when comparing with the summer image in (c) where all calm water surfaces appear black (left side of the image). (b) Winter image with strong surface scattering and partly frozen water areas (brighter shade of grey as compared to (a)). (d) Winter image showing melting phase (appearance of dot-like shapes on agricultural fields where frozen areas melted to puddles). (e) Winter image with a strong surface scatter due to snow and frozen areas. The red star highlights the Ketzin pilot site location.

Data set 1 (737 days)								
Date	$B_\perp$ (m)	B_T (days)	Date	$B_\perp$ (m)	B_T (days)	Date	$B_\perp$ (m)	B_T (days)
24 May 2009	142	-429	01 Feb 2010	-41	-176	20 Sep 2010	-39	55
04 Jun 2009	163	-41	12 Feb 2010	55	-165	23 Oct 2010	49	88
26 Jun 2009	59	-396	23 Feb 2010			03 Nov 2010	36	99
07 Jul 2009	24	-385	06 Mar 2010	-167	-143	14 Nov 2010	6	110
18 Jul 2009	3	-374	17 Mar 2010	90	-132	25 Nov 2010	79	121
29 Jul 2009	-133	-363	28 Mar 2010	166	-121	17 Dec 2010		
09 Aug 2009	219	-352	08 Apr 2010	-90	-110	28 Dec 2010	165	154
31 Aug 2009	-113	-330	30 Apr 2010			08 Jan 2011	106	165
22 Sep 2009	20	-308	22 May 2010	140	-66	30 Jan 2011	33	187
03 Oct 2009	-80	-297	02 Jun 2010	68	-55	04 Mar 2011	-90	220
14 Oct 2009	-69	-286	13 Jun 2010	205	-44	15 Mar 2011	2	231
25 Oct 2009	-156	-275	24 Jun 2010	89	-33	26 Mar 2011	-25	242
05 Nov 2009	142	-264	05 Jul 2010	-16	-22	17 Apr 2011	94	264
16 Nov 2009	128	-253	16 Jul 2010	-71	-11	28 Apr 2011	118	275
27 Nov 2009	179	-242	27 Jul 2010			09 May 2011	37	286
19 Dec 2009	172	-220	18 Aug 2010	-16	22	20 May 2011	99	297
30 Dec 2009	263	-209	29 Aug 2010	151	33	31 May 2011	107	308
21 Jan 2010	79	-187	09 Sep 2010	54	44	03 Jul 2011	39	341
Data set 2 (792 days)								
Date	$B_\perp$ (m)	B_T (days)	Date	$B_\perp$ (m)	B_T (days)	Date	$B_\perp$ (m)	B_T (days)
29 Sep 2011	122	-209	08 Jun 2012	54	44	05 Feb 2013	-76	286
10 Oct 2011	38	-198	19 Jun 2012	100	55	16 Feb 2013	-71	297
21 Oct 2011	35	-187	30 Jun 2012	107	66	27 Feb 2013	123	308
01 Nov 2011	132	-176	11 Jul 2012	-148	77	10 Mar 2013		
12 Nov 2011	164	-165	22 Jul 2012	201	88	21 Mar 2013		
04 Dec 2011	98	-143	02 Aug 2012	135	99	01 Apr 2013		
15 Dec 2011	94	-132	13 Aug 2012	79	110	12 Apr 2013	53	352
26 Dec 2011	271	-121	24 Aug 2012	-104	121	23 Apr 2013	-7	363
06 Jan 2012	101	-110	04 Sep 2012	-11	132	04 May 2013	15	374
17 Jan 2012	-16	-99	15 Sep 2012	86	143	15 May 2013	-59	385
28 Jan 2012			26 Sep 2012	-46	154	26 May 2013	63	396
08 Feb 2012			07 Oct 2012	177	165	17 Jun 2013	99	418
19 Feb 2012			18 Oct 2012	9	176	28 Jun 2013	68	429
01 Mar 2012	-101	-55	29 Oct 2012	181	187	09 Jul 2013	111	440
12 Mar 2012	-59	-44	09 Nov 2012	109	198	20 Jul 2013	129	451
23 Mar 2012	132	-33	20 Nov 2012	-45	209	13 Sep 2013	-222	495
03 Apr 2012	-43	-22	01 Dec 2012	220	220	05 Oct 2013	49	509
14 Apr 2012	16	-11	12 Dec 2012			27 Oct 2013	7	523
25 Apr 2012			23 Dec 2012			18 Nov 2013	-134	537
06 May 2012	45	11	03 Jan 2013	-3	253	29 Nov 2013	68	548
17 May 2012	12	22	14 Jan 2013					
28 May 2012	86	33	25 Jan 2013					

Table 4.1: Overview on acquired and processed data. Yellow dates are snow images that were excluded before InSAR processing. The red marked date represents the selected master image date for the PSI processing of the two individually analyzed data sets. The perpendicular ($B_\perp$) and temporal Baselines (B_T) according the PSI processing are also shown. Images of blue highlighted dates were included in PSI processing, but were excluded from SBAS processing due to bad coherence with other images or phase unwrapping issues.

After this first visual inspection, the remaining images were used to compute interferograms according to the time series methods of PSI and SBAS, two state-of-the art classes of techniques for MT-InSAR analysis. PSI summarizes all techniques which focus on dominant point scatterers within a resolution cell of a SAR image (strong signal response) that are phase-stable in time and less-affected by decorrelation issues. First, Ferretti et al. [4] developed the Permanent Scatterer Interferometry™, but several algorithms followed with changes in the methodology by Adam et al. [23], Werner et al. [24] and Hooper et al. [12] without changing the initial idea that is mentioned above, and therefore the class of different methods is named PSI. As PSI focuses on dominant scatterers in a stack of single-master interferograms, urban areas are mapped with a distinctly higher spatial scatter density as rural regions, because man-made objects cause usually double bouncing signal reflection due to their geometry, and therefore a strong signal response.

The SBAS approach, developed initially by Berardino et al. [8], is an extension of the classical differential SAR interferometry towards the usage of a large data sets and generation of a network of multi-master interferograms from SAR image pairs with small spatial and temporal baselines (temporally close images). This approach helps to overcome decorrelation issues in vegetated regions to a certain extent and to detect the underlying displacement signal [24-25]. Compared to PSI, SBAS focuses more on distributed scatterers than on dominant scatterers, allowing to increase the information content in rural areas at the expense of a high signal-to-noise ratio. As with the PSI, several developments in the SBAS methodology followed the work by Berardino et al. [8]. For example, the technique developed by Hooper [14] differs from Berardino et al. [8] in identifying slowly decorrelating filtered phase (SDFP) pixels for deformation analysis directly in single-look interferograms instead of using multi-looked interferograms. As spatial resolution is essential in such small areas of investigation as the Ketzin pilot site, Hooper's approach was employed here.

After computing the interferogams for the Ketzin pilot site, these were inspected towards their quality, where-by non-coherent interferograms were removed from further time series analysis. The overall number of investigated scenes by the SBAS procedure was finally reduced to 46 and to 54 for the first and second data sets, respectively. Table 4.1 summarizes the acquired images and highlights those that were excluded from processing.

The presented perpendicular ($B_\perp$) and temporal baseline (B_T) of each SAR image in Table 4.1 refer to the PSI processing with respect to the selected master image. For the SBAS processing B_T was limited to 99 days (approximately three months with respect to TSX acquisition interval of 11 days) to generate the interferogram network (Fig. 4.4). The maximum $B_\perp$ from SBAS interferogram computations were 349 m and 352 m for data sets 1 and 2, respectively. Generally, interferogram coherence is low for the area around the Ketzin pilot site, as expected according to the varying phenological states of the field crops, harvesting and seasonal conditions. Hence, in spring and summer time (May to September) the B_T in the SBAS interferogram network is short, in particular about one month (22/33 days). During the winter period the temporal decorrelation is slower. This allows to retrieve interferograms that cover B_T of about two months (66 days), which in turn helps to bridge data gaps due to snow imagery.

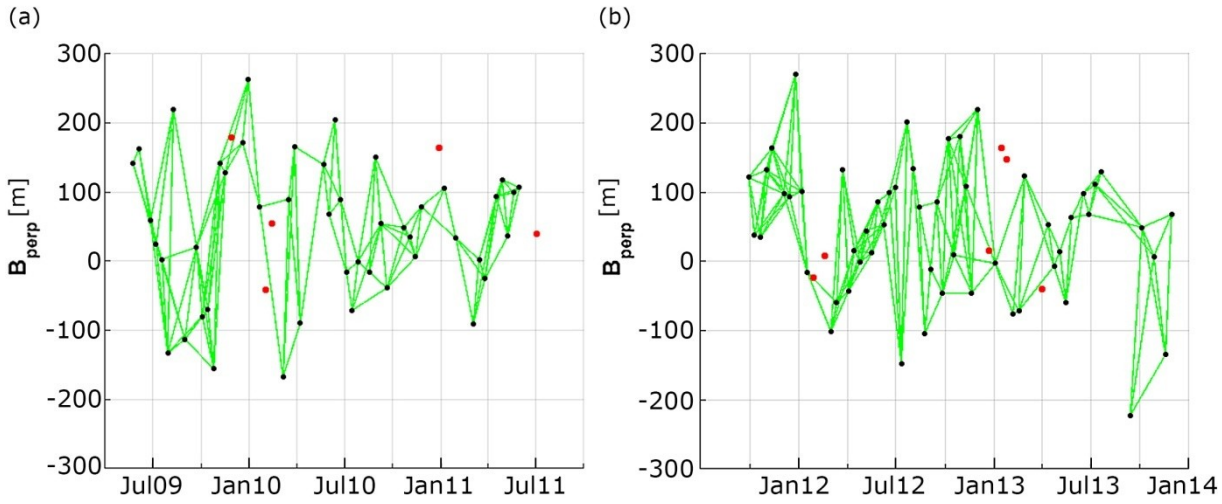

Fig. 4.4: SBAS network for data set 1 (a) and data set 2 (b). Red dots are the excluded SAR images that cause incoherent interferograms, black dots show all images used for interferogram generation and green lines represent the interferograms themselves.

After interferogram computation, a Digital Terrain Model (DTM) is required to remove the topographic phase contribution from the overall phase difference. The standard SRTM-3 DTM with about 90 m resolution is not sufficient in case of using high resolution SAR images, as it causes a geographic misfit of the investigated scatterers in the size of the DTM resolution after StaMPS geocoding step. In addition, the more details of the surface are represented in the model, the smaller is the remaining DTM error after topographic phase removal. Hence, if existing and available, applying a DTM with approximately similar spatial resolution as the used SAR images is recommended. For the Ketzin study a subset (area of interest) from the 10 m DTM of Germany was used.

With the topography-corrected interferograms as input, PS and SDFP pixels were selected according to the PSI [13] and SBAS methods [14] by first selecting an initial set of candidate pixels based on amplitude analysis and then refining them in an iterative process using phase stability analysis. Prior to final displacement time series calculation, the important step of phase unwrapping is required as phase values are measured modulo 2π radians and integer phase-cycle ambiguities can prevent correct displacement derivation. The better the spatial density of selected PS or SDFP pixels, the lesser unwrapping errors occur. Unwrapping was done in three dimensions (two in space and one in time [26]) and the following inversion for displacement time series was done by using least squares. Figure 4.4 shows the final network of SBAS interferograms for data sets 1 (4.4(a)) and 2 (4.4(b)) used for least-squares inversion. Images that cause totally non-coherent interferograms or phase unwrapping issues have been removed from the network and are marked here with a red dot (blue highlighted image dates in Table 4.1).

4.3.2 Pressure Measurements

As geodetic reference data for the validation of the InSAR results are not available, e.g. from ground surface leveling or GPS measurements, a correlation investigation against well bottomhole pressure data was considered for this purpose. These data exist from the beginning of CO_2 injection in up to 5-minute intervals. The daily bottomhole pressure recorded at 5 a.m. was used as it is close to the satellite's acquisition time. Kuehn et al. [5] have demonstrated that a correlation between surface motion and borehole pressure change can be found for a gas storage reservoir in Berlin, Germany.

4.3.3 Hydromechanical Simulations

Hydromechanical simulations were employed to determine the pore pressure-induced stress changes, resulting in vertical ground surface displacements at the Ketzin pilot site. These coupled simulations were undertaken using a one-way coupling between the numerical reservoir simulator Eclipse [27] and the geomechanical simulator FLAC^{3D} [28]. Hereby, pore pressures calculated with the reservoir simulator [29] were transferred to the geomechanical one at 14 selected simulation time steps. Following a general validation of the hydromechanical coupling procedure against analytical solutions that is beyond the scope of this work, the maximum vertical ground surface displacements in the boundaries of the modeling domain were derived.
For that purpose, the reservoir model of 5 km x 5 km x 74 m size was embedded in a regional-scale geomechanical model of 40 km x 40 km x 5 km size, including twelve lithological units and 24 major discrete faults. The geomechanical model is discretized by about 1.4 million elements with sizes of 50 m (near-well area) to 800 m (boundary elements) in horizontal and 20 m to 160 m in vertical direction, using a lateral grid refinement in the near-well area. Reservoir model parameterization is given in Kempka and Kühn [29], while geomechanical model parameters are listed in Kempka et al. [30-31]. We employed the Petrel software package [32] to upscale the pore pressures calculated by the reservoir simulator to the geomechanical simulation grid at each coupling time step.
Initial principal stress magnitudes and orientation were derived from stress analyses carried out at the Ketzin pilot site by Sinha et al. [33], whereby displacements perpendicular to the lateral and bottom model boundaries were fixed, while the top surface was allowed to displace in any direction. After model calibration, an initial equilibrated stress state was available as a starting point for the further 14 selected model coupling steps. The interested reader is requested to refer to Kempka and Kühn [29] for more details on the reservoir model and to Kempka et al. [30-31] for a thorough discussion of the geomechanical model implementations.

4.4 Results

4.4.1 InSAR Displacement Maps

As shown in Fig. 4.5, stable scatterers were detected by the PSI and SBAS methods for the first data set covering the period 24 May 2009 through 31 May 2011. Here, house facades or parts of roofs are scattering the microwave impulses. Therefore, settlements are clearly visible as point clouds that are connected by lines or curves of points that represent typical infrastructure like roads, railways or bridges. Some individual scatterers visible on agricultural fields represent power poles or wind turbines (indicated by numbers 1 and 2, respectively, in Fig. 4.6(b)). All scatterers together create a point pattern showing mainly artificial objects in the rural region. Only sparse natural scatterers are found within vegetated areas.
Point clouds of interest are found in the northern part of Fig. 4.6(c), representing a huge car park that is also shown in the close-up view 4.6(a).The landfill in the western part of Fig. 4.6(c) (close-up view 4.6(d)) shows cumulative LOS surface displacements over the second period ranging from -10.1 cm to 5.5 cm measured by InSAR and visualized by a color ramp that is adjusted to this value range.

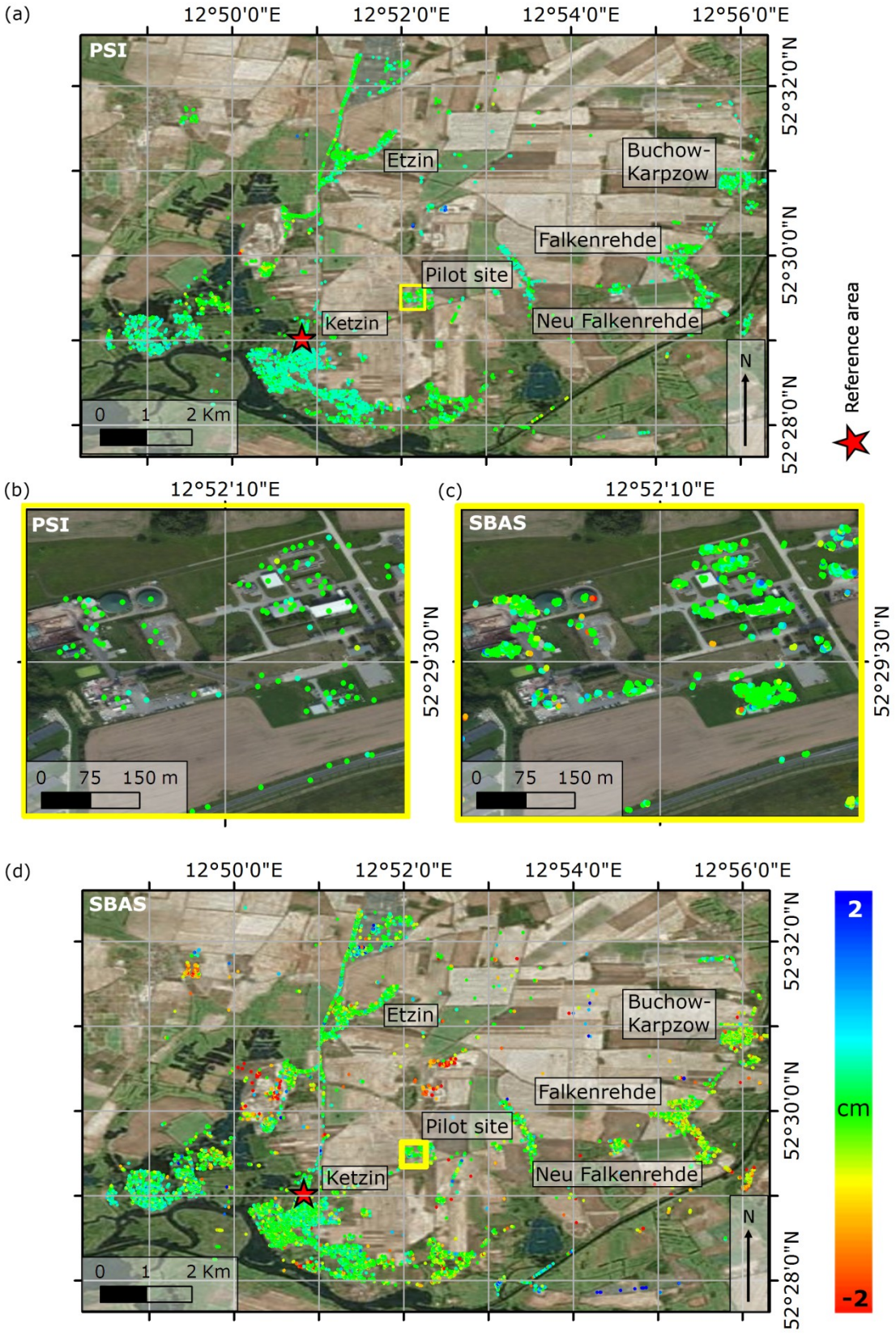

Fig. 4.5: Cumulative LOS InSAR results for the first data set covering the period from 24 May 2009 through 31 May 2011. (a) PSI result for the whole investigated region and its close-up view in (b) showing the pilot site. (c) Close-up view of the SBAS-derived average displacement map of the pilot site. (d) SBAS-derived cumulative displacement map for the whole region.

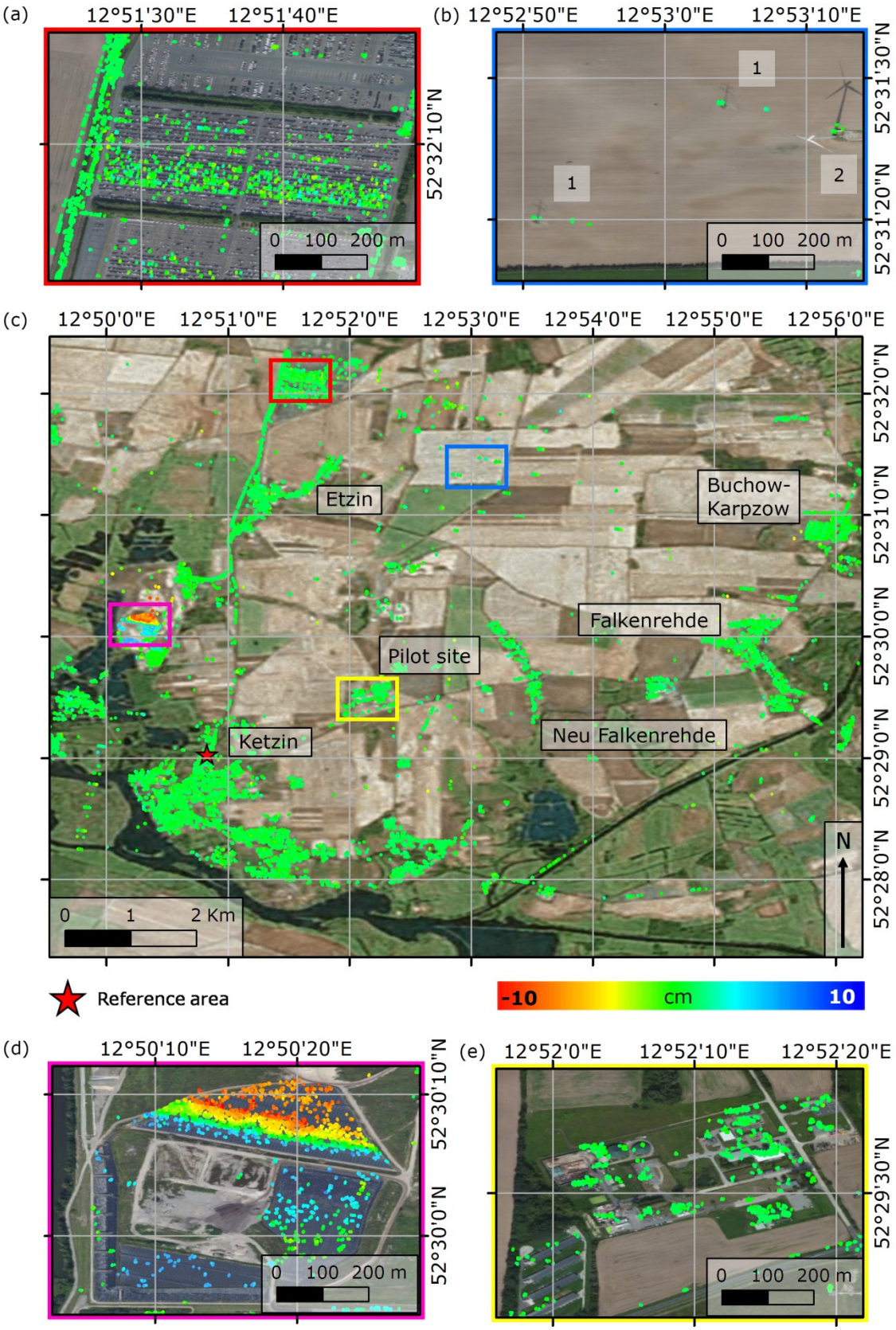

Fig. 4.6: SBAS-derived cumulative LOS results for the second data set that covers the period from 19 September 2011 through 29 November 2013. (c) Displacement map for the whole region with close-up views showing different objects: (a) car park, (b) power poles and wind turbines (identified with number 1 and 2, respectively), (d) landfill and (e) the Ketzin pilot site.

Compared to the clear indication of ongoing surface displacements at the landfill, the area at the pilot site does not show any significant surface displacement, neither for the first period (Fig. 4.5(b,c)), nor for the second one (Fig. 4.6(e)). For a better comparison, the presented result in Fig. 4.6(e) was adjusted to the color scale used in Fig. 4.5 and is shown in Fig. 4.7.
The PSI method as implemented in StaMPS failed for the second data set. Table 4.2 summarizes the used number of images and interferograms as well as the number of scatterers found by the respective method for the whole region and for the pilot site (highlighted in Fig. 4.7 with a red frame) for both data sets (time periods). Since PSI worked only for data set 1 and the SBAS procedure results in an about ten times higher number of scatterers at the pilot site, the further investigation on the scatterer's time series focuses on the SBAS outcome.

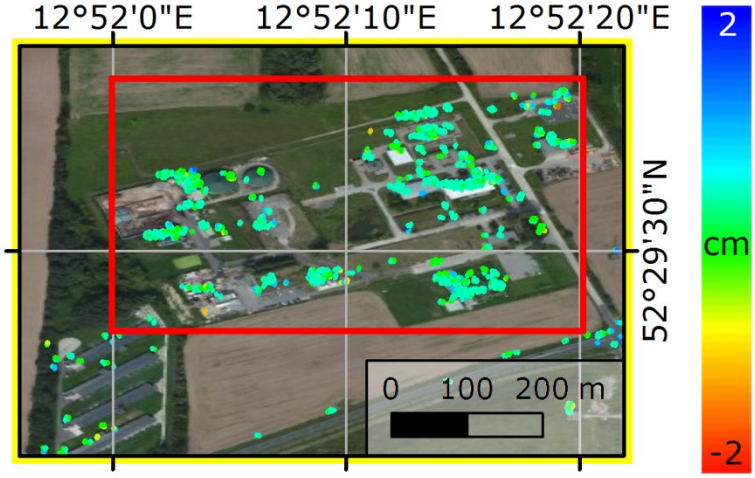

Fig. 4.7: Close-up view 4.6(e) adjusted to the color scale of Fig. 4.5. The red frame shows the extent of area for which the scatterers were counted in order to compare the outcome of the different methods summarized in Table 4.2. Background satellite image available through Esri World Imagery layer, in detail this image's credit is DigitalGlobe.

	Data set 1		Data set 2	
	PSI	SBAS	PSI	SBAS
# Images used for interferogram generation	51	46	-	54
# Interferograms	50	121	-	156
# Scatterers found in region under investigation	6497	50686	-	68377
# Scatterers found at test site	101	1017	-	1152

Table 4.2: Summary on PSI and SBAS input and output.

As shown in Fig. 4.8 the majority of scatterers found by PSI and SBAS represent cumulative LOS displacements between -4 mm and 4 mm within their specific periods. The mean value of all considered scatterers (Table 4.2, last row) is about -1 mm with standard deviations of 1.6 mm (PSI), and 3.6 mm (SBAS) for the first period and 1 mm ± 2.6 mm (SBAS) for the second period. Standard deviations of the SBAS results are higher compared to the PSI outcome, because the range of displacement values is higher and the interferometric phase of SDFP pixels tend to be noisier than of PS (lower SNR) due to their point characteristic. Single scatterers with cumulative displacement values larger than ±4 mm are distributed over the whole area that is indicated by the red frame in Fig. 4.7. Hence, no long-term, localized and distinct spatial surface displacements are visible.

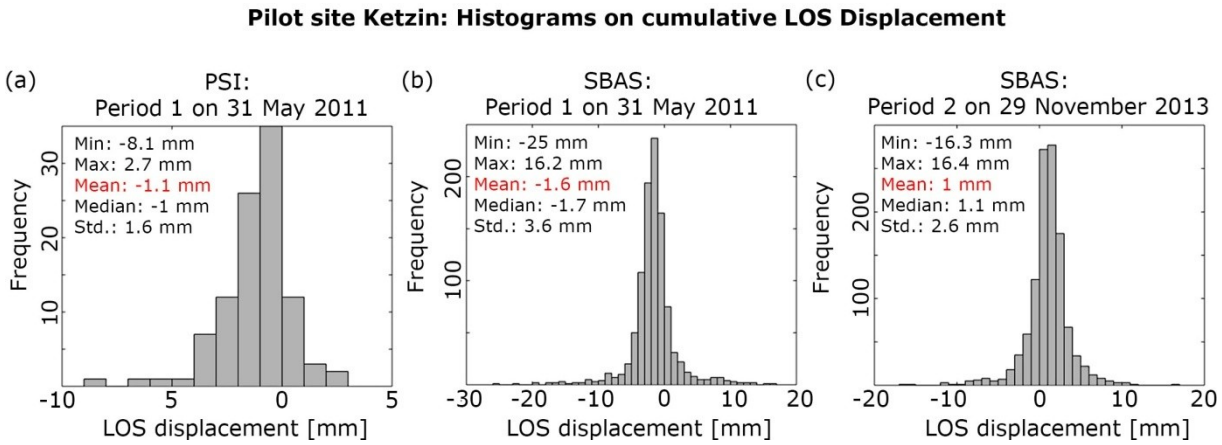

Fig. 4.8: Statistics and histograms on the InSAR-derived cumulative LOS displacement. Results of both PSI (a) and SBAS (b,c) methods and for both periods under investigation are presented. Input data are from scatterers found within the extent of the red frame shown in Fig. 4.7 and listed in Table 4.2.

Four corner reflectors were installed in March 2011 to support data collection at points of interest at the pilot site (Fig. 4.2(a)). Due to their late installation in comparison to the beginning of data acquisition, their signal is only continuously visible in the second data block. Moreover, due to different operational measures carried out at the site, all four corner reflectors are only visible for eight months until end of May 2012. One reflector, CR3, was removed from its position in order to build up a foundation for construction purposes prior to the drilling of the Ktzi 203 well (see Fig. 4.2(b)). This construction work lasted from 28 May 2012 until 7 October 2012. Also CO_2 injection was stopped during this time until end of December 2012. During this time, also the signal of reflector CR2 was lost due to a protective wooden fence installed in its vicinity. This fence's distance was so close to the reflector, that its and the reflector's signal response were not distinguishable (sampling distance issue according to image spatial resolution of about 3 m). Hence, half of the reflectors did not represent useful scatterers during the entire second period (29 September 2011 through 29 November 2013), because their signal was not persistent in time. The signals of the other two reflectors (CR1 and CR4, Fig. 4.2(a)) were also not clearly assignable after StaMPS processing. This is probably due to the fact that isolated movements of bright scatterers are not considered in the algorithm [13], because they are not spatially correlated. Since the point quality assessment in the pixel selection process assumes a spatially correlated deformation, the stability of points that do not undergo spatially correlated deformation are underestimated.

In general, during the construction and drilling phase of Ktzi 203, many strong but short-term scatterers are visible at the pilot site on the SAR images, because all required facilities and devices respond to the transmitted microwave impulses. Since their positions are not stable in time, their signal cannot be used for time series analyses.

Figure 4.9 shows a sequence of SAR amplitude image subsets of the pilot site that present the different signal appearances for the different conditions explained above.

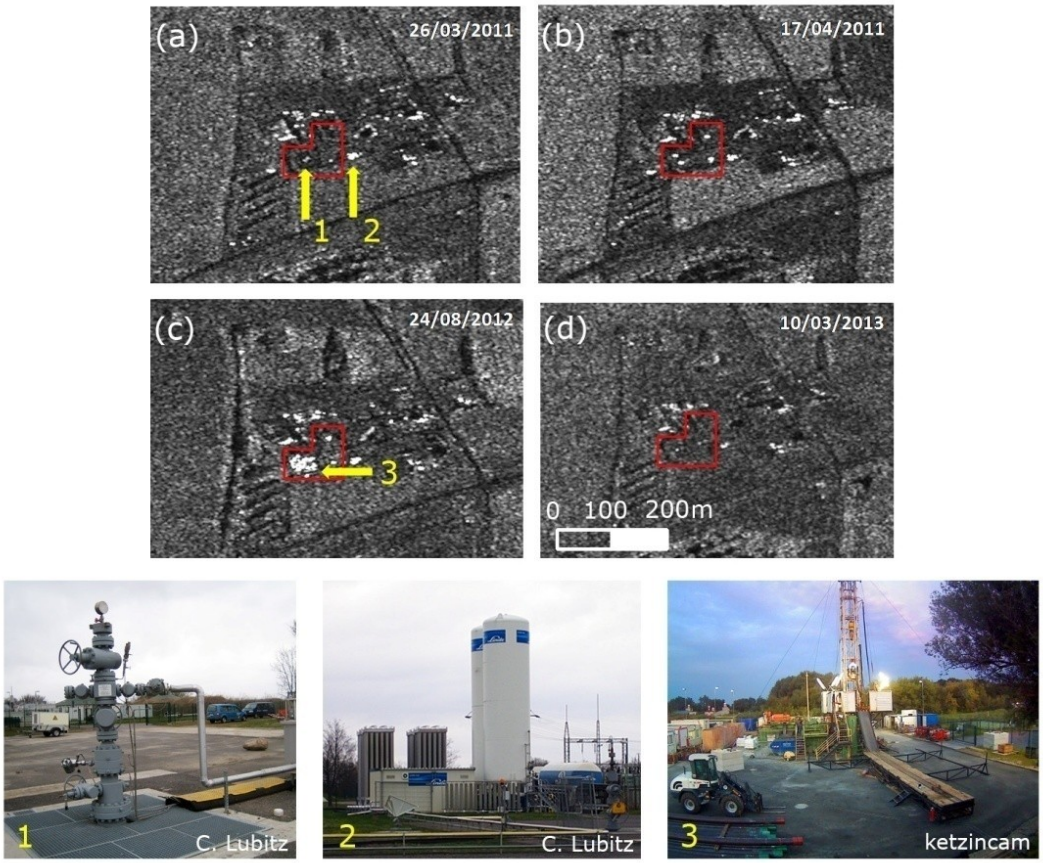

Fig. 4.9: Corner reflector signal appearance under varying conditions: (a) prior to installation, (b) four strong signals after installation, (c) during construction phase of well Ktzi 203 and (d) hidden by snow in winter season. Red frame indicates roughly the test site that is also highlighted in Fig. 4.2(a). Yellow arrows illustrate locations of objects that are shown in photographs 1 to 3 that cause the presented signal in the SAR amplitude image. Those are the well head of the injection well (1), the intermediate gas storage tanks and gas transformation facility (2) and the situation during construction of Ktzi 203 at time of SAR image acquisition (3).

4.4.2 Correlation Against Well Bottomhole Pressure

Suitable ground reference data (typically leveling or GPS) for comparison with InSAR data is not available at the Ketzin pilot site - neither before the start of CO_2 injection nor was it regularly collected during the injection phase. The only available information that can be used to evaluate the outcome of InSAR analysis is the bottomhole pressure that is collected in 5-minute intervals at the injection well Ktzi 201.

Additionally, the spatial gaseous CO_2 distribution within the Stuttgart Formation simulated based on the latest history-matched geological model [29,34] and *in-situ* data [35-36] can be used to assess the InSAR results. In this context, the spatial extent of potential ground surface displacements may be estimated, so that the area of investigation can be narrowed. However, as illustrated in Fig. 4.5(b,c) and 4.6(e), only a few pixels were found at the site associated with the local facilities, because the site is surrounded by agricultural fields. Hence, the spatial distribution of the gaseous CO_2 as well as displacements simulated for the northern and western directions cannot be compared directly to InSAR results due to lack of scatterers.

Regarding the displacement-pressure comparison, pressure values were directly opposed to the mean LOS displacement of all detected SDFP pixels within a 25 m-radius around the Ktzi 201 well with 24 SDFP pixels for the first and 25 SDFP pixels for the second period. The mean value of these SDFP pixels through time is plotted in blue in Fig. 4.10. It has to be mentioned that the presented

pressure data is the one recorded at 5 a.m. (closest value to TSX image acquisition time) and only those values have been included in this analysis from dates at which a SAR image acquisition was performed.

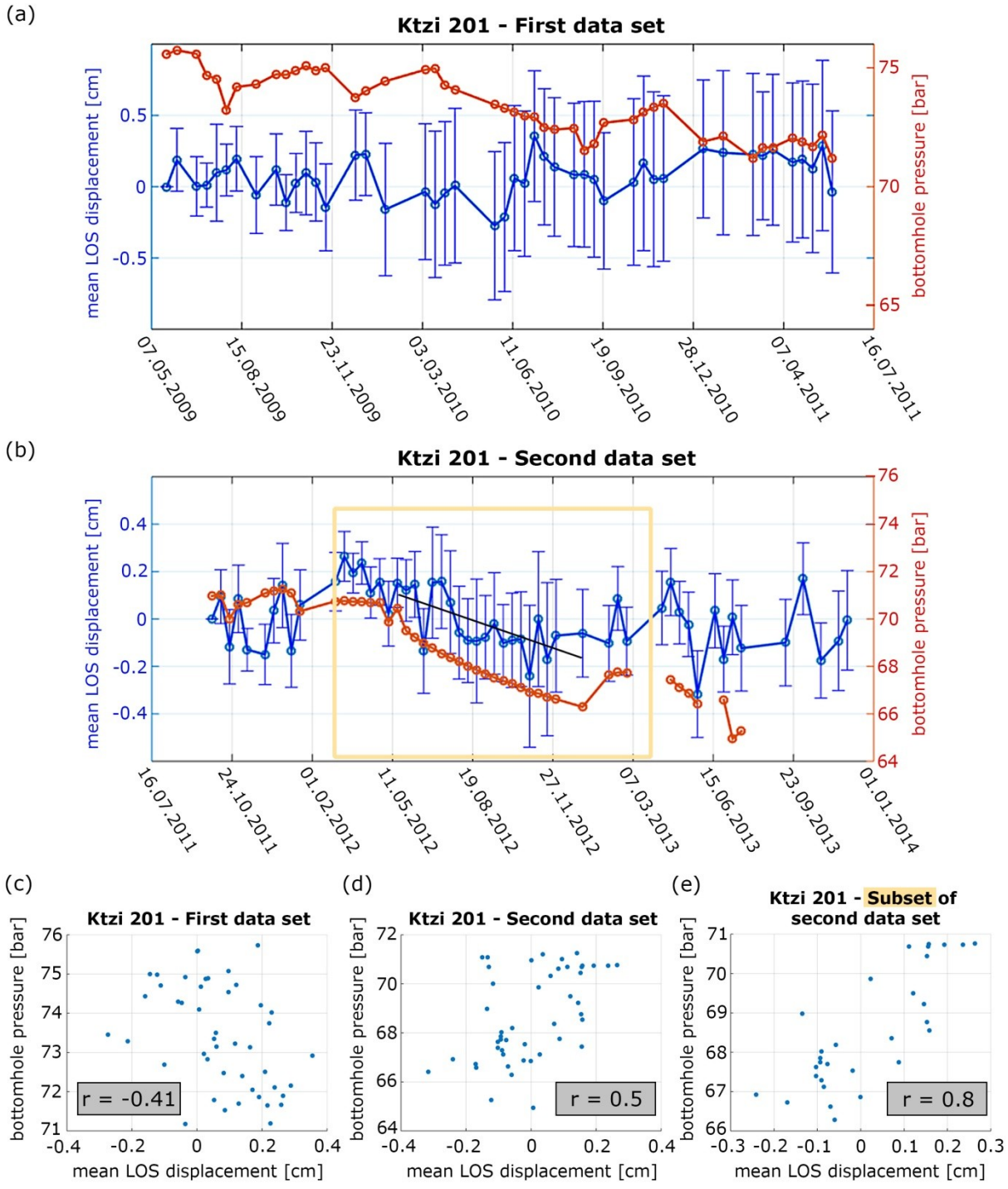

Fig. 4.10: Mean of SBAS derived LOS displacement from all scatterers detected in close distance to the injection well Ktzi 201 (location shown in Fig. 4.2(a)) for both periods under investigation, (a) refers to period 1 and (b) to period 2. Standard deviation is shown with error bars. Black line in (b) represents a least squares based line fit with the standard deviations as weights for the period of injection stop. For comparison, the bottomhole pressure is plotted [35-36]. Subplots (c), (d) and (e) show the scatter plots and correlation coefficients (r) between the mean InSAR LOS displacement and the bottomhole pressure for period one, two and a temporal subset of period two that is indicated with a light orange frame in (b), respectively.

The plots in Fig. 4.10 do not reveal a relevant trend in the mean time series of the investigated SDFP pixels (Fig. 4.10 (a,b)). In fact, the large standard deviation of up to 0.6 cm and 0.3 cm for data sets 1 and 2, respectively, confirm a low signal-to-noise ratio (SNR). The scatter plots in Fig. 4.10(c,d) and the associated correlation coefficients -0.41 and 0.5 between the InSAR LOS displacements and bottomhole pressures for the first and second periods, respectively, suggest a weak correlation. This is due to the contrary sign preventing a clear assignment of a positive or negative correlation and/or the low values themselves, which can be related to the noisiness of the InSAR data and the low pressure variations impeding a clear statement.
When looking precisely at the observed bottomhole pressure data in Fig. 4.10(a,b), several minor ups and downs of up to 1.6 bar occur between investigated dates due to changes in the injection schedule. Such features are associated with *in-situ* CO_2 density changes. The most striking pressure change is a decreasing trend and was recorded starting with the construction phase of the Ktzi 203 well (from 28 May 2012 until 7 October 2012) and thereafter (Fig. 4.10(b)). During this time bottomhole pressure decreases smoothly from 70.5 bar to 66.3 bar. Injection restart was in January 2013 followed by a nearly immediate pressure increase to 67.6 bar. Computing the scatter plot and correlation coefficient for a period that covers this event with a small temporal extension before and after (1 March 2012 - 27 February 2013, highlighted with a light orange frame in Fig. 4.10(b)), results in a value of 0.8 for the correlation coefficient (see Fig. 4.10(e)). This high value as compared to the coefficient for the whole second period is significant as it confirms an approximately positive, linear correlation between bottomhole pressure and surface displacement in the investigated time period.

4.4.3 Hydromechanical Simulations Results on Ground Surface Displacements

The coupled hydromechanical simulation results exhibit that the operational procedure undertaken at the Ketzin pilot site, especially considering the pilot-scale character of this experiment, generates ground surface displacements up to 4 mm in the modeling domain during the injection period from June 2008 to August 2013 (Fig. 4.11).

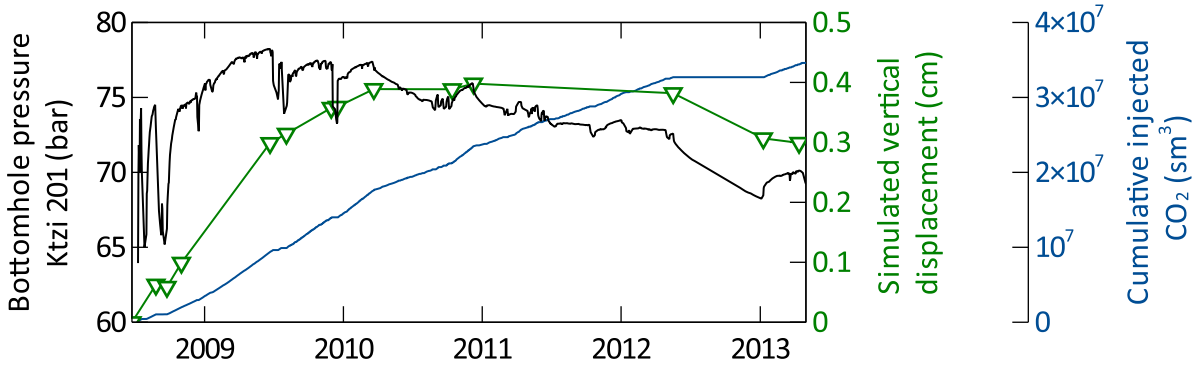

Fig. 4.11: Bottomhole pressure observed at the Ktzi 201 injection well [35-36], corrected to 639.5 m (reservoir level, black solid line) [29], simulated vertical ground surface displacements at the Ktzi 201 well location (green solid line with triangles representing the hydromechanical coupling time steps) and cumulative injected CO_2 into the Stuttgart Formation (blue solid line) in standard cubic meter (reservoir conditions: 15.6 °C and 1 atm).

Taking into account the relatively low amount of injected CO_2 with about 67 kt at the end of the storage operation at the Ketzin pilot site as well as the relatively low achieved maximum pressure elevation by 16 bar in the Stuttgart Formation during the overall injection period, the calculated ground surface displacements show up in a reasonably low range compared to those observed in industrial-scale storage operations such as at In Salah (1.6 cm vertical ground surface displacement, 100 bar pressure elevation [37]). Figure 4.11 further demonstrates that a direct correlation between bottomhole pressures and simulated vertical ground surface displacements can be derived for

injection stops exceeding a time period of a month, i.e., in September 2008 and May to December 2012, but also for injection periods where significant pressure increases occur, e.g., in October 2008 or October to December 2010. Simulated vertical displacements during the acquisition of the first InSAR data set (May 2009 to May 2011) exhibit a rate of about 2 mm/year, while those simulated for the period of the second data set acquisition (September 2011 – February 2013) are below 1 mm/year, and fall below the threshold detectability of InSAR. However, taking into account the significant time period May 2012 to December 2012, subsidence of about 0.75 mm were calculated by our coupled simulations.

4.5 Discussion

Applying the PSI method using TSX data turned out to be more challenging than the SBAS approach for monitoring deformation at the Ketzin pilot site for CO_2 storage. As PSI focuses on dominant point scatterers within a resolution cell, they are usually detected in urban areas or vegetation-free regions. For the Ketzin pilot site and other rural regions, the scattering objects are characterized by lower signal response and more varying signal strength over time. Typically, several of these scatterers appear within one resolution cell, so there is often not one dominant scatterer visible. Such scatterers, also known as Distributed Scatterers (DS), are not selected in the PSI method, because they are less coherent. Although Persistent Scatterers (PS) were found in the area of interest at different settlement locations forming point clouds, the number of PS in-between is not sufficient to connect these point clouds throughout the whole area. In consequence, unwrapping problems occur, not within the islands of points but in-between leading to error propagation and incorrect displacement values. Applying SBAS here, led to a ten times higher number of detected scatterers as compared to PSI (see Table 4.2). More scatterers were not only found at settlements, but also in-between reducing unwrapping problems and effects of error propagation.
At the Ketzin pilot site itself, the constructed facilities provide artificial scatterers that deliver SAR signal responses within the naturally strongly vegetated region for both PSI and SBAS method. Again, by using SBAS more scatterers were found, but they do not cover the entire spatial CO_2 distribution, observed by 3D seismics [38-41] and determined by numerical simulations [42]. More artificial scatterers set up on the surrounding fields would be required to overcome the issue to a certain extent, but in general, an overall equally distributed high scatterer density is necessary for a substantiated analysis.
Moreover, in PSI the interferograms are computed with respect to a single master image. Investigation periods of two years, as in this case, may be too long (long B_T) for regions with fast temporal decorrelation leading to strongly reduced number of PS and a low spatial sampling. For the second investigation period (2011-2013), the situation turned out to be even more severe. Several master selections were tested for interferogram generation and the afterwards PSI processing, but all failed regarding sufficient PS detection. This problem occurs only when considering the whole second period (from 19 September 2011 through 29 November 2013). Reducing the period of investigation to about one year, from 19 September 2011 to 18 October 2012 , resulted in sufficient number of PS and no significant phase unwrapping issues. However, the result of this one-year test (results not shown here) does not show any significant difference with respect to the results obtained from the two-year analyses based on SBAS.
Although temporal decorrelation is also a strong problem when using the multiple-master approach of SBAS, because it reduces the maximum selectable B_T (see section 4.3.1.2) for interferogram computation to just a few months here, the method delivers more points to get information on potential deformations. Therefore, in rural regions with strong seasonal variations, especially snowy winters, but also with strong agricultural activities as field preparation and harvesting, or other factors as soil shrinkage/swelling, canopy development through the year and falling Autumn leafs, SBAS is method of choice when PSI is the only other option. Alternatives are the recently developed advanced techniques SqueeSAR™ by Ferretti et al. [43], the DS algorithm by Goel and Adam [44] or

the Intermittent SBAS (ISBAS) method developed at University of Nottingham by Sowter et al. [45] all promising a drastically increased number of scatterers for InSAR time series analysis.
As the InSAR time series in Fig. 4.10 show high standard deviations, a noise reduction by applying SAR image multi-looking prior to interferogram computation may be a solution. Such a step, often applied to strengthen the signal, could be implemented at the expense of image resolution. This might be acceptable when monitoring large-scale surface deforming events, but in small areas where each single scatterer counts as in our study area, the information content would be dramatically decreased. The available image resolution for this project was about 3 m in azimuth and range, given by using TSX Stripmap data. The highest possible resolution would be given by TSX high-resolution Spotlight data (about 1 m) or the recently developed and tested TSX Staring Spotlight mode with up to 0.24 m azimuth resolution [46]. Such data were not available during the entire monitoring process. Within another recent CO_2 injection-related project in Hastings, Texas, United States of America, which is located in a similar vegetation-rich setting as Ketzin, an InSAR-based monitoring was conducted by using TSX high-resolution Spotlight data from 2012-2014. A strong multi-looking with a factor of 16 was applied for noise reduction before interferogram generation resulting in a spatial resolution of about 15 m in azimuth and range [47]. Since the initial image resolution was very high, the signal smoothing at the expense of resolution still resulted in sufficient number of scatterers that delivered a clear signal of several surface displacement locations with velocities of up to 2 mm/y. Their InSAR processing was based on a modified SBAS approach and differences to StaMPS, which was used here, are neither to be discussed nor evaluated at this point.
MT-InSAR results presented in the previous section mainly indicate the absence of a major trend through the overall period such as a potential surface uplift due to the gas injection at the Ketzin pilot site. Our hydromechanical simulations demonstrate the relationship between bottomhole pressure and vertical displacements (section 4.4.3). The maximum simulated ground surface displacement rates of about 2 mm/year in the first period (May 2009 to May 2011) and of <1 mm/year in the second period (September 2011 to November 2013) could not be captured by the satellite-based monitoring techniques due to the strong noise influence. However, the injection stop during the time period May 2012 to December 2012 results in a simulated ground subsidence rate of about 1.5 mm/year (about -0.75 mm vertical displacement in 6 months).This subsidence is also detected by the employed analysis of the InSAR data for this period. Using the InSAR time series result visible in Fig. 4.10(b) and applying a least squares estimation to fit a line, weighted by the standard deviations, results in a subsidence of 2.8 mm. Due to unavailability of TSX-data prior to May 2009, no InSAR-based statement can be made concerning the situation before and shortly after CO_2 injection has started in June 2008.
The question that arose from the previous section was, although no long-term trend is observable, whether transient pressure variations or at least the significant injection stop related pressure change, as all visible in the simulated data, cause an immediate response in the InSAR displacement time series. The most probable correlation was assumed in the close vicinity of the injection well. Such assumption is appropriate as the fastest and strongest response on pressure variations due to injection rate changes is occurring there. This explains the applied selection of SDFP pixels for the comparison in Fig. 4.10 that was explained previously. As shown in Section 4.4.2, a potential link between displacement and pressure was found, although of weak character due to the noise in the InSAR results (standard deviation of up to 0.6 cm and 0.3 cm for data sets 1 and 2, respectively) and due to the low pressure variations observed (below 2 bar). Only the period of the distinct injection stop and associated pressure decrease of about 4 bar exhibits a correlation coefficient of 0.8. This finding is also confirmed by the hydromechanical simulation results, exhibiting a negative vertical of about 0.75 mm for this period. The indication of a positive linear correlation between the two variables allows to consider subsurface pressure variations for comparison purposes with InSAR data, as also confirmed by Kuehn et al. [5], but requires a good SNR in the InSAR data. Strong noise as in the present case hampers the actual signal which in turn reduces the significance of correlation investigations. The noise problem is related to the applied MT-InSAR method. It is a trade-off between less point density of PS with high SNR and a higher point density of low SNR SDFP pixels when considering full resolution images of a rural region.

Presented minor variations in the time series of Fig. 4.10(a,b) may be related to the observed pressure variations. Large-scale industrial volumes as for example at In Salah (about one million tonnes per year), have caused surface displacements up to 5 mm/year [10], but were injected significantly deeper than at the Ketzin pilot site (about 1800 m) and with notably higher pressure increase (maximum of about 100 bar at in Salah against 16 bar at Ketzin).

4.6 Conclusion

In this study we used MT-InSAR time-series techniques based on TerraSAR-X data to assess ground surface deformation at the Ketzin pilot site for geological CO_2 storage. Although very challenging due to not ideal interferometric conditions in the region, MT-InSAR analysis detected more than 1000 coherent pixels on the pilot site, which showed no statistically significant LOS motion in the years 2009-2011 and 2011-2013. We attribute this stability to the relatively low amount of injected CO_2 (67 kt in 4 ½ years) and the low overall pressure elevation of maximum 16 bar as compared to other industrial-scale storage operations.
Despite the long-term stability, our results show a temporary direct correlation (0.8) between observed InSAR displacements and bottomhole pressures, when the latter changes by 4 bar within half a year during the injection stop period between May and December 2012. Considering the conformity of satellite-based observations (subsidence of 2.8 mm) and numerical modeling (< 1 mm) for this period of no injection in 2012, we conclude that the integration of both methods has been successfully carried out at the Ketzin pilot site.
The main hindering factors for InSAR usage at Ketzin are the varying weather conditions and the vegetation coverage, both preventing temporally stable (coherent) and equally distributed signals in space. InSAR time series investigations over several years are usually demanded, but need the temporal connection of interferograms through the whole time. If SAR data gaps occur as in summer 2011 due to acquisition problems or unusable images, the continuous monitoring is limited as the seasonal effects make bridging of data gaps complicated. At least, a consequent image acquisition at short intervals is beneficial.
The recently launched and long-term scheduled Copernicus Sentinel-1 satellite mission provides SAR imagery free of charge and a global coverage on a six-day interval at C-band, which is less affected by vegetation, and hence, decorrelation effects as compared to shorter wavelength of X-band satellites as TSX/TDX. This is a low-cost opportunity with a temporally dense data availability that can serve the increasing international demand for long-term carbon storage site monitoring at varying local conditions by using MT-InSAR.

4.7 Acknowledgement

This study was supported by the Initiative and Networking Fund of the Helmholtz Association in the frame of Helmholtz Alliance “Remote Sensing and Earth System Dynamics”. All TerraSAR-X data are kindly provided by DLR under proposal GEO0301. The applied DTM is available through a Web Map Service (www.geodatenzentrum.de) by the German Federal Agency for Cartography and Geodesy.
Special thanks go to Jan Anderssohn initiating the project, to Mahmud Haghshenas Haghighi for support in scripting, to Fabian Möller for support in all questions and tasks regarding the on-site work and to Sonja Martens being a valuable source in all general questions regarding the overall Ketzin pilot project.

4.8 References

[1] Ringrose, P.S., Mathieson, A.S., Wright, I.W., Selama, F., Hansen, O., Bissell, R., Saoula, N. and Midgley, J.(2013): The In Salah CO_2 storage project: lessons learned and knowledge transfer, Energy Procedia, 37, 6226-6236.

[2] Onuma, T. and Ohkawa, S. (2009): Detection of surface deformation related with CO_2 injection by DInSAR at InSalah, Algeria, Energy Procedia, 1, 2177-2184.

[3] Vasco, D.W., Rucci, A., Ferretti, A., Novali, F., Bissell, R., Ringrose, P., Mathieson, A. and Wright, I.(2010): Satellite-based measurements of surface deformation reveal fluid flow associated with the geological storage of carbon dioxide, Geophys. Res. Lett., 37, L03303, doi: 10.1029/2009GL041544.

[4] Ferretti, A., Prati, C. and Rocca, F. (2001): Permanent Scatterers in SAR Interferometry, IEEE Transactions on Geoscience and Remote Sensing, 39,1.

[5] Kuehn, F., Hoth, P., Stark, M., Burren, R. and Hole, J. (2009): Experience with Satellite Radar for Gas Storage Monitoring, Erdöl, Erdgas, Kohle, 125, 11, 452-460.

[6] Werner, C., Wegmüller, U., Strozzi, T. and Wiesmann, A. (2003): Interferometric Point Target Analysis for Deformation Mapping, IEEE International Geoscience and Remote Sensing Symposium (IGARSS), 21-25 July 2003, Toulouse, France, Proceedings, doi: 10.1109/IGARSS.2003.1295516.

[7] Yang, Q., Zhao, W., Dixon, T.H., Amelung, F., Han, W.S., Li, P. (2015): InSAR monitoring of ground deformation due to CO_2 injection at an enhanced oil recovery site, West Texas, International Journal of Greenhouse Gas Control, 41, 20-28.

[8] Berardino, P., Fornaro, G., Lanari, R. and Sansosti, E. (2002): A New Algorithm for Surface Deformation Monitoring Based on Small Baseline Differential SAR Interferograms, IEEE Transactions on Geoscience and Remote Sensing, 40, 11, 2375-2383.

[9] National Energy Technology Institute: NETL's Carbon Capture and Storage Database - Version 5, https://www.netl.doe.gov/research/coal/carbon-storage/strategic-program-support/database (26th May 2017).

[10] Rutqvist, J., Vasco, D.W. and Myer, L. (2009): Coupled reservoir-geomechanical analysis of CO_2 injection at In Salah, Algeria, Ernergy Procedia, 1, 1847-1854.

[11] Lubitz, C., Motagh, M., Wetzel, H.-U. and Kaufmann, H. (2013): Remarkable Urban Uplift in Staufen im Breisgau, Germany: Observations from TerraSAR-X InSAR and Leveling from 2008-2011, Remote Sensing, 5, 3082-3100, doi: 10.3390/rs5063082.

[12] Hooper, A., Zebker, H., Segall, P. and Kampes, B.(2004): A new method for measuring deformation on volcanoes and other natural terrains using InSAR persistent scatterers, Geophys. Res. Lett., 31, L23611, doi: 10.1029/2004GL021737.

[13] Hooper, A., Segall, P., and Zebker, H. (2007): Persistent scatterer interferometric synthetic aperture radar for crustal deformation analysis, with application to Volcán Alcedo, Galápagos, Journal of Geophysical Research, 112, B07407, doi: 10.1029/2006JB004763.

[14] Hooper, A. (2008): A multi-temporal InSAR method incorporating both persistent scatterer and small baseline approaches, Geophys. Res. Lett., 35, L16302, doi: 10.1029/2008GL034654.

[15] Martens, S., Liebscher, A., Möller, F., Henninges, J., Kempka, T., Förster, A., Schöner, R., Förster, H.J., Norden, B., Blaschke, A.W., Luckert, J., Beutler, G., Gaupp, R. and Rhede, D. (2010): Reservoir characterization of a CO_2 storage aquifer: The Upper Triassic Stuttgart Formation in the Northeast German Basin, Marine and Petroleum Geology, 27, 10, 2156-2172.

[16] Norden, B., Förster, A., Vu-Hoang, D., Marcelis, F., Springer, N. and Le Nir, I. (2010): Lithological and petrophysical core-log interpretation in CO_2SINK, the European onshore research storage and verification project, SPE Reservoir Evaluation & Engineering, 179-192, doi: 10.2118/115247-PA.

[17] Norden, B. and Frykman, P. (2013): Geological modelling of the Triassic Stuttgart Formation at the Ketzin CO_2 storage site, Germany, International Journal of Greenhouse Gas Control, 19, 756-774.

[18] Liebscher, A., Martens, S., Möller, F., Lüth, S., Schmitt-Hattenberger, C., Kempka, T., Szizybalski, A. and Kühn, M.(2012): Überwachung und Modellierung der geologischen CO_2-Speicherung - Erfahrung von Pilotstandort Ketzin, Brandenburg (Deutschland), Geotechnik, 35, 177-186

[19] Würdemann, H., Möller, F., Kühn, M., Heidug, W., Christensen, N.P., Borm, G., Schilling, F.R. & the CO2 SINK Group (2010): CO_2SINK – from site characterisation and risk assessment to monitoring and verification: one year of operational experience with the field laboratory for CO_2 storage at Ketzin, Germany, International Journal of Greenhouse Gas Control, 4,6, 938–951.

[20] Martens, S., Kempka, T., Liebscher, A., Lüth, S., Möller, F., Myrttinrn, A., Norden, B., Schmidt-Hattenberger, C., Zimmer, M., Kühn, M., The Ketzin Group (2012): Europe's longest-operating on-shore CO_2 storage site at Ketzin, Germany: a progress report after three years of injection, Environmental Earth Sciences, 67, 323-334.

[21] Martens, S., Liebscher, A., Möller, F., Henninges, J., Kempka, T., Lüth, S., Norden, B., Prevedel, B., Szizybalski, A., Zimmer, M., Kühn, M. & the Ketzin Group (2013): CO_2 Storage at the Ketzin Pilot Site, Germany: Fourth Year of Injection, Monitoring, Modelling and Verification, Energy Procedia, 37, 6434–6443.

[22] Prevedel, B., Wohlgemuth, L., Henninges, J., Krüger, K., Norden, B., Förster, A., CO_2SINK Drilling Group (2008): The CO_2SINK boreholes for geological storage testing, Scientific Drilling, 6, 32-37, doi: 10.2204/iodp.sd.6.04.2008.

[23] Adam, N., Kampes, B., Eineder, M., Worawattanamateekul, J. and Kircher, M. (2003): The development of a scientific permanent scatterer system, ISPRS Hannover Workshop, 6.-8. October 2003, Leibniz University Hannover, Inst. for Photogramm. and Geoinf., Hannover, Germany.

[24] Neri, M., Casu, F., Acocella, V., Solaro, G., Pepe, S., Berardino, P., Sansosti, E., Caltabiano, T., Lundgren, P. and Lanari, R. (2009): Deformation and eruptions at Mt. Etna (Italy): A lesson from 15 years of observations, Geophys. Res. Lett.,36, L02309, doi:10.1029/2008GL036151.

[25] Akbarimehr, M., Motagh, M. and Haghshenas-Haghighi, M. (2013): Slope Stability Assessment of the Sarcheshmeh Landslide, Northeast Iran, Investigated Using InSAR and GPS Observations, Remote Sensing, 5, 3681-3700,doi:10.3390/rs5083681.

[26] Hooper, A., and Zebker, H. (2007): Phase unwrapping in three dimensions with application to InSAR time series, Journal of Optical Society of America, 24, 9, 2737-2747.

[27] Schlumberger (2011a) Eclipse reservoir engineering software, version 2011.3

[28] Itasca (2016) FLAC3D v5.01 – Fast Lagrangian Analysis of Continua in 3 Dimensions. User's Manual.

[29] Kempka, T. and Kühn, M. (2013): Numerical simulations of CO_2 arrival times and reservoir pressure coincide with observations from the Ketzin pilot site, Germany, Environmental Earth Sciences, Special Issue, 1-11, doi:10.1007/s12665-013-2614-6.

[30] Kempka, T., Klapperer, S. and Norden, B. (2014a) Coupled hydro-mechanical simulations demonstrate system integrity at the Ketzin pilot site for CO2 storage, Germany, Rock Engineering and Rock Mechanics: Structures in and on Rock Masses - Proceedings of EUROCK 2014, ISRM European Regional Symposium, 1317-1322.

[31] Kempka, T., De Lucia, M. and Kühn, M. (2014b): Geomechanical integrity verification and mineral trapping quantification for the Ketzin CO_2 storage pilot site by coupled numerical simulations, Energy Procedia, 63, 3330-3338m, doi: 10.1016/j.egypro.2014.11.361.

[32] Schlumberger (2011b) Petrel Seismic-to-Evaluation software, version 2011.2.

[33] Sinha, B.K., Ouellet, A. & Bérard, T. (2010): Estimation of principal horizontal stresses using radial profiles of shear slownesses utilizing sonic data from a CO_2 storage site in saline aquifer in Germany, SPWLA 51st annual logging symposium, June 19–23 2010, 16 pp.

[34] Kempka, T., Class, H., Görke, U.-J., Norden, B., Kolditz, O., Kühn, M., Walter, L., Wang, W. and Zehner, B. (2013): A Dynamic Flow Simulation Code Intercomparison based on the Revised Static Model of the Ketzin Pilot Site, Energy Procedia, 40, 418-427, doi: 10.1016/j.egypro.2013.08.048.

[35] Möller, F., Liebscher, A., Martens, S., Schmidt-Hattenberger, C. and Kühn, M. (2012): Yearly operational datasets of the CO_2 storage pilot site Ketzin, Germany, Scientific Technical Report, Data, published online only, doi: 10.2312/GFZ.b103-12066.

[36] Möller, F., Liebscher, A., Martens, S., Schmidt-Hattenberger, C. and Kühn, M. (2013): Yearly operational datasets of the CO_2 storage pilot site Ketzin, Germany, (Supplement of data from2012 published in Möller et al., 2012), Scientific Technical Report, Data, published online only, doi: 10.5880/GFZ.b103-12066.2012.

[37] Jonny Rutqvist, Donald W. Vasco, Larry Myer (2010): Coupled reservoir-geomechanical analysis of CO_2 injection and ground deformations at In Salah, Algeria, International Journal of Greenhouse Gas Control, 4, 2, 225-230.

[38] Lueth, S., Ivanova, A., Kempka, T.(2015): Conformity assessment of monitoring and simulation of CO_2 storage: A case study from the Ketzin pilot site, International Journal of Greenhouse Gas Control, 42, 329-339, doi: 10.1016/j.ijggc.2015.08.005.

[39] Huang, F., Juhlin, C., Kempka, T., Norden, B., Zhang, F. (2015): Modeling 3D time-lapse seismic response induced by CO_2 by integrating borehole and 3D seismic data – A case study at the Ketzin pilot site, Germany, International Journal of Greenhouse Gas Control, 36, 66-77, doi: 10.1016/j.ijggc.2015.02.020.

[40] Huang, F., Juhlin, C., Han, L., Kempka, T., Lueth, S., Zhang, F. (2016): Quantitative evaluation of thin-layer thickness and CO_2 mass utilizing seismic complex decomposition at the Ketzin CO_2 storage site, Germany, Geophysical Journal International, 207, 1,160-173.

[41] Huang, F., Juhlin, C., Han, L., Sopher, D., Ivandic, M., Norden, B., Deng, W., Zhang, F., Kempka, T., Lueth, S.(2017): Feasibility of utilizing wavelet phase to map the CO_2 plume at the Ketzin pilot site, Germany, Geophysical Prospecting, 65, 2, 523-543, doi: 10.1111/1365-2478.12383.

[42] Class, H., Mahl, L., Ahmed, W., Norden, B., Kühn, M., Kempka, T.(2015): Matching Pressure Measurements and Observed CO_2 Arrival Times with Static and Dynamic Modelling at the Ketzin Storage site, Energy Procedia, 76, 623-632,doi: 10.1016/j.egypro.2015.07.883.

[43] Ferretti, A., Fumagalli, A., Novali, F., Prati, C., Rocca, F. and Rucci, A. (2011): A New Algorithm for Processing Interferometric Data-Stacks: SqueeSAR ,IEEE Transactions on Geoscience and Remote Sensing, 49, 9, 3460-3470.

[44] Goel, K. and Adam, N. (2012): An advanced algorithm for deformation estimation in non-urban areas, ISPRS Journal of Photogrammetry and Remote Sensing, 73, 100-110.

[45] Sowter, A., Bateson, L., Strange, P., Ambrose, K. and Syafiudin, M.F.(2013): DInSAR estimation of land motion using intermittent coherence with application to the South Derbyshire and Leicestershire coalfields, Remote Sensing Letters, 4:10, 979-987, doi: 10.1080/2150704X.2013.823673.

[46] Mittermayer, J., Wollstadt, S., Prats-Iraola, P. and Scheiber R. (2014): The TerraSAR-X Staring Spotlight Mode Concept, IEEE Transactions on Geoscience and Remote Sensing, 52, 6, 3695-3706.

[47] Zhao, W. (2017): Small Deformation detected from InSAR Time-Series and their Applications in Geophysics, Open Access Dissertations,1795, http://scholarlyrepository.miami.edu/oa_dissertations/1795.

5. Chapter: Discussion and Conclusion

5.1 Discussion of Results

The overall aim of this thesis is to investigate the suitability of standard MT-InSAR methods for a regular geodetic surveillance of surface displacements associated with small-scale anthropogenic activities. In this context, several key questions and objectives were defined in Chapter 1.1, which will now be considered with respect to the outcomes of the previously presented case studies of Staufen (Chapters 2 and 3) and Ketzin (Chapter 4). Whereas the first two subchapters focus on the comparison with leveling measurements and the linkage of surface displacement with subsurface processes, the third subchapter concentrates on the technical aspects from a user's point of view.

5.1.1 Spatio-Temporal Assessment of MT-InSAR and Leveling Measurements

One focus of this doctoral thesis is the assessment of the capabilities of the state of the art MT-InSAR techniques to precisely map deformation fields compared to the classical terrestrial leveling measurements. The following section presents and discusses the results of the case study at Staufen in this respect. The investigations at the Ketzin pilot site (Chapter 4) cannot comprehensively support this specific discussion as leveling measurements were not conducted there. Instead, the InSAR results obtained in the Ketzin case study contribute to the discussion on the limitations of MT-InSAR techniques in Chapter 5.1.3.2. Here, this specific case study can only indirectly assess the relevance of leveling measurements by evaluating the impacts of their absence.

By using the SBAS methodology, a spatially limited elliptical-shaped deformation field with 290 m by 190 m extension could be clearly mapped at the city center of Staufen. As presented in Chapter 2.5.1 and illustrated in Figure 2.9, the density of the measurement points is significantly higher than the leveling survey point network that was established. The resulting higher level of detail is essential for a clear delineation of the affected area, for any geological interpretation or the enhancement of existing ones, for a suitable interpolation when areal calculations are required as well as for damage assessment of affected buildings and associated claims for damages.

The use of imaging radar satellites is beneficial here for two main reasons. First, an urban setting with many artificial objects provides ideal scattering conditions for microwave impulses, and hence a high amount of measurement points. As mentioned in Chapter 1.3, such scatterers often cause geometry-induced double-bouncing, for example, at building facades that are oriented in the viewing direction of the sensor. The resultant high energetic backscattering allows precise discrimination from other signals. This is important for the distance measurement (range) of the scattering object. As such objects are usually persistent, their signal is detectable in time, and the variations in their range to the sensor enable to draw conclusions on their stability. In the context of range accuracy, influencing factors such as atmosphere and topography will be discussed in Chapter 5.1.3.2., where MT-InSAR limitations will be considered with respect to localized displacement monitoring. Second, the establishment of a leveling network is labor-intensive, and thus time-consuming, whereas a satellite image is a snapshot that collects information of all the measurement points in the area under investigation at one time.

When using satellite-based InSAR techniques in urban areas, building facades and roofs are the main sources of information for drawing conclusions on surface stability. These objects are not considered for terrestrial leveling measurements, because the vertical displacement information is directly collected on the ground surface. Consequently, the area that is covered by buildings cannot be measured. Instead, leveling is usually performed on streets and walking areas, which in turn might be located in the radar shadow of buildings in dense settlements, where no InSAR data can be collected. This also applies for historic cities like Staufen, where narrow alleys are typical. As leveling requires visibility between survey points, the city structure influences the location and the density of leveling points. Therefore, both techniques are rather complementary, and a well-planned combined surveillance can compensate for the deficits of the individual techniques. This is especially interesting when larger parks prevent any SAR signal correlation in time, and result in missing information as is the case in the north-east part of the deformation ellipse at Staufen.

Another important difference in both methods, which need to be discussed here, is the actual measurement. Whereas leveling provides the direct vertical displacement, InSAR LOS results comprise vertical and horizontal motion contributions in one measurement. The case study of Staufen clearly shows the associated effects in Chapter 2.5.2. The magnitude discrepancies in leveling and InSAR time series were revealed, and these were explained as significant horizontal displacements. Data acquisition of additional TSX/TDX images from an opposing orbit and decomposition calculations, as presented in Chapter 3.5.2.2, confirm this assumption as they show a clear horizontal motion pattern in east- and westward directions. Generally, the near-polar orbit geometry and the right-looking sensing direction of the observing SAR satellite are fixed. This results in certain angles (satellite's heading and look angle) under which the objects on the Earth's surface can be monitored. Hence, 1D-LOS SAR measurements are mostly sensitive for the vertical motion contribution and have the lowest sensitivity for the north-south horizontal motion component. As illustrated in Fig. 2.11 and discussed in Chapter 2.5.2, 1D-LOS results can be misleadingly interpreted depending on the look angle, the magnitude of vertical motion as well as the magnitude and the direction of the horizontal displacement components. Thus, a combined data analysis of the ascending and descending images (opposing orbits) is beneficial to better capture the deformation field. But it is also subject to restrictions due to the limited sensitivities for the individual 3D-components and geometry-driven uncertainties with respect to the glancing intersection. Investigations into the glancing intersection were not performed in this thesis, but are recommended for future uncertainty assessments as it can have a considerable effect.

In fact, it is rather uncertain that the same point on the surface is observed from an ascending and a descending orbit, because the signal's backscatter is influenced, amongst others, by the object's orientation towards the satellite's viewing direction. An urban setting with buildings and alleys exacerbates this effect. For the decomposition of vertical and east-west displacements at Staufen, the measurement point locations of the ascending result were used to select and average the surrounding descending measurement points. The high density of InSAR data points is again valuable here as it ensures appropriate point selection at close distance.

Much effort was put in for the regular leveling measurements at Staufen for monitoring the displacement. It started with once a month in 2008, was increased to a two-week interval during the period of fast motion rates in the order of 1cm/month (March 2009 to June 2010), and was again reduced to a two-month periodicity till the end of 2012. Finally, the measurements were repeated once a quarter. These intervals were adjusted according to the relevance and measurability of motion rates. Evolution monitoring is also possible by using multi-temporal InSAR datasets. SAR images can be operationally acquired at fixed intervals that depend on the orbit-related revisit time of the SAR satellite. The TSX/TDX satellites with an 11-day revisit time provide an opportunity for dense image repetition that matches the two-week interval, which was required by the survey authorities. Adjustments according to the needs of the surveillance are possible by a multiple of the 11-day cycle.

As shown in the Staufen case study, the trend of approximate linear uplift as detected with leveling was also captured by the MT-InSAR SBAS method. Figures 2.10 and 3.6 (Chapters 2.5.1 and 3.5.2.1) illustrate this. The decrease in motion rate was discovered with both geodetic techniques, and was associated with the temporally correlating countermeasures. They were initiated shortly after the cause of deformation was related to the drilling activities. The countermeasures comprise the sealing of the boreholes and the pumping of groundwater to prevent further water contact with anhydrite.

Based on the findings in the Staufen case study, it can be concluded that MT-InSAR techniques have the potential for revealing surface displacement information with a high level of detail, but cannot fully replace terrestrial ground measurements such as leveling. The latter are still indispensable when the surface topography (i.e. the townscape) leads to radar shadow. The Ketzin pilot site case study (Chapter 4) further demonstrates the need for additional ground measurements. Strong vegetation coverage and weather variations triggered temporal decorrelation issues, and prevented an appropriate and equally distributed InSAR measurement point density. An aerial analysis of the surface displacements associated with the subsurface storage of CO_2 is possible in a limited form only, and it could be improved by leveling campaigns.

5.1.2 Surface-Subsurface Connection in the View of InSAR

The occurrence of surface displacements is always linked to the question over their sources. Which indirect conclusions can be drawn about subsurface processes based on the MT-InSAR displacement measurements at the top surface? This was one key question in Chapter 1.1. Such measurements can provide information on the stability of individual objects directly or indirectly on ground stability, when considered in spatial correlation to other surrounding objects. This is the first decision that must be made when interpreting InSAR measurements. In some cases, it can also be both—a combination of subsurface deformation and structure instability—when the first causes the second.

Applying a simple geophysical model, as it has been done in the Staufen case study by the inversion of the InSAR observation (Chapter 3), can support the interpretation of the spatially mapped and temporally monitored areal surface displacement. It can be used to constrain depth, extent, and orientation of a single source underground, and its temporal evolution. For Staufen, the Okada finite rectangular opening-mode dislocation source in a homogeneous elastic half-space was applied. It delivered a fit in accordance with the InSAR observation, and the knowledge gained from independent investigations by the National Agency for Resources and Mining (LGRB). The LGRB identified the water driven, volume-increasing anhydrite-gypsum transformation as the process that triggered the deformation. The depth of the related swellable region was detected by *in-situ* measurements (61.5 m–99.5 m below ground level), and the estimated depth (89 m ± 9 m) of the deformation source from the joint inversion of the ascending and the descending InSAR LOS results fit well with it (Chapter 3.4.2 and 3.5.3). This depth estimation again shows the benefit of the combined InSAR investigations, as well as that of the results of the performed single-data inversion (ascending data only) at an estimated depth (51 m ± 6 m) that is hardly connected to the anhydrite layers, which were found by the LGRB drill core analyses. It must be noted that a weak and shallow source can lead to the same surface displacement observations as a strong and deep source. The additional information of the independent LGRB analyses here helps to interpret the modeled source parameters, and demonstrates the usefulness of comprehensive data collections for understanding complex processes as well.

When comparing the modeled source with the observed surface displacement, the occurring deviations (Fig. 3.4) can reflect several aspects that must be considered when assessing the use of a simple geophysical model. First, residuals can point out individual building stresses in association with different building foundations and loads (construction variety). Moreover, building ages and their locations (stronger forces on the deformation center than on its edges) influence the buildings' reaction to the subsurface opening process, and hence, the appearance of their displacement in the InSAR observations. Second, a complex geological heterogeneity can be indirectly discovered from the residuals. A simple model, as applied for the Staufen case study, does not include local geological structures, e.g. faults or different groundwater levels. These can act as barriers or contribute to hydromechanical processes that can influence the deformation process. Also, crustal layering is not considered, i.e. heterogeneous or homogeneous strata can occur that have different material properties and varying capacities to hamper the opening forces of the underground volume increase. Third, the applied model assumes a single source that leads to the ground surface displacements, but many smaller sources that act in combination are also a possibility. Anhydrite occurs as individual lenses rather than as a compact layer. Such factors can all lead to the discovered model-observation deviations.

From the temporal perspective, the InSAR observation inversion can support the evaluation of the changes in the deformation process, when different periods are investigated. This is shown in Chapter 3.4.2 (Table 3.2), where the opening rate (strength) of the finite rectangular opening-mode dislocation source had decreased by a factor of 5 in the five years of observation. As discussed in Chapter 2.5.3, some natural possibilities can account for the deceleration, including a gypsum crust around the anhydrite lenses that prevents further water contact, and hence stops the chemical transformation. However, the temporal correlation with the counteractions (borehole sealing and groundwater pumping) is the most reasonable explanation for the InSAR observation and the modeled opening rate reduction.

In summary, when InSAR observations are available, their inversion can be used to constrain a simple geophysical model that provides the first information on the underground source location, and can provide hints on unknown geological barriers (faults). By including temporal evolution, indications of process changes can be concluded. Although limited in complexity, such information is generally helpful in cases where there are no other data sources. Additional information on the hydro-geological situation, as available at Staufen, through drill core analyses, seismic surveys, temperature logging, etc., contextualizes the InSAR results and the modeling outcome. All of them together allow a detailed assessment of this specific anthropogenic-induced deformation process. Nevertheless, a complex hydro-mechanical simulation with a detailed description of faults, strata properties, and the option to include multiple swelling sources would enhance the integrated assessment of the deformation by modeling and InSAR measurements. It may solve the current geophysical issue of the insufficiently explained spatial limitation of the surface displacement, especially towards the north and west (Fig. 2.12 (a) and 3.9 (b)).
The Staufen case study has confirmed the constructed relation between the visible ground surface displacements and the existence of a triggering ground surface process, indirectly measured by MT-InSAR. In the Ketzin pilot site case, this relation can also be confirmed, but from the opposite side. The pore pressure-induced stress changes in the subsurface due to the injected CO_2 are generally not severe enough to cause ground surface displacements that can be observed with InSAR (Chapter 4.4.2). The low cumulative amount of CO_2 (67 kt in about five years versus million t/year at large scale CCS sites, as for example at In Salah) and the consequent low pressure changes were attributed to it. However, independent hydro-mechanical simulations demonstrate ground surface displacements even for the tiniest pressure variations (Fig. 4.11). Nevertheless, a validation of the simulations is required, and since leveling or GPS surveys were not conducted, InSAR measurements are the alternative, but expose their boundaries here. Only the strongest pressure change of about 4 bar during a several-month-long period of injection stop (May 2012 to December 2012) led to 2.8 mm surface subsidence as detected with InSAR (Fig. 4.10 (b)). Here, the relevance of temporal monitoring becomes evident. Even though these MT-InSAR-based displacement signs are very small in magnitude and strongly influenced by a high noise level, their significance is shown in their temporal continuity. This is further supported by the high correlation of 80% with the bottomhole pressure in the injection well (Fig. 4.10 (e)), and by the integrated assessment of the complex hydromechanical simulations, which show a vertical subsidence of 0.75 mm for this period (Chapter 4.4.3).
The Ketzin case study has demonstrated that although geodetic reference data are lacking, e.g. leveling surveys, an integration of MT-InSAR techniques and numerical modeling can be carried out to assess ground surface displacements. Nonetheless, such an assessment could be improved by a denser and equally distributed InSAR measurement point cloud and an enhanced SNR. Some methodological alternatives are considered in Chapter 5.1.3.2. Furthermore, the complexity of the underlying model for the simulations as described in Chapter 4.3.3 is beneficial here because it allows the simulations to point out the tiniest changes in the subsurface process. In comparison to the simple geophysical model in the Staufen case study, it comprises all the missing additional information therein such as faults, groundwater levels and several lithological units.

5.1.3 Technical and Performance Aspects

5.1.3.1 Data Evaluation

All the presented case studies are based on the use of X-band SAR data of the TSX and TDX satellites of the German Aerospace Center (DLR). There are several reasons for this decision. For instance, the advantage of using TSX-/TDX-data is the high resolution of about 3 m in azimuth and range in the standard image acquisition mode (Stripmap mode). Since both case studies were supposed to show very local surface displacements, high resolution images were a prerequisite for a detailed analysis. The 30 m range resolution of C-Band sensors on board the ESA's satellites, ERS-2 and Envisat, is not sufficient here. Additionally, the data policy of DLR for the TSX-/TDX-data is considered as so-called

costs of fulfilling user requests with the possibility of discounts under certain conditions. An example is the contribution of institutions to the TSX mission [46], which is the case for the German Research Centre (GFZ). This means a free data access after proposal acceptance, which is generally a relevant aspect for each kind of work, whether driven scientifically or commercially.
Moreover, for both study areas, a long-term monitoring over several years was planned and a system must have been found that would provide data for this time (Fig. 5.1). Both ERS-2 and Envisat were already operating longer than their planned lifetime when data acquisition for Staufen started in 2008: ERS-2 for 13 years and Envisat for six years. Envisat would have been one reasonable option here, but the decision was made in favor of the higher spatial resolution of the younger TSX that was launched in 2007. The C-band alternatives from Canada (Radarsat-1/-2) as well as the X-band satellites from Italy (Cosmo-SkyMed) were not considered here. The associated data regulations restricted the data amount of free or discounted SAR images for foreign investigation areas and/or institutions when the investigations into the case studies presented herein had started. In general, free data is only available for the scientific community. Any commercial project that requires SAR data must include data costs in the cost calculations.

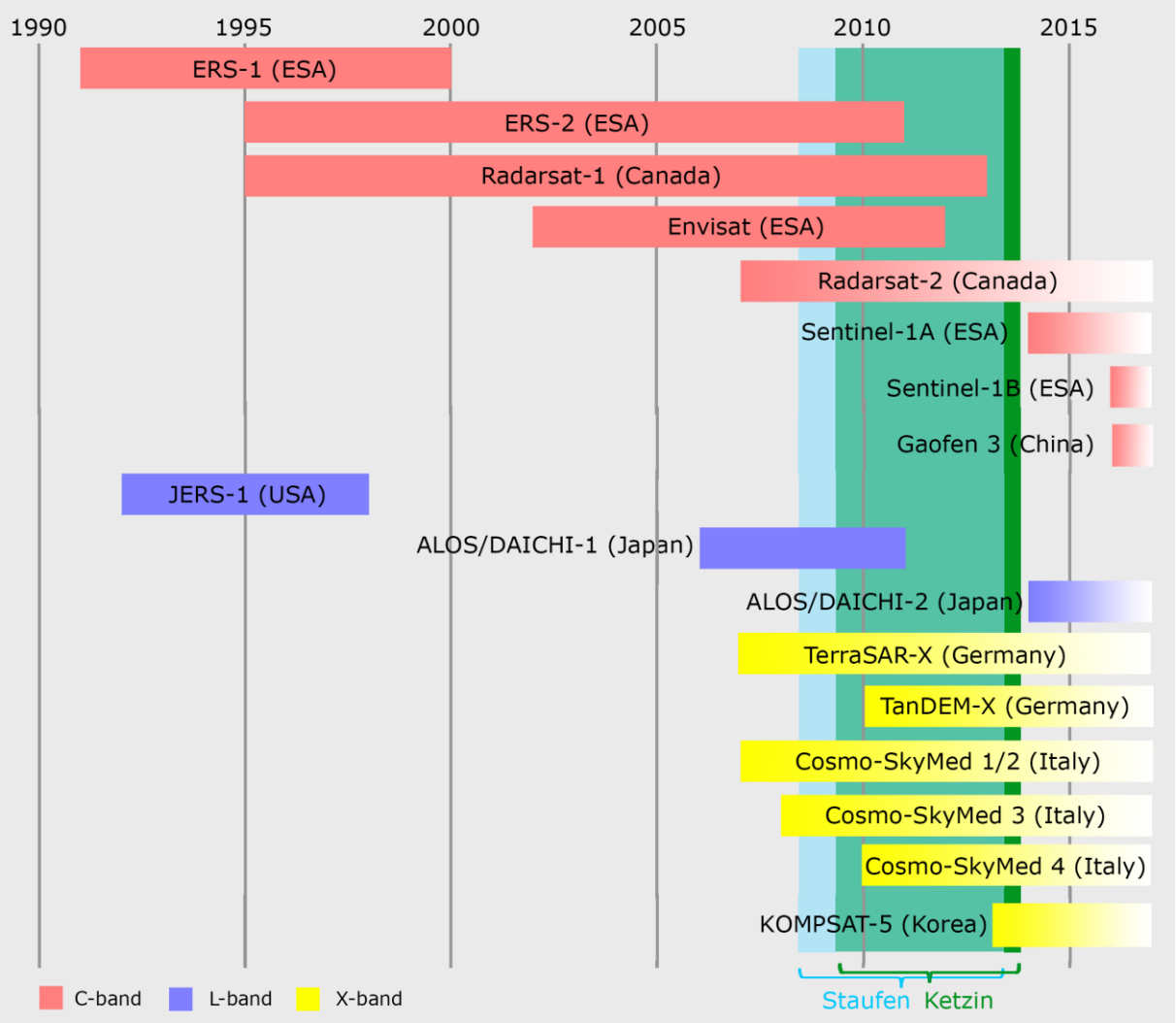

Fig. 5.1: Overview of civilian SAR imaging satellites operating at different wavelengths (bands) that have been available since the 1990s [47], [48]. The investigation periods of the Staufen and Ketzin case studies have been added to highlight the possible data sources [figure by Christin Lubitz].

As all scientific work was in progress, ESA's Copernicus-Program reached the satellite launch phase of Sentinel-1A in 2014, shortly after image acquisition stopped for Staufen and Ketzin. The launch of this C-band SAR satellite not only provides a continuation of the ERS-1/-2 and Envisat archives, but also

an increase in spatial resolution (5 m in azimuth and range direction). Together with Sentinel-1B that was launched in 2016, the global SAR mapping is now possible with a revisit time of six days (12 days with single satellite usage). This is an enhancement with respect to TSX/TDX. In addition, the data policy has evolved towards free access for all user groups (scientific and commercial), which makes the usage of Sentinel-1 data an interesting option. Such enhancements in technology and data policy lead to the following theoretical question for which prognostic statements will be given here:

- Would the Sentinel-1 InSAR time series analysis deliver different or better results or more information in comparison to the X-band data of TSX/TDX for the Staufen and Ketzin case studies, and how would they look like?

Three aspects must be considered to answer this question: the spatial resolution, the temporal resolution, and the wavelength-dependent sensitivity.
Both test sites, Staufen and Ketzin, spatially reflect a very limited area of surface deformation. Considering only the extent in these cases and the affected buildings at Staufen, a high spatial resolution is required for a detailed analysis. When Sentinel-1A/B would be used, the spatial resolution would be slightly worse. For completeness of this theoretical analysis, I have included here Japan's Daichi-2 satellite with an on board L-band sensor, which was launched in 2014. It provides up to 3 m spatial resolution in the high resolution mode, and is thus comparable to TSX/TDX. A resolution of 3 m and 5 m (Sentinel-1), respectively, may be considered sufficient at Staufen due to the high signal coherence in time in this urban setting. Regarding the rural site character of Ketzin, a higher resolution would enhance the detectability of smaller scattering objects. Moreover, using a higher resolution here, e.g. the spotlight mode of TSX/TDX and Daichi-2 with 1 m resolution, would allow noise reduction by spatial filtering options. Such filtering always comes at the expense of spatial resolution, and the use of such high resolution data end up with moderate image resolution with reduced noise level. The most recent developments reach spatial resolutions of about 25 cm (e.g. TSX Staring SpotLight mode [49]) that enables a drastic increase in detail level. This is important for all small displacement surveillances regardless of their environmental settings.
Similar revisit times were designed for TSX/TDX (11 days), Sentinel-1A/B (12 days with a single satellite, 6 days when using both) and Daichi-2 (14 days). The use of the satellite constellation of Sentinel-1A/B is advantageous here. A reduced revisit time is preferable when strong motion rates occur, leading to a fast loss of signal coherence (temporal decorrelation) that makes the application of MT-InSAR difficult, like at Ketzin. Furthermore, it can compensate for data gaps due to mission maintenance or other orbit maneuvers. In cases where surface responses to subsurface process changes need to be assessed, a fast image repetition can also be useful because it allows for a close temporal connection.
The third point is the most complex one in this analysis. Wavelength-dependent sensitivity can be considered from different points of views. Generally, short wavelengths are sensitive to small scale objects, i.e. signals from such sensors are scattered by objects of similar size. In detail, this means that short X-band signals (TSX/TDX: 3.1 cm wavelength) are already scattered at the leaf level of vegetation, whereas C-band signals (Sentinel-1: 5.6 cm wavelength) can reach the ground surface in less dense vegetated regions. L-band (Daichi-2: 24 cm wavelength) is least affected by vegetation coverage. Similarly, X-band signals can backscatter in the atmosphere, when there is strong rain or ice crystals. What seems to be disadvantageous in this context can be considered advantageous when the surface displacements with very small rates need to be observed. Here, the sensitivity to map displacements is half the wavelength in the LOS direction (TSX/TDX: 1.5 cm, Sentinel-1: 2.8 cm, Daichi-2: 12 cm). This leads to a preference for short wavelength sensors.
So, the use of Sentinel-1 data for Staufen would not deliver higher level of detail about the uplift ellipse as the resolution is slightly coarser, and the townscape (artificial geometry and material properties, see Chapter 1.3) provides many good scattering objects for both wavelengths. Perhaps, the north-eastern vegetated area is the only exception, because no TSX-based measurement points could be found due to temporal decorrelation. Here, increased information content through C-band measurements would support the sharp delineation of the deformation field. This can be essential

for the source and the subsurface process analyses and to evaluate claims for damages as well. In general, I would suggest the TSX high resolution spotlight mode (1 m) or the higher resolution modes that are currently being developed. Any monitoring of surface displacement in urban areas would benefit from the spatially highest level of detail that is possible, and the consequent high displacement sensitivity, especially for damage assessment of individually affected buildings. Sentinel-1 data would only be advantageous here given the nearly halved temporal resolution and access to free data.
Regarding the Ketzin case study, Sentinel-1 data is assumed to lead to a higher measurement point density, and hence spatially increased information content, especially at the agricultural fields around the pilot site. This is due to the fact that the potentially scattering objects would rather represent the ground surface than the vegetation top, which results in less temporal decorrelation. Nearly no TSX-based measurement points were found there, but the area still covers the spatial extent of the subsurface CO_2 distribution, and is thus important for process analyses. Here, the slightly lower spatial resolution of Sentinel-1 would not have so much of an impact. The use of L-band data from Daichi-2 would be even more beneficial from this point of view, but the very small surface displacements based on the hydromechanical simulations (4 mm in 5 years) could not be measured. The required displacement sensitivity is not possible with such long wavelengths, and most probably also not when using Sentinel-1 data. Therefore, displacement monitoring of the pilot site, where no vegetation is present, benefits from images with the highest resolution possible as it allows the detection of the tiny surface displacement responses to the low pressure changes in the injection well. In conclusion, a combination of the high resolution spotlight mode of TSX/TDX (1 m) and of Sentinel-1 data would have been the best monitoring option. First, it would have led to increased information content on the fields, and second, there would have been improved probability to detect the very small displacements at the well site.

5.1.3.2 Software and Method Assessment

In this thesis, the user friendliness of MT-InSAR is also discussed. Therefore, the questions pertaining to who requires such surface displacement measurements and who will process the data need to be considered. In general, displacement monitoring is a security-driven task. Private clients or public-sector customers (commercial users) can commission a geodetic surveillance during the planning phase of a project in order to minimize the risks to humans and infrastructure or to provide a kind of early warning. Mostly, they task a company or a public surveillance office with acquiring and processing the data.
When an InSAR time series monitoring is needed, the contractor most probably uses the state of the art methods. These methods are the PSI and SBAS approaches. Both are implemented in the mainly used commercial SAR processing software SARscape from Sarmap [50] and Gamma from the Gamma Remote Sensing Research and Consulting AG [51], both located in Switzerland. The Gamma software is command-based, whereas SARscape is implemented as a graphical user interface in the ENVI software environment. Alternatively, there are public-domain tools, e.g. StaMPS (Stanford Method for Persistent Scatterers)[52], [53], but their use is usually restricted to non-commercial projects. Furthermore, the in-house solutions of universities and research institutes, which are hardly accessible to external or commercial users, are not presented here.
At the beginning of data processing for Staufen and Ketzin, SARscape and StaMPS were available at GFZ. Since software development is a continuous process, some issues with SARscape pertaining to SAR image co-registration needed to be fixed during this time. For temporal reasons, a decision was taken to work with StaMPS instead. Therefore, the suitability of the main commercial software SARscape and Gamma for the two case studies cannot be evaluated here.
StaMPS provides PSI and SBAS algorithms for interferograms that were previously computed with DORIS, which is also an open access radar processing tool [54]–[56]. In the following subchapters, the methods as implemented in StaMPS will be assessed on the basis of the results from the case studies, statements regarding software usage will be given, and some further methodological aspects that can cause issues will be discussed.

Comparison of PSI versus SBAS

All the case studies presented in Chapter 2, 3 and 4 focus on MT-InSAR results based on the SBAS approach. Applying the PSI method led to several problems, which prevented adequate analyses at Staufen and Ketzin. As the PSI result of Staufen is not shown in the published manuscript (neither in Chapter 2 nor in Chapter 3), it is presented in Appendix B.1a for the purpose of completeness. The PSI-derived displacement map clearly shows the absence of data points at the center of the deformation ellipse at Staufen as compared to the SBAS outcome (Chapter 2, Fig. 2.6 and B.1b). The missing information prevents the further assessment of the PSI-based InSAR measurements as compared to leveling, and also complicates the geological interpretation and the evaluation of the surface-subsurface connection, which are all important objectives of this thesis (Chapters 5.1.1 and 5.1.2).

The poor PSI performance for the localized deformation monitoring at Staufen and Ketzin is mainly visible by a significantly reduced number of measurement points (Chapter 4.4.1 and Appendix B.1), and unwrapping issues (Appendix B.2). Unwrapping issues occur when the phase difference between neighboring data points is larger than π radians, which leads to an aliasing effect [26] and prevents the correct unwrapping of the wrapped interferometric phase. This results in disconnected areas, and consequently wrong displacement calculations. Such phase differences can be either due to true discontinuities in the data or due to low data sampling. Using a 3D unwrapping algorithm instead of a 2D or even a 1D one, reduces the probability of disconnected regions as the effective data sampling is increased by the dimension of time. Although a 3D algorithm was used in the StaMPS PSI processing, the phase unwrapping issues, especially at Ketzin, can be attributed to the low scatter point density between the individual settlements that leads to disconnected regions (Appendix B.2). The reason is the temporal decorrelation of the scattered SAR signals due to seasonal variations in the rural and vegetation-rich agricultural setting, which results in an overall low coherence in this region. As PSI focuses on long-term stable scatterers that are visible in all interferometric image pairs (Chapter 1.4.1), a long time span between an image pair (temporal baseline) amplifies this effect. Exceptions are artificial elements, e.g. settlements, wind turbines or the facilities at the Ketzin pilot site. They are the only scatterers with high phase stability.

The temporal baseline problem at Ketzin became obvious when the two-year PSI time series investigation failed to detect a sufficient number of PS, whereas a reduction of the observation period to one year delivered a valuable result (Chapter 4.5). In comparison, the SBAS method helps in overcoming these temporal decorrelation-related issues to a certain extent as it is based on a multi-master image approach (Chapter 1.4.2). This enables the processing of several years of observations as a whole. Here, a short revisit time of the satellite is beneficial as it increases the number of suitable image pairs for the interferogram network computation. As shown in Chapter 4.3.1.2, even the short 11-day revisit time of TSX/TDX can be critical in regions such as Ketzin, where temporal decorrelation is very fast. Nevertheless, the SBAS approach allows a time series analysis of the scatterers with lower coherence than PS, and thus, includes more data points for displacement monitoring.

Another aspect that is related to the estimation of phase stability in the PSI algorithm of StaMPS may account for the comparatively low PS density at Staufen, especially visible in the center of the deformation ellipse. Schunert et al. [57] state that the algorithm assumes a spatially correlated deformation during point quality assessment, which must not be necessarily true for localized deformations, but which then leads to an underestimation of the stability of points that do not undergo spatially correlated deformation. The consequence is the exclusion of these points from the final set of PS. They solved this problem by estimating the localized deformation via a linear trend, and subtracted it prior to the point stability assessment. As known from the leveling measurements, the assumption of an approximately linear motion is correct. Nonetheless, such a procedure actually contradicts the general objective of the StaMPS algorithm to be independent of a temporal model as such knowledge is not always available prior to an InSAR analysis [20]. Therefore, I again focused on the SBAS method of StaMPS as it delivered a sufficient data point density without the necessity of including a temporal model.

In a direct comparison, the difficulties in the InSAR time series processing by using PSI for both case studies demonstrate that the SBAS approach is versatile, i.e. usable for urban and non-urban areas as well as for short and long monitoring periods, but associated with higher uncertainty in the values (Chapter 4.4.1, Fig. 4.8). Nevertheless, the data point density issue, especially for non-urban regions, triggered the invention of alternative methods about 10 years after the development of PSI and SBAS in 2001 and 2002: the SqueeSAR™ [58] and the DS algorithm [59]. With SqueeSAR™, the PS and the distributed scatterers (DS) are jointly processed, whereas the DS algorithm solely focuses on the DS, but with a different procedure from SBAS. If there is need to use SqueeSAR™, TRE Altamira, a company with branches in Italy, Spain and Canada, provides the data processing service. It is not a software distributor like Gamma Remote Sensing or Sarmap.
In 2013, another new method was developed at the University of Nottingham, the so-called Intermittent SBAS (ISBAS), which improved the SBAS methodology of Berardino et al. [25] by also considering the intermittently coherent pixels for interferometric time series processing [60]. This leads to a significant increase in the number of detected scatterers in vegetated or agriculturally used lands (rural regions), which usually suffer from temporal decorrelation. Therefore, testing this new method on the data gained from Ketzin is recommended. Initial studies on the ISBAS algorithm used C-band data from ERS-2 and Envisat at low spatial resolution (100 m x 100 m) [60], [61], as only larger deformation phenomena were of interest. The conference contributions by Novellino et al. in 2015 [62] and the recently published paper by Novellino et al. [63] also confirm its usability on the high-resolution X-band data from TSX and Cosmo-SkyMed. Here, spatial resolutions of 15 m x 15 m and 9 m x 9 m, respectively, were used after applying multi-looking with the same effect of a drastically increased number of detected scatterers. The very low resolutions of the initial studies would not be sufficient for details at Ketzin, but the latest investigations into the high resolution data promise a better spatial distribution of scatterers at the site. As the ISBAS method builds upon the Berardino method, which is implemented in SARscape, there are two possibilities for testing this new approach. Either one can demand its implementation by Sarmap (in case of a commercial user) or one needs to program the algorithm by oneself based on the publication [60]. The latter requires appropriate programming skills and expert knowledge of the existing and the new algorithms.
Companies that offer InSAR surveillance as well as software distributors benefit from the fast implementations of new methodologies in existing software. Such new techniques allow enhancing product significance, to broaden the fields of application, and therefore a company's portfolio, which in turn increases the economic efficiency. At present, ISABS has neither been implemented in SARscape nor in Gamma.

Methodological Limitations

This subchapter will discuss two limiting aspects that were mentioned previously, but not considered in detail with respect to their relevance for small-scale displacement monitoring: atmospheric artifacts and topography.
In general, interferometric analysis requires the estimation of spatially correlated atmospheric effects (ionosphere and troposphere) [64] to subtract their phase contribution from the differential phase between two independent measurements. Such atmospheric phase artifacts can be modeled by using weather models, meteorological or GPS data [65]–[67], or must be estimated by using spatial and temporal filtering methods [17], [19]. Usually, atmospheric correction is very important on the regional scale. In order to save computational costs and due to the fact that only very local displacements were considered, data processing at Staufen and Ketzin were done only on a spatially very small subset of the SAR image. Therefore, complex atmospheric modeling of the ionosphere as well as of the troposphere was not conducted. Nonetheless, the StaMPS algorithm includes an iterative estimation process to remove, amongst others, the spatially correlated atmospheric phase contribution [20] without including weather models.
Some atmospheric effects are introduced by the topography of the observed region, especially when very steep and high mountains are present [68]. This is usually not the case in urban areas, where localized deformations can occur. Here, it would be interesting to investigate the effects of the so-

called urban heat islands on range measurements at different times, especially as the spatial resolution of SAR satellites is increasing more and more to reach the decimeter level. This certainly allows for a more detailed analysis of the localized displacements, but also requires a more detailed phase analysis of the contributing, but unwanted factors. Different aspects influence heat islands, e.g. city form (green space, materials, geometry, and building heights and density), occurrence of pollution, water areas, city size, geographical region, and day time [69], which lead to high variability from location to location. This is also of interest when satellite constellations are planned for MT-InSAR usage (e.g. Senitnel-1A/B, Cosmo-SkyMed), because image acquisition then potentially covers different daytimes. Research on urban heat islands and their effect on localized displacement observations by using InSAR is an interesting topic for future investigations.
The local topography is another factor that can negatively influence the range measurement, and hence correct displacement retrieval. Its phase contribution must be removed from the differential phase, and the accuracy in doing so depends on the existing topographic model (e.g. Digital Elevation Model (DEM) or Digital Surface Model (DSM)) of the investigated area. Global DEMs exist, e.g. from the Shuttle Radar Topography Model or the recently available WorldDEM^{TM} based on the TSX/TDX mission. It is important that with increasing spatial SAR image resolution, the spatial resolution and accuracy of the topographic model must also increase in order to reduce DEM errors. For Staufen, a 1 m Light Detection and Ranging (LiDAR) model that includes the surface, i.e. also building heights, was used to synthetically calculate the topographic phase contribution and to subtract it from the measured interferometric phase. The DEM for Ketzin includes several data sources (amongst others, LiDAR measurements and terrestrial, point wise height measurements), which were interpolated to a final grid of 10 m. The quality of this DEM was probably not sufficient enough, and could have caused the DEM errors that still may contribute to the displacement. For future products, I recommend selecting the most suitable DSM available (similar spatial resolution as the SAR image) or, if a commercial project is planned, to order a LiDAR DSM for minimizing the DEM error.

5.1.3.3 Efficiency

A regular InSAR surveillance of the existing or the potential localized deformations for safety purposes must consider certain performance-oriented aspects for an efficient work concept. Data availability and costs go hand in hand with the requested SAR-Band (X, C, and L). Its choice depends on the vegetation cover and the strength of the expected or the existing surface displacements (displacement sensitivity of the wavelength, Chapter 5.1.3.1.), which in turn influence the sensor's revisit time requirements. In addition, when there is an accompanying surveillance, data acquisition must be continued for the whole project duration and even longer, e.g. to monitor the potential long-term effects when CO_2 storage in a storage layer has stopped. A several-year-long campaign is usually possible, but longer periods require continued satellite missions that operate under the same conditions and with overlapping satellite lifetimes, such as that planned for ESA's Sentinels.
Another aspect is associated with data collection and processing: storage and hardware capacities. The acquired images require large disc space, which has been increasing with the new generation of SAR satellites, image resolution, and covered region (e.g. Envisat ASAR Single-Look Complex (SLC) Image product: 741 MB/product, TSXT/TDX SLC Stripmap product: up to 1.8 GB/product, and Sentinel-1 SLC product: 8 GB/product). Moreover, the increasing number of images for the time series analyses and the processing itself with all its intermediate products at least need intermediate large storage capacities. Some intermediate products can be usually deleted after certain procedures are finished. For example, interferograms can be deleted after StaMPS has converted the data into Matlab matrices that are necessary for further processing of PSI or SBAS. Nevertheless, storage has become a general issue. One possibility for file size reduction when undertaking localized investigations is to only process the area of interest (subset) and not the whole image (several tens of kilometers in range and azimuth) as it was done for the case studies presented herein (Staufen subset: about 470 x 580 pixels, and Ketzin subset: about 4000 x 4000 pixels). Table 5.1 shows how the file size reduces drastically when using a subset instead of processing the whole image, and how much storage space is needed for all the interferograms according to the specific MT-InSAR method.

	Delivered SLC image	Subset Interferogram	Number of Interferograms (Sum of storage capacities for Interferograms)		Matrix with final phase values in Stamps	
			PSI	SBAS	PSI	SBAS
Staufen	~ 1.7 GB	2.1 MB	50 (105 MB)	249 (523 MB)	1 MB	40 MB
Ketzin	0.4 -1.8 GB*	123 MB	50 (6 GB)	277 (34 GB)	2 MB (data set 1)	44 MB (data set 1) 73 MB (data set 2)

Table 5.1: Overview of the different product sizes from the Staufen and Ketzin case studies. * Delivered image products vary in size for the Ketzin case study, because the covered area in azimuth direction varies according to different users who desire data from this path.

Another current issue that is associated with large data volume and complex algorithms is the processing time needed to retrieve the desired surface displacement information. Data processing for such large data sets as in the cases of Staufen and Ketzin can still require several days without considering the refinement iterations due to, for example, unwrapping issues. An important aspect here is hardware capabilities. Using a computer center that provides parallel processing is advantageous here. For example, the company TRE Altamira has built an in-house data center that uses a Linux-based parallel processing system of about 100 servers and 276 cores for their InSAR processing services, and which have 200 TB storage capacities [70]. Usually, smaller companies or public authorities that are tasked with InSAR surveillance do not have such computing capabilities, but an investment in suitable hardware is recommended to reduce the processing time. In the past several years, high-performance techniques and infrastructures, e.g. clusters, distributed networks or cloud computing, have garnered interest for remote sensing data processing [71]. The growing amount of data and fast product demands in many fields of applications (e.g. hazard tracking and monitoring, oil spill detection, etc.) make them necessary. In order to efficiently use high-performance computing capacities, the existing MT-InSAR algorithms need to be adjusted accordingly [72]. This is a very complex and challenging task, but recent research work on this topic has demonstrated, for example, time saving by using cloud computation [73].
In this context, process automation is also getting more and more important, especially since near-real-time data delivery is possible, e.g. within 1 hour for Sentinel-1 [74] or in 2-4 hours for TSX/TDX when accepting low orbit accuracy [75]. Image delivery with precise orbits for interferometry purposes still requires several days. Appropriate algorithms are required, which are not only applicable to the delivery of the desired product for varying kinds of locations, but which are also fast. However, trained personnel with fundamental background knowledge in radar theory are still needed for MT-InSAR analyses. Intermediate products must be interpreted and evaluated for further usage within the processing chain. Problems and error sources must be recognized and solved. Especially when using the Gamma software, scripting skills are required. Hence, a fully automated MT-InSAR processing without any human interaction is not yet possible.

5.2 Conceptual Thoughts for Future Projects

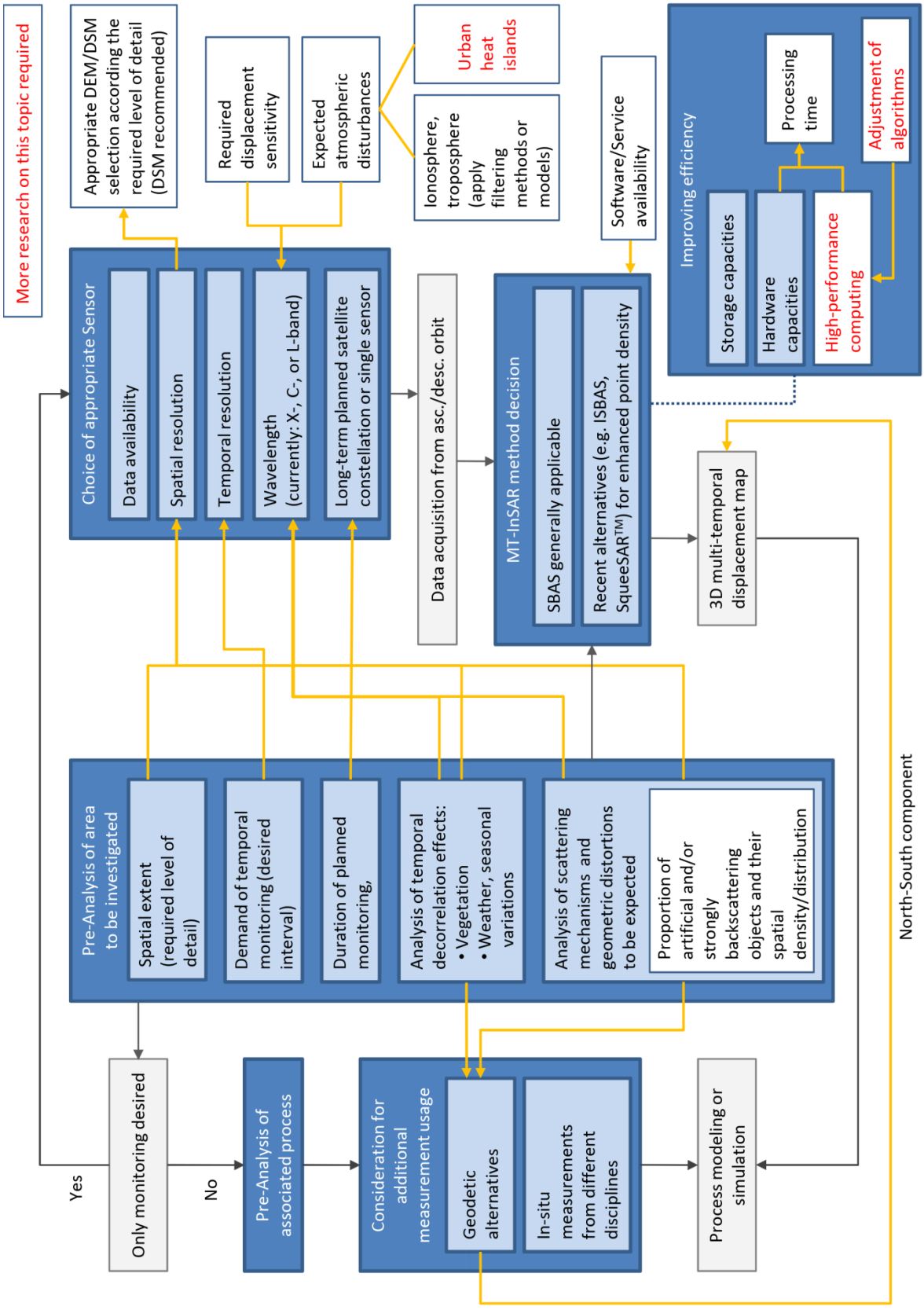

Fig. 5.2: Definition of the decisions and dependencies in MT-InSAR displacement monitoring based on the findings in this thesis [figure by Christin Lubitz].

5.3 Conclusion

The detection and monitoring of local surface displacements has become reliable due to the increasing availability of high-resolution SAR satellites (1 m–5 m) and developments towards further increase in spatial resolution (< 1 m). The main findings of this doctoral thesis are:

Terrestrial, labor-intensive and usually sparse, point-wise leveling measurements cannot reach the level of detail in mapping surface displacements as it is possible by using satellite-based SAR images. Standard MT-InSAR techniques have proved their suitability even for monitoring the smallest displacement when certain conditions are given.
First, SAR sensors with high-resolution imaging capabilities are essential; 3 m appear to be sufficient in urban areas, but 1 m or even higher resolutions are recommended for very small displacements. Second, a detailed displacement map requires a sufficient number of measurement points. The local setting, i.e. the vegetation coverage, the existence and density of artificial objects, as well as seasonal variations influence signal coherence, and hence the final number of available survey points. Long signal persistence is usually given in urban areas, which simplifies long-term InSAR surface displacement monitoring. In cases of strong vegetation cover, but also in areas of radar shadow due to topography or city structure, a combination with terrestrial geodetic measurements provides additional survey points. This improves the point density, and therefore the level of detail in the desired displacement map.
Third, based on the environmental situation, the SAR wavelength must be chosen. On condition that the same spatial resolution is available, sensors with longer wavelengths are more suitable for vegetation-rich regions. In cases of displacements with very low magnitudes, X-band is the appropriate choice.
Finally, to achieve the best possible result, SAR data from an ascending and a descending orbit should be used. It supports the clear delineation of the affected area, especially in east-west direction, and enables a differentiation between horizontal and vertical motion contributions. The orbit-related low north-south displacement sensitivity is still a problem for the desired 3D monitoring. Research on this topic comprises the development of alternative methods, e.g. Multiple Aperture Interferometry (MAI) [76], and discussions on satellites with left and right looking capability as well as on alternative non-polar orbit paths [77].

A temporally dense displacement monitoring is possible without much effort through the designed revisit time of modern satellites, especially when satellite constellations are used. A prerequisite is acquisition reliability, which must be guaranteed by the data provider.

In the view of generality, SBAS is preferable over PSI. There are many variations of algorithms that are adjusted to local conditions of the investigated area, but which are not implemented in standard software. Since this thesis also focuses on a user-friendly application of MT-InSAR techniques, a self-coded adaption is not considered to be a prerequisite for their successful usage. Furthermore, new techniques that have the potential to replace SBAS or PSI such as SqueeSAR™ or ISBAS are either only available as service from a certain company or not yet implemented in existing software. This hampers their non-scientific usage.

The constructed relation between surface displacements and associated subsurface processes can be indirectly confirmed by using MT-InSAR and simple inverse source modeling. Nevertheless, the combination of comprehensive *in-situ* data from independent geophysical measurements for complex simulations of the subsurface situation is recommended. Such detailed simulations enhance the understanding of the existing or the potential deformations, and they can be used for comparison with the InSAR results.

In summary, displacement monitoring is possible by standard MT-InSAR techniques with a high level of detail and less *in-situ* effort, but the surface-subsurface relation still requires intensive research.

6. List of Cited Literature

[1] N. Deichmann and D. Giardini, "Earthquakes Induced by the Stimulation of an Enhanced Geothermal System below Basel (Switzerland)," *Seismological Research Letters*, vol. 80, no. 5, pp. 784–798, 2009.

[2] S. Stramondo, M. Moro, C. Tolomei, F. R. Cinti, and F. Doumaz, "InSAR surface displacement field and fault modelling for the 2003 Bam earthquake (southeastern Iran)," *Journal of Geodynamics*, vol. 40, pp. 347–353, 2005.

[3] M. Motagh *et al.*, "Subduction earthquake deformation associated with 14 November 2007, Mw 7.8 Tocopilla earthquake in Chile: Results from InSAR and aftershocks," *Tectonophysics*, vol. 490, pp. 60–68, 2010.

[4] B. Delouis, D. Giardini, P. Lundgren, and J. Salichon, "Joint inversion of InSAR, GPS, teleseismic, and strong-motion data for the spatial and temporal distribution of earthquake slip: Application to the 1999 İzmit mainshock," *Bulletin of the Seismological Society of America*, vol. 92, no. 1, pp. 278–299, 2002.

[5] M. Simons, Y. Fialko, and L. Rivera, "Coseismic deformation from the 1999 Mw 7.1 Hector Mine, California, earthquake as inferred from InSAR and GPS observations," *Bulletin of the Seismological Society of America*, vol. 92, no. 4, pp. 1390–1402, 2002.

[6] Y. Fialko, M. Simons, and Y. Khazan, "Finite source modelling of magmatic unrest in Socorro, New Mexico, and Long Valley, California," *Geophysical Journal International*, vol. 146, no. 1, pp. 191–200, 2001.

[7] P. Lundgren, "Gravity and magma induced spreading of Mount Etna volcano revealed by satellite radar interferometry," *Geophysical Research Letters*, vol. 31, no. 4, pp. 1–4, 2004.

[8] M. E. Pritchard and M. Simons, "An InSAR-based survey of volcanic deformation in the southern Andes," *Geophysical Research Letters*, vol. 31, no. 15, pp. 1–42, 2004.

[9] J. Anderssohn, M. Motagh, T. R. Walter, M. Rosenau, H. Kaufmann, and O. Oncken, "Surface deformation time series and source modeling for a volcanic complex system based on satellite wide swath and image mode interferometry: The Lazufre system, central Andes," *Remote Sensing of Environment*, vol. 113, no. 10, pp. 2062–2075, 2009.

[10] D. Massonnet *et al.*, "The displacement field of the Landers earthquake mapped by radar interferometry," *Nature*, vol. 364, pp. 138–142, 1993.

[11] I. Colomina and P. Molina, "Unmanned aerial systems for photogrammetry and remote sensing: A review," *ISPRS Journal of Photogrammetry and Remote Sensing*, vol. 92, pp. 79–97, 2014.

[12] T. M. Lillesand, R. W. Kiefer, and J. W. Chipman, *Remote Sensing and Image Interpretation*, 6th Editio. Hoboken, New Jersey: John Wiley & Sons, 2008.

[13] C. Elachi and J. Van Zyl, *Introduction to the Physics and Techniques of Remote Sensing*, 2nd Editio. Hoboken, New Jersey: John Wiley & Sons, 2006.

[14] H. A. Zebker and J. Villasenor, "Decorrelation in Interferometric Radar Echoes," *IEEE Transactions on Geoscience and Remote Sensing*, vol. 30, no. 5, pp. 950–959, 1992.

[15] B. M. Kampes, "Displacement Parameter Estimation using Permanent Scatterer Interferometry," 2005.

[16] T. H. Dixon, "SAR Interferometiy and Surface Change Detection : Workshop Held," *Eos*, vol. 75, no. 24, 1994.

[17] A. Hooper, P. Segall, and H. Zebker, "Persistent scatterer interferometric synthetic aperture radar for crustal deformation analysis, with application to Volcán Alcedo, Galápagos," *Journal of Geophysical Research*, vol. 112, no. B7, p. B07407, Jul. 2007.

[18] E. Rodriguez and J. M. Martin, "Theory and design of interferometric synthetic aperture radars," *IEEE Proceedings F (Radar and Signal Processing)*, vol. 139, no. 2, pp. 147–159, 1992.

[19] A. Ferretti, C. Prati, and F. Rocca, "Permanent scatterers in SAR interferometry," *IEEE Transactions on Geoscience and Remote Sensing*, vol. 39, no. 1, pp. 8–20, 2001.

[20] A. Hooper, H. Zebker, P. Segall, and B. Kampes, "A new method for measuring deformation on

volcanoes and other natural terrains using InSAR persistent scatterers," *Geophysical Research Letters*, vol. 31, no. 23, 2004.

[21] N. Adam, B. M. Kampes, M. Eineder, J. Worawattanamateekul, and M. Kircher, "The development of a scientific permanent scatterer system," *ISPRS Workshop High Resolution Mapping from Space, Hannover, Germany, 2003*, p. 6 pp., 2003.

[22] C. Werner, U. Wegmuller, T. Strozzi, and A. Wiesmann, "Interferometric point target analysis for deformation mapping," *IGARSS 2003. 2003 IEEE International Geoscience and Remote Sensing Symposium. Proceedings (IEEE Cat. No.03CH37477)*, vol. 7, no. 1, pp. 4362–4364, 2003.

[23] R. M. Goldstein, H. A. Zebker, and C. L. Werner, "Satellite radar interferometry: Two-dimensional phase unwrapping," *Radio Science*, vol. 23, no. 4, pp. 713–720, 1988.

[24] A. Hooper and H. A. Zebker, "Phase unwrapping in three dimensions with application to InSAR time series.," *Journal of the Optical Society of America*, vol. 24, no. 9, pp. 2737–2747, 2007.

[25] P. Berardino, G. Fornaro, R. Lanari, and E. Sansosti, "A new algorithm for monitoring localized deformation phenomena based on small baseline differential SAR interferograms," *IEEE Transactions on Geoscience and Remote Sensing*, vol. 40, no. 11, pp. 2375–2383, 2002.

[26] A. Hooper, "A combined multi-temporal InSAR method incorporating persistent scatter and small baseline approaches," *Geophysical Research Letters*, vol. 35, no. 16, 2008.

[27] O. Mora, R. Lanari, J. J. Mallorqui, P. Berardino, and E. Sansosti, "A new algorithm for monitoring localized deformation phenomena based on small baseline differential SAR interferograms," *IEEE International Geoscience and Remote Sensing Symposium*, vol. 2, no. 11, pp. 2375–2383, 2002.

[28] A. J. Hooper, "A multi-temporal InSAR method incorporating both persistent scatterer and small baseline approaches," *Geophysical Research Letters*, vol. 35, no. 16, 2008.

[29] J. A. Steketee, "On Volterra's dislocation in a semi-infinite elastic medium," *Canadian Journal of Physics*, vol. 36, no. 2, pp. 192–205, 1958.

[30] Y. Okada, "Surface deformation due to shear and tensile faults in a half-space," *International Journal of Rock Mechanics and Mining Sciences Geomechanics Abstracts*, vol. 75, no. 4, pp. 1135–1154, 1985.

[31] D. Massonnet and K. L. Feigl, "Radar interferometry and its application to changes in the Earth's surface," *Reviews of Geophysics*, vol. 36, no. 4, p. 441, 1998.

[32] D. Massonnet and K. Feigl, "Satellite rada interferimetric map of the coseismic defromation field of the M=6.1 Eureka Valley, California earthquake of May 17, 1993," vol. 22, no. 12, pp. 1541–1544, 1995.

[33] K. Mogi, "Relations between the eruptions of various volcanoes and the deformations of the ground surfaces around them," *Bulletin of the Earthquake Research Institute*, vol. 36. pp. 99–134, 1958.

[34] P. M. Davis, "Surface Deformation Due to Inflation of an Arbitrarily Oriented Triaxial Ellipsoidal Cavity in an Elastic Half-Space With Reference to Kilauea Volcano, Hawaii," *Journal of Geophysical Research*, vol. 91, no. B7, pp. 7429–7438, 1986.

[35] F. T. Lee and J. F. J. Abel, "Subsidence from underground mining: Environmental analysis and planning considerations," in *Publications of the Geological Survey*, 1983.

[36] B. N. Whittaker and D. J. Reddish, *Subsidence–Occurrence, Prediction and Control*, 1st Editio. Amsterdam, The Netherlands: Elsevier Science Publishers B.V., 1989.

[37] X. L. Yao, B. N. Whittaker, and D. J. Reddish, "Influence of overburden mass behavioural properties on subsidence limit characteristics," *Mining Science and Technology*, vol. 13, pp. 167–173, 1991.

[38] K. B. Singh and T. N. Singh, "Ground movements over longwall workings in the Kamptee coalfield, India," *Engineering Geology*, vol. 50, pp. 125–139, 1998.

[39] W. Münch, H. P. Sistenich, C. Bücker, and T. Blanke, "Möglichkeiten der geothermischen Stromerzeugung in Deutschland," *VGB PowerTech*, pp. 1–11, 2005.

[40] B. Pancevski, "Geothermal probe sinks German city," *The Telegraph*, 2008. [Online]. Available: http://www.telegraph.co.uk/news/worldnews/1583323/Geothermal-probe-sinks-German-

city.html. [Accessed: 27-Nov-2017].
[41] C. Atkinson, “Green good intentions cause chaos in two German towns,” *Deutsche Welle*, 2009. [Online]. Available: http://www.dw.com/en/green-good-intentions-cause-chaos-in-two-german-towns/a-4473382. [Accessed: 27-Nov-2017].
[42] D. Charter, “Earth moves for geothermal clean energy town Staufen as cracks appear,” *The Times*, 2017. [Online]. Available: https://www.thetimes.co.uk/article/cracks-appear-in-staufen-s-geothermal-heating-plan-mdw9dx0lr. [Accessed: 27-Nov-2017].
[43] Global CCS Institute, “Large-scale CCS facilities,” 2017. [Online]. Available: https://www.globalccsinstitute.com/projects/large-scale-ccs-projects. [Accessed: 30-Mar-2017].
[44] National Energy Technology Laboratory, “NETL’s Carbon Capture and Storage Database - Version 5,” 2014. [Online]. Available: https://www.netl.doe.gov/research/coal/carbon-storage/strategic-program-support/database. [Accessed: 30-Mar-2017].
[45] British Geological Survey, “Why monitor CO2 storage projects.” [Online]. Available: http://www.bgs.ac.uk/discoveringGeology/climateChange/CCS/whyMonitorCO2Storage.html. [Accessed: 30-Mar-2017].
[46] A. Roth, “TerraSAR-X Science Plan,” 2004.
[47] European Space Agency, “Satellite Missions Database,” *Earth Observation Portal*. [Online]. Available: https://directory.eoportal.org/web/eoportal/satellite-missions. [Accessed: 10-Jan-2017].
[48] “Gaofen (High Resolution),” *China Space Report*, 2017. [Online]. Available: https://chinaspacereport.com/spacecraft/gaofen/#gf3. [Accessed: 27-Nov-2017].
[49] Airbus Defence and Space, “TerraSAR-X Image Product Guide - Basic and Enhanced Radar Satellite Imagery,” 2014.
[50] Sarmap, “SARscape.” [Online]. Available: http://www.sarmap.ch/page.php?page=sarscape. [Accessed: 30-Mar-2017].
[51] GAMMA Remote Sensing AG, “GAMMA Software.” pp. 1–10, 2017.
[52] A. Hooper, D. Bekaert, and K. Spaans, “StaMPS / MTI Manual Version 3.3b1,” pp. 1–36, 2013.
[53] A. Hooper, “STAMPS.” [Online]. Available: https://homepages.see.leeds.ac.uk/~earahoo/stamps/. [Accessed: 14-Nov-2017].
[54] Delft University of Technology, “DORIS.” [Online]. Available: http://doris.tudelft.nl/. [Accessed: 14-Nov-2017].
[55] Delft Institute of Earth Observation and Space Systems (DEOS), “Delft Object-oriented Radar Interferometric Software User’s manual and technical documentation,” 2008. [Online]. Available: http://doris.tudelft.nl/usermanual/index.html. [Accessed: 14-Nov-2017].
[56] B. M. Kampes, R. F. Hanssen, and Z. Perski, “Radar interferometry with public domain tools,” in *Third International Workshop on ERS SAR Interferometry, `FRINGE03’*, 2003, p. 6 pp.
[57] A. Schunert, M. Even, U. Sörgel, and K. Schulz, “A modified version of StaMPS for the detection of localized surface displacement,” in *8th European Conference on Synthetic Aperture Radar*, 2010, pp. 1–4.
[58] A. Ferretti, A. Fumagalli, F. Novali, C. Prati, F. Rocca, and A. Rucci, “A new algorithm for processing interferometric data-stacks: SqueeSAR,” *IEEE Transactions on Geoscience and Remote Sensing*, vol. 49, no. 9, pp. 3460–3470, 2011.
[59] K. Goel and N. Adam, “An advanced algorithm for deformation estimation in non-urban areas,” *ISPRS Journal of Photogrammetry and Remote Sensing*, vol. 73, pp. 100–110, 2012.
[60] A. Sowter, L. Bateson, P. Strange, K. Ambrose, and M. F. Syafiudin, “DInSAR estimation of land motion using intermittent coherence with application to the South Derbyshire and Leicestershire coalfields,” *Remote Sensing Letters*, vol. 4, no. 10, pp. 979–987, 2013.
[61] D. Gee, A. Sowter, A. Novellino, S. Marsh, and J. Gluyas, “Monitoring land motion due to natural gas extraction: Validation of the Intermittent SBAS (ISBAS) DInSAR algorithm over gas fields of North Holland, the Netherlands.,” *Marine and Petroleum Geology*, vol. 77, pp. 1338–1354, 2016.
[62] A. Novellino *et al.*, “Intermittent small baseline subset (ISBAS) InSAR analysis to monitor

landslides in Costa della Gaveta, Southern Italy," in *International Geoscience and Remote Sensing Symposium (IGARSS)*, 2015, pp. 3536–3539.

[63] A. Novellino, F. Cigna, A. Sowter, M. Ramondini, and D. Calcaterra, "Exploitation of the Intermittent SBAS (ISBAS) algorithm with COSMO-SkyMed data for landslide inventory mapping in north-western Sicily, Italy," *Geomorphology*, vol. 280, pp. 153–166, 2017.

[64] R. F. Hanssen, *Radar Interferometry Data Interpretation and Error Analysis*. New York: Springer, 2001.

[65] Z. Li, J. P. Muller, P. Cross, and E. J. Fielding, "Interferometric synthetic aperture radar (InSAR) atmospheric correction: GPS, Moderate Resolution Imaging Spectroradiometer (MODIS), and InSAR integration," *Journal of Geophysical Research*, vol. 110, no. 3, pp. 1–10, 2005.

[66] J. Foster, B. Brooks, T. Cherubini, C. Shacat, S. Businger, and C. L. Werner, "Mitigating atmospheric noise for InSAR using a high resolution weather model," *Geophysical Research Letters*, vol. 33, no. 16, pp. 1–5, 2006.

[67] X. L. Ding, Z. W. Li, J. J. Zhu, G. C. Feng, and J. P. Long, "Atmospheric effects on InSAR measurements and their mitigation," *Sensors*, vol. 8, no. 9, pp. 5426–5448, 2008.

[68] C. Delacourt, P. Briole, and J. A. Achache, "Tropospheric corrections of SAR interferograms with strong topography. Application to Etna," *Geophysical Research Letters*, vol. 25, no. 15, pp. 2849–2852, 1998.

[69] J. Voogt, "How Researchers Measure Urban Heat Islands."

[70] TRE ALTAMiRA, "Company," 2017. [Online]. Available: http://tre-altamira.com/company/. [Accessed: 23-Jun-2017].

[71] C. A. Lee, S. D. Gasster, A. Plaza, C.-I. Chang, and B. Huang, "Recent Developments in High Performance Computing for Remote Sensing : A Review," *IEEE Journal of Selected Topics in Applied Earth Observations and Remote Sensing*, vol. 4, no. 3, pp. 508–527, 2011.

[72] F. Casu *et al.*, "SBAS-DInSAR Parallel Processing for Deformation Time-Series Computation," *IEEE Journal of Selected Topics in Applied Earth Observations and Remote Sensing*, 2014.

[73] I. Zinno *et al.*, "A First Assessment of the P-SBAS DInSAR Algorithm Performances Within a Cloud Computing Environment," *IEEE Journal of Selected Topics in Applied Earth Observations and Remote Sensing*, vol. 8, no. 10, pp. 4675–4686, 2015.

[74] European Space Agency, "Sentinel Online - Data Distribution Schedule." [Online]. Available: https://sentinel.esa.int/web/sentinel/missions/sentinel-1/data-distribution-schedule. [Accessed: 25-Nov-2017].

[75] Airbus Defence and Space, "TerraSAR-X Image Product Guide - Basic and Enhanced Radar Satellite Imagery," 2014.

[76] N. B. D. Bechor and H. A. Zebker, "Measuring two-dimensional movements using a single InSAR pair," *Geophysical Research Letters*, vol. 33, no. 16, pp. 1–5, 2006.

[77] T. J. Wright, "Toward mapping surface deformation in three dimensions using InSAR," *Geophysical Research Letters*, vol. 31, 2004.

7. Appendix

A Overview on largest industrial CCS sites worldwide in operation, under construction, or planned [43].

EOR = Enhanced Oil Recovery, DGS = Dedicated Geological Storage, dsp = deep saline formations

Project name	**Project lifecycle stage**	**Country**	**Operation date**	**Primary storage type**
Val Verde Natural Gas Plants	Operate	UNITED STATES	1972	EOR
Enid Fertilizer CO2-EOR Project	Operate	UNITED STATES	1982	EOR
Shute Creek Gas Processing Facility	Operate	UNITED STATES	1986	EOR
Sleipner CO2 Storage Project	Operate	NORWAY	1996	DGS - offshore dsp
Great Plains Synfuel Plant and Weyburn-Midale Project	Operate	CANADA	2000	EOR
Snøhvit CO2 Storage Project	Operate	NORWAY	2008	DGS - offshore dsp
Century Plant	Operate	UNITED STATES	2010	EOR
Air Products Steam Methane Reformer EOR Project	Operate	UNITED STATES	2013	EOR
Coffeyville Gasification Plant	Operate	UNITED STATES	2013	EOR
Lost Cabin Gas Plant	Operate	UNITED STATES	2013	EOR
Petrobras Santos Basin Pre-Salt Oil Field CCS Project	Operate	BRAZIL	2013	EOR
Boundary Dam Carbon Capture and Storage Project	Operate	CANADA	2014	EOR
Uthmaniyah CO2-EOR Demonstration Project	Operate	SAUDI ARABIA	2015	EOR
Quest	Operate	CANADA	2015	DGS - onshore dsp
Abu Dhabi CCS Project (Phase 1 being Emirates Steel Industries (ESI) CCS Project)	Operate	UNITED ARAB EMIRATES	2016	EOR
Petra Nova Carbon Capture Project	Operate	UNITED STATES	2017	EOR
Illinois Industrial Carbon Capture and Storage Project	Operate	UNITED STATES	2017	DGS - onshore dsp
Gorgon Carbon Dioxide Injection Project	Execute	AUSTRALIA	2017	DGS - onshore dsp
Kemper County Energy Facility	Execute	UNITED STATES	2017	EOR
Alberta Carbon Trunk Line ("ACTL") with Agrium CO2 Stream	Execute	CANADA	2018	EOR

Alberta Carbon Trunk Line ("ACTL") with North West Sturgeon Refinery CO2 Stream	Execute	CANADA	2018	EOR
Yanchang Integrated Carbon Capture and Storage Demonstration Project	Execute	CHINA	2018	EOR
Sinopec Qilu Petrochemical CCS Project	Define	CHINA	2019	EOR
Rotterdam Opslag en Afvang Demonstratieproject (ROAD)	Define	NETHER-LANDS	2019-20	DGS - offshore depleted oil and/ or gas resevoir
Texas Clean Energy Project	Define	UNITED STATES	2021 (Institute estimate)	EOR
CarbonNet Project	Define	AUSTRALIA	2020's	DGS - offshore dsp
Sinopec Shengli Power Plant CCS Project	Define	CHINA	2020's	EOR
Riley Ridge Gas Plant	Evaluate	UNITED STATES	2020	EOR
Sinopec Eastern China CCS Project	Evaluate	CHINA	2020	EOR
Huaneng GreenGen IGCC Project (Phase 3)	Evaluate	CHINA	2020's	EOR important, DGS options under review
Korea-CCS 1	Evaluate	SOUTH KOREA	2020's	DGS - offshore dsp
Korea-CCS 2	Evaluate	SOUTH KOREA	2020's	DGS - offshore dsp
Teesside Collective Project	Evaluate	UNITED KINGDOM	2020's	DGS - offshore dsp
Caledonia Clean Energy Project	Evaluate	UNITED KINGDOM	2022	DGS, offshore dsp with potential for EOR
South West Hub	Evaluate	AUSTRALIA	2025	DGS - onshore dsp
China Resources Power (Haifeng) Integrated Carbon Capture and Sequestration Demonstration Project	Identify	CHINA	2020's	DGS - offshore dsp
Shanxi International Energy Group CCUS project	Identify	CHINA	2020's	Under evaluation
Shenhua Ningxia CTL Project	Identify	CHINA	2020's	Under evaluation

B.1 Cumulated LOS displacement of Staufen based on a) SBAS and b) PSI procedure of StaMPS for the period July 2008-May 2011. The red star highlights the reference point. With SBAS 23608 measurement points were detected and with PSI 3189 measurement points.

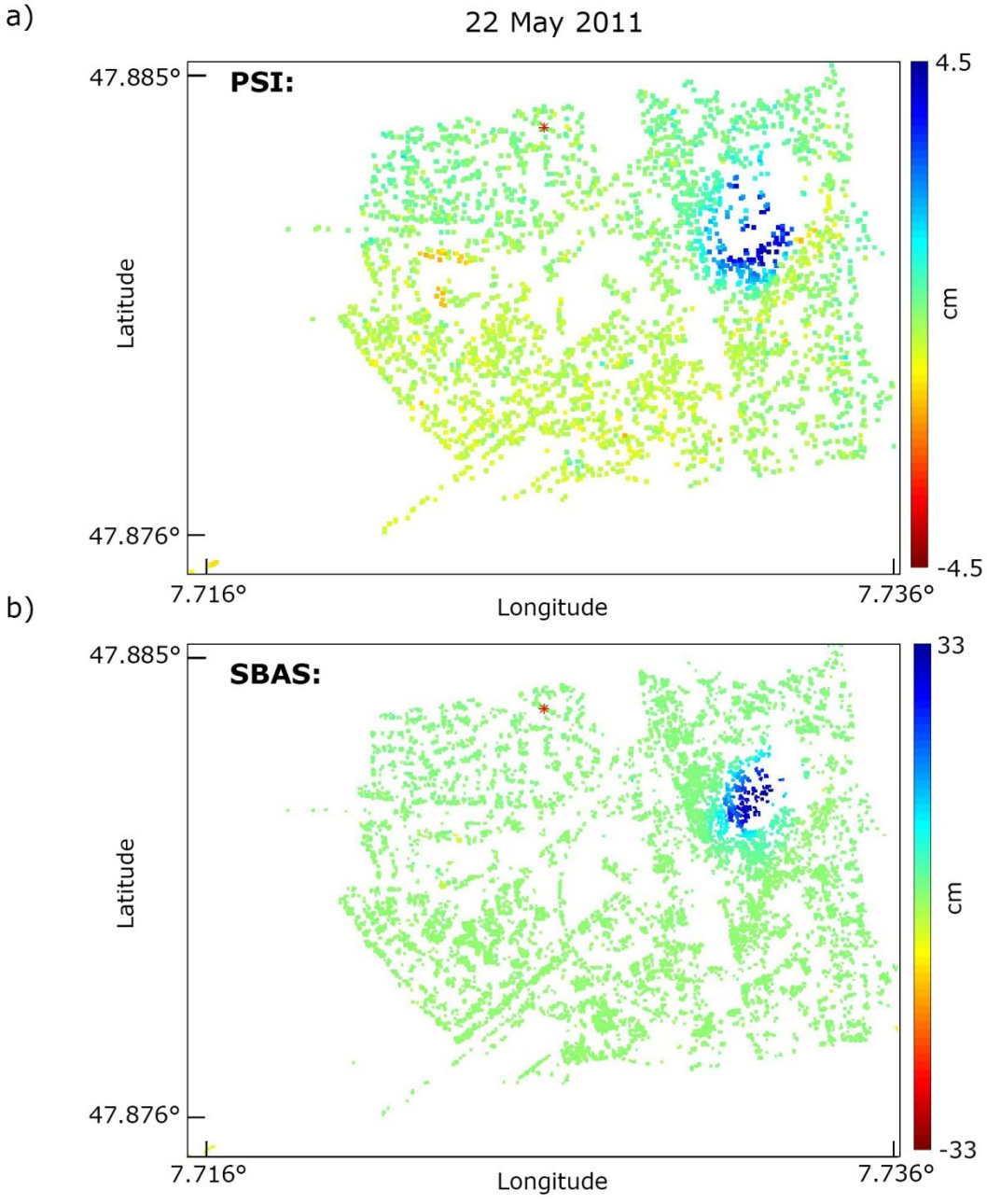

B.2 Unwrapping issues due to insufficient scatterer density that lead to wrong displacement values at the Ketzin test site.

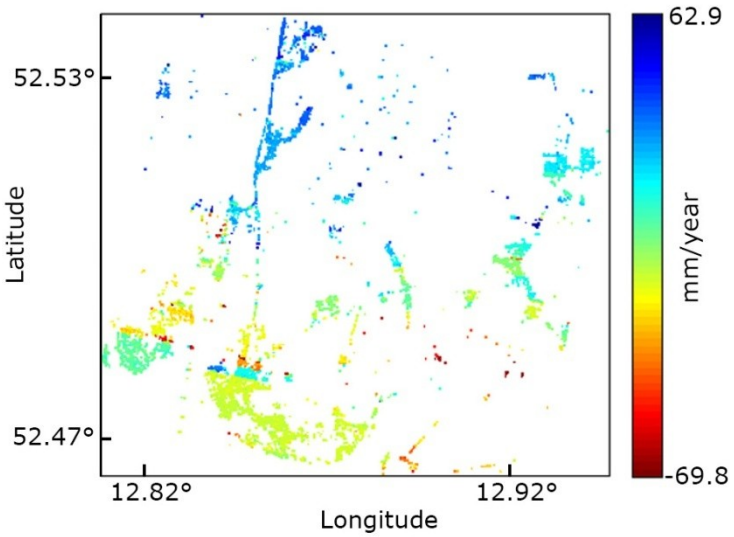

List of Figures

List of Tables